June 8, 2021 Docket No: 99902082

U.S. Nuclear Regulatory Commission
ATTN: Document Control Desk
Washington, DC 20555-0001

Subject: Transmittal of White Paper on the Energy Multiplier Module (EM^2) Accelerated Fuel Qualification Strategy

General Atomics Electromagnetic Systems (GA-EMS) is submitting to the NRC the Energy Multiplier Module (EM^2) Accelerated Fuel Qualification (AFQ) Strategy white paper for pre-application license review. The AFQ strategy takes a stepwise approach to developing and qualifying a new nuclear fuel form for use in the EM^2 gas-cooled fast reactor, which has a fuel lifetime of up to 30 years. The AFQ strategy seeks to reduce the time and cost of fuel qualification by using advances in multi-scale modeling combined with miniature fuel irradiations. The aim of this strategy would reduce, but not totally eliminate, the need for in-core radiation experiments without compromising safety.

This activity is in support of the DOE award for the industry-led DE-NE0008331. GA-EMS has budgeted 160 staff hours for this review. GA-EMS requests that the NRC complete its review and provide its feedback and any requests for additional information within 90 days of receipt of this letter.

To aid in the efforts to advance the reactor concept, GA-EMS requests that the following three areas be placed in priority in the feedback:

1. The science-based approach includes the use of both fuel performance models and separate effects testing to validate predictive capabilities, which are intended to increase both the quantity and quality of "data" from experiments, and modeling and simulation that provides the basis for the fuel qualification process. The science-based approach promotes a reduction in performance uncertainties and strengthens the safety case. GA-EMS requests concurrence, or further guidance on implementation of this science-based approach.

2. Accelerated fuel irradiations may provide significant understanding of fuel behavior even though they have an alternative fuel irradiation time history. INL is developing the FAST capability, which may hold much promise to extend science-based modeling to long-lived and high burnup fuels as long as the range of validity is determined. Targeted experiments, coupled with predictive performance analysis, would then be able to address the integral fuel test requirements. GA-EMS would like input from the NRC on their view of incorporating accelerated fuel irradiations as part of the science-based modeling.

3. Even with advanced modelling, practical demonstration of 30-year lifetime of this and other long-lived fuels will need to be built up from cumulative performance based on shorter segments of time. GA-EMS plans to conduct fuel surveillance, inspection and testing during the prototype phase of a demonstration reactor along with Versatile Test Reactor (VTR) testing to establish interim burnup limits for a conditional operating license. GA-EMS is seeking NRC staff agreement that a conditional operating license is possible for the EM^2 long core life reactors prior to obtaining full burnup fuel test data under prototypical conditions.

GA-EMS requests the NRC staff to provide advice and guidance on this summary and expected application of Accelerated Fuel Qualification methodology into the licensing framework for EM^2 and advanced reactors.

If you have any questions or need any additional information, please contact John Bolin by email at john.bolin@ga.com or by phone at 858-762-7576.

Best regards,

Dr. Christina Back
Vice President, Nuclear Technologies and Materials Division

Enclosure: "Energy Multiplier Module (EM^2) Accelerated Fuel Qualification Strategy," GA-EMS document 30533R00003/A, May 6, 2021.

CC: Samuel.CuadradoDeJesus@nrc.gov
John.Segala@nrc.gov
Amy.Cubbage@nrc.gov
Raymond.Furstenau@nrc.gov

30533R00003
Revision A

PRE-APPLICATION LICENSE REVIEW OF SILICON CARBIDE COMPOSITE CLAD URANIUM CARBIDE FUEL FOR LONG-LIFE GAS-COOLED FAST REACTOR CORES

ENERGY MULTIPLIER MODULE ACCELERATED FUEL QUALIFICATION STRATEGY

Prepared by General Atomics – Electromagnetic Systems

Grant Agreement DE-NE0008831

DISCLAIMER

GA Project 30533

GENERAL ATOMICS

REVISION HISTORY

Revision	Date	Description of Changes
A	06MAY21	Initial Release

POINT OF CONTACT INFORMATION

PREPARED BY:			
Name	**Position**	**Email**	**Phone**
John Bolin	Principal Investigator	John.Bolin@ga.com	858-762-7576
Hangbok Choi	Senior Staff Engineer	Hangbok.Choi@ga.com	858-762-7554
APPROVED BY:			
Name	**Position**	**Email**	**Phone**
C. Back	Division Director	Christina.Back@ga.com	858-762-7552
K. Partain	Quality Engineer	Katherine.Partain@ga.com	858-455-3225

DESIGN CONTROL SYSTEM DESCRIPTION

		DISC	QA LEVEL	SYS
☒	R & D			
☐	DV&S			
☐	DESIGN			
☐	T&E	N	II	N/A
☐	NA			

ACKNOWLEDGEMENT

This material is based upon work supported by the Department of Energy under Award Number DE-NE0008831.

TABLE OF CONTENTS

REVISION HISTORY ii
POINT OF CONTACT INFORMATION ii
DESIGN CONTROL SYSTEM DESCRIPTION ii
ACKNOWLEDGEMENT iii
ACRONYMS vii
1 INTRODUCTION 1
2 REGULATORY BASES 3
2.1 NRC Regulations 3
2.2 NRC Guidance 4
2.2.1 Standard Review Plan 4
2.2.2 Principal Design Criteria for Non-Light-Water Reactors 8
2.3 GA Position on Adaptation of Non-LWR Criteria to EM^2 8
3 DESCRIPTION OF EM^2 SYSTEM 9
3.1 EM^2 Plant and Major Components 9
3.2 EM^2 Fuel System 12
3.3 EM^2 Safety Features 16
4 FUEL DESIGN BASES AND CRITERIA 18
4.1 Thermal Design Bases and Criteria 18
4.1.1 Fuel Temperature 18
4.1.2 Cladding Temperature 19
4.2 Mechanical Design Bases and Criteria 20
4.2.1 Cladding Stress Limit 20
4.2.2 Cladding Strain Limit 21
4.2.3 Fuel Element Fatigue 22
4.2.4 Element Internal Pressure 22
4.3 Chemical Design Bases and Criteria 23
4.4 Summary of Design Bases and Criteria 23
5 ANALYSIS METHODS AND MATERIAL PROPERTIES 24
5.1 Thermal-Mechanical Analysis Methods 24
5.2 Material Properties 25
5.2.1 Fuel Material Properties 25
5.2.2 Cladding Material Properties 29
5.3 Uncertainties in Properties and Models 35
5.3.1 Uranium Carbide Fuel 35
5.3.2 Silicon Carbide Composite Cladding 37
6 PERFORMANCE EVALUATION 38
6.1 Approach to EM^2 Fuel Performance Evaluation 38
6.2 Normal Operation 39
6.3 Accident Conditions 41
6.3.1 Control Rod Withdrawal 42
6.3.2 Loss of Primary Cooling Capability 44
6.4 Remarks 46
7 LEGACY APPROACH TO FUEL QUALIFICATION 47
8 STRATEGY FOR ACCELERATED FUEL QUALIFICATION 50
8.1 AFQ Phase 1 for EM^2 Fuel 53

8.2 AFQ Phase 2 for EM^2 Fuel 55
8.2.1 Fundamental material properties and characterization of UC 56
8.2.2 Atomistic to Mesoscale Modeling and Simulation - Low Length-Scale Models 57
8.2.3 Phase 2 Targeted Experiments: MiniFuel Irradiation Tests 61
8.2.4 Phase 2 Models and Tests for Fuel Form (Pellet) Design and Analysis: Fission Accelerated Steady-state Testing (FAST) 63
8.2.5 Phase 3: Integral Fuel Testing 65
8.3 Overall EM^2 Qualification Plan 65
8.4 Summary of Key Elements in Accelerated Fuel Qualification 68

9 REFERENCES 68

LIST OF FIGURES

Figure 1 AFQ approach uses modeling and simulation with experimental validation 2
Figure 2 EM2 plant layout on 9 hectares of land 10
Figure 3 EM^2 primary heat transport system enclosed in two-chamber sealed containment 11
Figure 4 EM^2 PCU components and Brayton cycle helium flow 12
Figure 5 Configuration of EM^2 reactor core 13
Figure 6 EM^2 tri-bundle fuel assembly 15
Figure 7 GA-fabricated bulk kernels and pellets with magnified cross-sections 16
Figure 8 Routing of FPCS collection lines to HTA 17
Figure 9 Passive DRACS heat exchangers and water loops 18
Figure 10 Melting temperature of carbide fuel as a function of plutonium content [1-7] 19
Figure 11 Radiation induced swelling in bulk SiC as a function of irradiation temperature [9]. 20
Figure 12 Irradiation stability (irradiated-to-non-irradiated ultimate strength ratio) of different SiC_f/SiC composite types [13]. 21
Figure 13 Components and distribution types for simplified stress-strain model of SiGA cladding using GA analysis and data [15]. 22
Figure 14 Tentative instantaneous creep rate model of SiGA under different operating conditions [46]. 32
Figure 15 Tentative transient creep rate model of SiGA [46]. 34
Figure 16 SiGA stress-strain model for selected temperatures of 1270K and 830K [41] 35
Figure 17 Power history of reference EM^2 fuel element 39
Figure 18 Reference EM^2 fuel element operating temperature profile 40
Figure 19 Reference EM^2 fuel pellet radial temperature distribution 40
Figure 20 Comparison of EM^2 fuel element cladding hoop stresses. 41
Figure 21 Comparison of EM^2 fuel element cladding hoop strains. 41
Figure 22 Transient EM^2 reactor core power during a single CR withdrawal 42
Figure 23 Transient EM^2 temperatures during a single CR withdrawal 43
Figure 24 Transient EM^2 cladding circumferential stress during a single CR withdrawal 43
Figure 25 Transient EM^2 cladding circumferential strain during a single CR withdrawal 43
Figure 26 Comparison of EM^2 primary system pressure with cooldown on one DRACS loop 44
Figure 27 Comparison of EM^2 helium mass flow during LOFA and LOCA 45
Figure 28 Comparison of EM^2 transient temperatures during LOFA and LOCA 45
Figure 29 Comparison of EM^2 transient cladding circumferential stress during LOFA and LOCA 46

Figure 30 Comparison of EM^2 transient cladding circumferential strain during LOFA and LOCA....46
Figure 31 Predicted thermal creep behavior of HT9 steel as a function of von-Mises stresses at 600ºC 51
Figure 32 Detail of Phase 2 of the Accelerated Fuel Qualification Methodology 55
Figure 33 Comparison of diffusion coefficient of ^{133}Xe in UC....57
Figure 34 Possible sites for Xe within the UC lattice (courtesy UT-Knoxville) 59
Figure 35 MiniFuel capsule for irradiation of UC kernels in HFIR (courtesy ORNL) 62
Figure 36 X-ray computed tomography images of UC kernel (courtesty ORNL) 63
Figure 37 GA Simulation of Post-Irradiation Heating of 3- and 6-Cycle HFIR Irradiated UC Kernels 63

LIST OF TABLES

Table 1 Fuel Damage Criteria....5
Table 2 Fuel Failure Criteria 6
Table 3 Fuel Coolability Criteria....7
Table 4 EM^2 core characteristics 14
Table 5 Summary of EM^2 fuel specifications....15
Table 6 Comparison of CVD SiC and SiC-SiC creep strain models 33
Table 7 Application of TRLs to reactor fuel development and qualification [1] 49
Table 8 AFQ Phases....52
Table 9 Gap assessment in uranium carbide fuel properties and models 54
Table 10 Gap assessment in silicon carbide composite cladding properties and models 54

ACRONYMS

Acronym	Description
AFCI	Advanced Fuel Cycle Initiative
AFQ	Accelerated Fuel Qualification
AGR	Advanced gas reactor
AMT	Assessment matrix table
AOO	Anticipated operational occurrence
ARDC	Advanced reactor design criteria
ASME	American Society of Mechanical Engineers
ATF	Accident tolerant fuel
ATR	Advanced test reactor
BOL	Beginning of life
BPV	Bypass prevention valve
CFR	Code of Federal Regulations
COL	Combined (Construction and Operating) License
CR	Control rod
CTE	Coefficient of thermal expansion
CVD	Chemical vapor deposition
CVI	Chemical vapor infiltration
DC	Design certification
DD	Dislocation dynamics
DFT	Density functional theory
DOE	Department of Energy
DOE-NE	DOE – Office of Nuclear Energy
DRACS	Direct reactor auxiliary cooling system
DU	Depleted uranium
ECCS	Emergency core cooling system
EM^2	Energy Multiplier Module
EM^2-DC	EM^2 design criteria
EOL	End of life
FAST	Fission accelerated steady-state testing
FEM	Finite element method

Acronym	Description
FGR	Fission gas release
FPCS	Fission product collection system
GA	General Atomics
GA-EMS	GA – Electromagnetic Systems
GDC	General design criteria
GFR	Gas-cooled fast reactor
HBS	High burnup structure
HFIR	High flux isotope reactor
HPS	Helium purification system
HTA	High temperature absorber
IAEA	International Atomic Energy Agency
ID	Inner diameter
INL	Idaho National Laboratory
ITAAC	Inspections, tests, analyses, and acceptance criteria
JRR	Japanese research reactor
JMTR	Japanese materials testing reactor
LANL	Los Alamos National Laboratory
LB	Large break
LBLOCA	Large break loss of coolant accident
LDRD	Laboratory-directed research and development
LEU	Low enriched uranium
LOCA	Loss of coolant accident
LOFA	Loss of flow accident
LTA	Lead test assembly
LTR	Lead test rod
LWR	Light-water reactor
M&S	Modeling and simulation
MD	Molecular dynamics
MHTGR-DC	Modular high-temperature gas-cooled reactor design criteria
MIT	Massachusetts Institute of Technology
MOL	Middle of life
MSA	Minimum solid area

Acronym	Description
mSiC	Monolithic silicon carbide
NEAMS	Nuclear energy advanced modeling and simulation
NFI	Nuclear Fuels Industries
NGNP	Next Generation Nuclear Plant
NPR	New Production Reactor
NRC	Nuclear Regulatory Commission
NRC-RES	NRC Office of Nuclear Regulatory Research
NRC-NRR	NRC Office of Nuclear Reactor Regulation
ORC	Organic Rankine cycle
ORNL	Oak Ridge National Laboratory
PCS	Primary coolant system
PCU	Power conversion unit
PIE	Post-irradiation examination
PIRT	Phenomena identification and ranking table
PLS	Proportional limit stress
QA	Quality assurance
RIA	Reactivity-initiated accident
SAFDL	Specified acceptable fuel design limit
SB	Small break
SBLOCA	Small break loss of coolant accident
SFR-DC	Sodium fast reactor design criteria
SiGA®	Silicon carbide technology developed by General Atomics
SRP	Standard review plan
T/C	Turbo-compressor
TD	Theoretical density
TM	Trade Mark
TRISO	Tri-structural isotropic
TRL	Technology readiness level
UTK	University of Tennessee – Knoxville
UTS	Ultimate tensile stress
VASP	Vienna ab initio simulation package
VTR	Versatile test reactor

Acronym	Description
VXF	Vertical experiment facility
WTA-HX	Water-to-air heat exchanger
XCT	X-ray computed tomography

1 INTRODUCTION

The purpose of this white paper is to lay out a strategy for significantly reducing the time and cost of qualifying new nuclear fuel and materials as part of licensing new advanced reactors. Most advanced reactor designs rely on fuel types that differ, substantially in many cases, from zircaloy-clad uranium dioxide (UO_2) fuel. Likewise, nearly all advanced reactors have operating conditions that differ significantly from those of light-water reactors (LWRs). These reactors must confront the challenge of producing a substantial amount of data and analyses to assure their safe performance per Nuclear Regulatory Commission (NRC) requirements for licensing. The essential data and validation of analyses has been empirical. The recent precedent for Tri-structural Isotropic (TRISO) particle fuel shows the time to develop such data can take over 20-25 years with costs of up to $350 million [1]. This represents a significant barrier to the introduction of new reactors that could be safer and more economic than present day LWRs.

Cost and schedule of an empirical fuel qualification approach is a particularly significant barrier for the Energy Multiplier Module (EM^2), an advanced reactor being developed by General Atomics Electromagnetic Systems (GA-EMS). EM^2 is a 500 MWt gas-cooled fast reactor (GFR) using pressurized helium coolant in a direct Brayton cycle. It is designed to be economically competitive with natural gas electricity generation and has a 30-year core life in order to reduce fuel cost and minimize waste generation to only one-fifth of an LWR. The EM^2 fuel consists of uranium carbide (UC) pellets enclosed in a silicon carbide (SiC) composite cladding – a SiGA® technology developed by GA-EMS. For the purposes of this paper, a SiC composite is defined as ceramic matrix composite composed of reinforcing silicon carbide fibers within a silicon carbide matrix.

Because of the long core life, it is impractical to accumulate full-burnup fuel performance data for licensing EM^2. Therefore, GA is spearheading an effort with several national laboratories and universities to develop a methodology to expedite the licensing qualification of fuel and material. This methodology, referred to as Accelerated Fuel Qualification (AFQ), combines advances in atomistic-to-mesoscale fuel performance modeling and simulation with new, targeted irradiation measurement capabilities [2]. A graphical comparison between AFQ and the typical empirical approach to fuel qualification is shown in Figure 1. As the predictive modeling capability is developed and experimentally validated, uncertainties in the predictive capability decrease and confidence in safety performance increase associated with design and regulatory decision-making.

Two industry-led projects have been funded by the Department of Energy (DOE) to help develop this methodology. One is a project to demonstrate the effectiveness of AFQ for EM^2 fuel to address UC kernel swelling and fission product release titled "Combining Multi-Scale Modeling with Microcapsule Irradiation to Expedite Advanced Fuels Deployment" [2]. GA, Oak Ridge National Laboratory (ORNL) and the University of Tennessee – Knoxville (UTK) are jointly executing this work. The other project is to develop a fuel qualification strategy titled "Pre-Application License Review Of Silicon Carbide Composite Clad Uranium Carbide Fuel For Long-

Life Gas-Cooled Fast Reactor Cores" based on the AFQ methodology, which is the subject of this white paper. An additional project is funded by Idaho National Laboratory (INL) using their Laboratory-Directed Research and Development (LDRD) funds to apply one of the AFQ methodologies to advance EM² UC pellet fuel development and qualification [3].

Several other companies working on advanced reactors, national laboratories, and universities have joined GA in the effort to develop and implement AFQ. These include Westinghouse, Framatome, Lightbridge Corporation, Walsh Engineering, Aerospace Corporation, TerraPower, University of Tennessee-Knoxville, University of Florida, INL, Los Alamos National Laboratory (LANL), ORNL, and Argonne National Laboratory (ANL). DOE Office of Nuclear Energy (DOE-NE) and the NRC Office of Nuclear Regulator Research (NRC-RES) and Office of Nuclear Reactor Regulation (NRC-NRR) participate as observers in the AFQ efforts to develop the methodology as documented in two workshops held in 2019 and 2020 [4, 5].

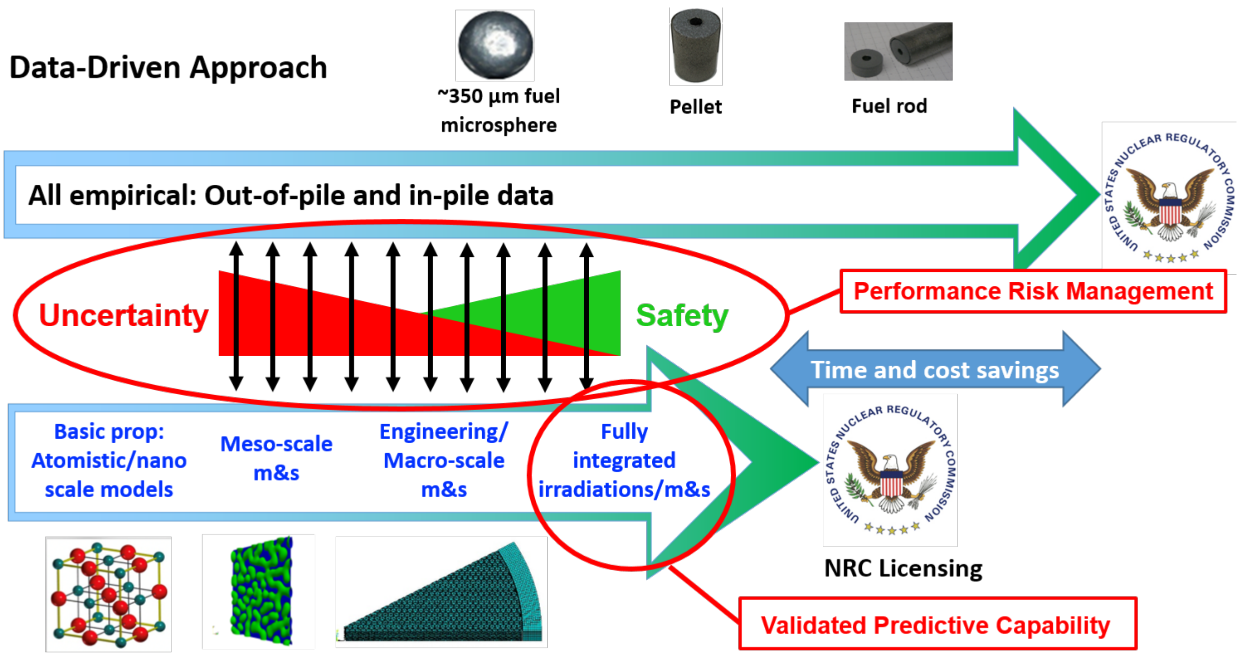

Figure 1 AFQ approach uses modeling and simulation with experimental validation

This white paper will cover the following topics:

- Identify existing regulations and regulatory guidance relevant to fuel qualification; and provide EM²-specific guidance.
- Present EM² reactor design, fuel specifications and safety approach, followed by design bases and criteria of fuel and cladding materials.
- Summarize the fuel performance analysis method and existing material data, followed by discussion of issues related to EM²-specific materials.

- Provide preliminary EM^2 fuel performance analysis results for the normal operation and transient cases including assessment of uncertainties and operational variations.
- Present historic fuel qualification practices.
- Present the AFQ methodology, outlining the irradiation and testing strategy that incorporates modern M&S capabilities and escalates GFR fuel technology readiness level (TRL). This section includes a brief description of advanced technologies such as atomistic-to-mesoscale modeling and simulation (M&S), microscale measurement, and mini-fuel tests that can accelerate the fuel qualification

The desired outcome of this white paper is to define EM^2 fuel licensing strategy for use in the EM^2 reactor that can serve as the driver of a time-efficient and cost-effective fuel qualification plan with application to other advanced reactor fuel forms.

2 REGULATORY BASES

The NRC regulations and guidance were originally developed for the conventional fuel and reactors. For the advanced reactors, these regulations and guidance are being revised and updated to reflect the mechanism and consequence of the fuel and reactor response to abnormal operating conditions. Ultimate goal of the NRC's non-LWR licensing framework is rulemaking to create a new 10 CFR Part 53. The following sections review the most relevant regulations and guidance to EM^2.

2.1 NRC Regulations

The General Design Criteria (GDC) in Appendix A to 10 Code of Federal Regulations (CFR) Part 50 establish minimum requirements for water-cooled nuclear power plants and are considered to be generally applicable to other types of nuclear power units. GDC 10 and 35 are generally applicable to fuel.

GDC 10 – Reactor design. The reactor core and associated coolant, control, and protection systems shall be designed with appropriate margin to assure that specified acceptable fuel design limits are not exceeded during any condition of normal operation, including the effects of anticipated operational occurrences (AOOs).

GDC 35 – Emergency core cooling. A system to provide abundant emergency core cooling shall be provided. The system safety function shall be to transfer heat from the reactor core following any loss of reactor coolant at a rate such that (1) fuel and clad damage that could interfere with continued effective core cooling is prevented and (2) clad metal-water reaction is limited to negligible amounts.

GDCs 12, 17, 20, 25, 26, 33, and 34 also provide criteria related to assuring specified acceptable fuel design limits (SAFDLs) are not exceeded due to power oscillations, electric power system capability, protection system functions and capabilities, reactor coolant makeup, and residual heat removal.

Acceptance criteria for emergency core cooling systems (ECCS) for LWRs are regulated by 10 CFR Part 50.46 and Appendix K ECCS Evaluation Models. These regulations provide additional requirements for meeting GDC 35.

2.2 NRC Guidance

2.2.1 Standard Review Plan

Detailed guidance for the review of LWR safety analysis reports is provided in NUREG-0800, Standard Review Plan (SRP). Fuel System Design under SRP 4.2 provides assurance that the fuel design meets the requirements of GDC 10 and 35, and the core coolability requirements of 10 CFR 50.46. Specific areas of review in SRP 4.2 are as follows:

1. Design Bases. Design bases for the safety analysis shall address <u>fuel system damage mechanisms</u> and provide <u>limiting values</u> for important parameters to prevent damage from exceeding acceptable levels.
2. Description and Design Drawings. The fuel system description and design drawings shall emphasize <u>product specifications</u> rather than process specifications.
3. Design Evaluation. The performance of the fuel system during <u>normal operation, AOOs, and postulated accidents</u> shall show that all design bases are met.
4. Testing, Inspection, and Surveillance Plans. The licensee performs testing and inspection of new fuel to ensure that the fuel is fabricated in accordance with the design and that it reaches the plant site and is loaded in the core without damage.
5. Inspections, Tests, Analyses, and Acceptance Criteria (ITAAC). For design certification (DC) and combined license (COL) reviews, the proposed ITAAC associated with the structures, systems, and components (SSCs) shall follow SRP Section 14.3, "Inspections, Tests, Analyses, and Acceptance Criteria."
6. COL Action Items and Certification Requirements and Restrictions. For a DC application, the COL action items, requirements, and restrictions (e.g., interface requirements and site parameters) shall be addressed.

2.2.1.1 Fuel Damage

Fuel damage criteria should assure that fuel system dimensions remain within operational tolerances and that functional capabilities are not reduced below those assumed in the safety analysis. When applicable, the fuel damage criteria should consider high burnup effects based on irradiated material properties data. Complete damage criteria should address the following:

a. <u>Stress limits</u> that are obtained by methods similar to those given in Section III of the Boiler and Pressure Vessel Code of ASME are acceptable.
b. The cumulative number of <u>strain fatigue cycles</u> on the structural members should be significantly less than the design fatigue lifetime, including a safety factor.
c. <u>Fretting wear</u> at contact points on the structural members should be limited.

d. Oxidation, hydriding, and the buildup of corrosion products (crud) should be limited, with a limit specified for each fuel system component.

e. Dimensional changes should be limited to prevent fuel failures or thermal-hydraulic limits being exceeded.

f. Fuel and burnable poison rod internal gas pressures should remain below the nominal system pressure during normal operation.

g. An evaluation of worst-case hydraulic loads should be performed for normal operation, AOOs, and accidents.

h. Control rod reactivity and insertability must be maintained.

Fuel damage criteria established for LWR provide guidance to establishing relevant criteria for EM² fuel system. The applicability and status of EM² fuel damage criteria are presented in Table 1.

Table 1 Fuel Damage Criteria

Fuel Damage Criteria	Applicability	Current Status
Stress limits	Yes	Final stress, strain, and loading limits remain to be established for all members of the fuel system. See Sections 4.2.1 and 4.2.2.
Strain fatigue cycles	Yes	Final strain fatigue limits remain to be established for all members of the fuel system. See Section 4.2.3.
Fretting Wear	Yes	Fretting wear tests and allowable limits remain to be established.
Oxidation, hydriding, buildup of corrosion	Partial	No hydriding or buildup of corrosion products observed. Final oxidation limits remain to be established.
Dimensional changes	No	Irradiation resistance of SiC composite materials exhibit minimal dimensional changes.
Internal gas pressure	Yes	Final internal gas pressure limits remain to be established based on cladding stress and strain. See Section 4.2.4.
Worst-case hydraulic loads	Yes	Final worst-case hydraulic loads and potential of unseating fuel assembly remain to be established.
Control rod insertability	No	Irradiation resistance of SiC composite materials expected to eliminate most concerns with control rod insertability.

2.2.1.2 Fuel Failure

Fuel rod failure is defined as the loss of fuel rod hermeticity. Fuel rod failures are permitted during postulated accidents, but they must be accounted for in the dose analysis. Complete fuel failure criteria should address the following items listed below in Table 2. Because no metal cladding is used in the EM^2 fuel design, some of the below failure mechanisms are not directly applicable such as hydriding, cladding collapse, and bursting.

Table 2 Fuel Failure Criteria

Fuel Failure Criteria	Applicability	Current Status
Hydriding	No	No hydriding of SiC composite materials has been observed.
Cladding collapse	No	Low ductility and high strength at high temperatures of SiC composite materials eliminates metallic cladding collapse phenomena.
Overheating of cladding	Yes	Final thermal margin criteria remain to be established. See Section 4.1.2.
Overheating of fuel pellets	Yes	Final fuel melting criteria remain to be established. See Section 4.1.1.
Excessive fuel enthalpy	Yes	Final fuel enthalpy criteria from a reactivity initiated accident (RIA) remain to be established.
Pellet/cladding interaction	Yes	No chemical interactions that lead to cladding failure have been observed with SiC composite materials. Final criteria for mechanical interaction between pellet and cladding remain to be established.
Bursting	Partial	Low ductility and high strength at high temperatures of SiC composite materials preclude classic ballooning and bursting of cladding. Final failure criteria for cladding loss of hermeticity remain to be established.

Fuel Failure Criteria	Applicability	Current Status
Mechanical fracturing	Yes	Final mechanical fracturing of SiC composite cladding remains to be established.

2.2.1.3 Fuel Coolability

Fuel coolability criteria should be provided for all severe damage mechanisms. Coolability, or coolable geometry, has traditionally implied that the fuel assembly retains its rod-bundle geometry with adequate coolant channels to permit removal of residual heat. Complete criteria should address the following items listed below in Table 3. Some of the below criteria are not applicable to the EM^2 fuel design. For example, the SiGA cladding will not melt but can decompose at extremely high temperatures. The cladding ballooning is expected for the metallic cladding with high internal pressure and ductility but is not credible for ceramic matrix cladding like SiGA. As such, EM^2 fuel design-specific requirements for coolability will be defined.

Table 3 Fuel Coolability Criteria

Fuel Coolability Criteria	Applicability	Status
Cladding embrittlement	No	High strength at high temperature of SiC composite cladding and its postquench characteristics preclude coolability issues.
Violent expulsion of fuel	Partial	Violent expulsion of fuel from SiC composite cladding has not been observed due to the high strength at high temperature of SiC composite cladding. Final criteria quantifying fuel dispersal from cracks in SiC composite cladding remain to be established.
Generalized cladding melting	No	SiC composite materials preclude cladding melt. Final cladding temperature limits remain to be established. See Section 4.1.2.
Fuel rod ballooning	No	Low ductility and high strength at high temperatures of SiC composite materials

Fuel Coolability Criteria	Applicability	Status
		preclude classic ballooning and bursting of cladding.
Structural deformation	Yes	Criteria to ensure control rod insertability from structural deformation associated with external loads from earthquakes and postulated pipe breaks remain to be established.

2.2.2 Principal Design Criteria for Non-Light-Water Reactors

In April 2018, the NRC issued Regulatory Guide 1.232 "Guidance for Developing Principal Design Criteria for Non-Light-Water Reactors." The Reg. Guide describes proposed guidance on how the GDC in Appendix A of 10 CFR Part 50 may be adapted for non-LWR designs. The guidance includes three appendices: A – Advanced Reactor Design Criteria (ARDC), B – Sodium-Cooled Fast Reactor Design Criteria (SFR-DC), and C – Modular High-Temperature Gas-Cooled Reactor Design Criteria (MHTGR-DC). The ARDC is intended to apply to a wide variety of advanced reactor technologies; however, in some instances, one or more of the criteria from the SFR-DC or MHTGR-DC may be more applicable to a design or technology than the ARDC. Because the EM² is a fast reactor as well as a gas-cooled reactor, it has design characteristics that are addressed by criteria in the ARDC, SFR-DC, and MHTGR-DC. GA has worked on adapting LWR GDC into non-LWR PDC since the 1980s including the MHTGR design submitted to the NRC, the New Production Reactor (NPR) designed for DOE, and the conceptual design for the Next Generation Nuclear Plant (NGNP).

2.3 GA Position on Adaptation of Non-LWR Criteria to EM²

Most of the damage and failure criteria identified in the SRP still apply to the EM² fuel. However, material specific criteria need to be reconsidered and revised. For example, SiC does not go through a melting process, but it dissociates at a very high temperature. Stress limits and safety factors of the ASME metal tube may not be directly applicable to the ceramic tube. As mentioned above, hydriding, oxidation, and ballooning are unlikely for the SiC cladding when compared with zircaloy and these characteristics will be verified during qualification testing.

Regarding Regulatory Guide 1.232, GA is proposing EM²-DC 10, a modified version of ARDC 10, in which "coolant" is replaced with "heat removal" because helium coolant inventory control for normal operation and AOOs is not necessary to meet SAFDLs, due to the reactor system design. Inventory control is provided in EM² but it is not a necessary safety system to meet SAFDLs due to the use of helium as a single phase coolant so that cooling remains effective even at reduced pressure.

GDC 35 is deleted based on similar arguments applied to the MHTGR-DC. Maintaining the helium coolant inventory is not necessary to maintain acceptable core cooling under accident conditions. Postulated accident heat removal is accomplished by the passive heat removal system. EM^2-DC 34 incorporates the accident residual heat removal requirements contained in GDC 35.

The two proposed EM^2 design criteria are as follows:

EM^2-DC 10 – Reactor design. The reactor core and associated heat removal, control, and protection systems shall be designed with appropriate margin to assure that specified acceptable fuel design limits are not exceeded during any condition of normal operation, including the effects of anticipated operational occurrences.

EM^2-DC 34 – Passive residual heat removal. A passive system to remove residual heat shall be provided. For normal operations and anticipated operational occurrences, the system safety function shall be to transfer fission product decay heat and other residual heat from the reactor core to an ultimate heat sink at a rate such that specified acceptable fuel design limits and the design conditions of the primary coolant pressure boundary are not exceeded. During postulated accidents, the system safety function shall provide effective core cooling.

3 DESCRIPTION OF EM^2 SYSTEM

3.1 EM^2 Plant and Major Components

The conceptual EM^2 plant consists of four reactor modules for a total electrical output of 1 GWe. The overall site covers ~9 hectares as shown in Figure 2. The reactor building with containment structure is located below grade. The maintenance hall that serves all four reactors is at grade level and is covered by an integral shield designed to protect against aircraft crashes and other external threats. Each reactor module is independent, consisting of a complete power train from reactor to heat rejection so the modules can be built sequentially and operated independently. The reactor building is divided into two sets of two modules mounted on seismic isolation platforms and separated by waste handling, electrical distribution facilities, and access entry. The lower portion of the reactor chamber is enclosed in a concrete shield structure to enable access to the direct reactor auxiliary cooling system (DRACS) (upper reactor chamber) and power conversion unit (PCU) in a separate containment chamber.

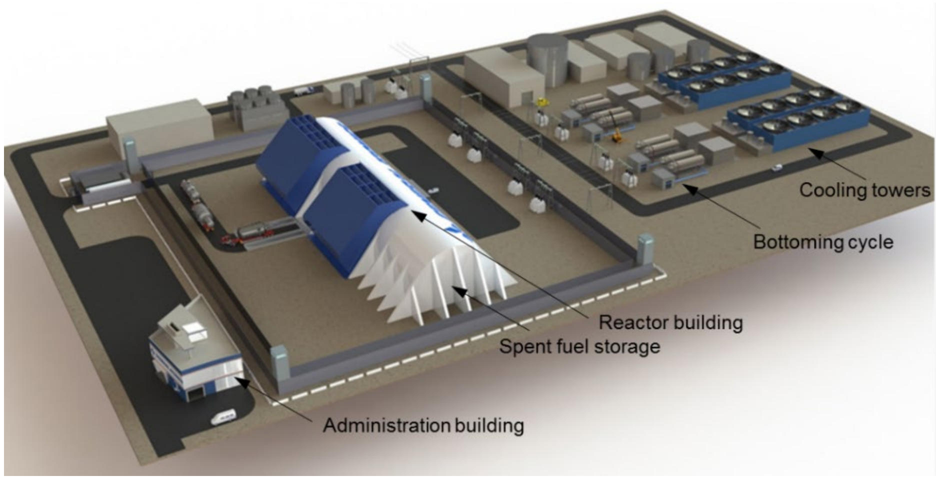

Figure 2 EM2 plant layout on 9 hectares of land

The primary coolant system (PCS) is enclosed within a sealed containment consisting of two chambers connected by a duct. The PCS includes the reactor system and PCU whose respective vessels are connected by a concentric connecting vessel. Figure 3 shows the flow path of the primary coolant during normal operation. Hot helium from the core at 850°C flows at 320 kg/s to the PCU through the inner hot duct. It expands through the turbine to the recuperator and then to the precooler, which is the cold sink of the thermodynamic cycle. The compressor increases the helium pressure from 6 to 13 MPa and returns it to the cold side of the recuperator. The helium exits the recuperator at 550°C and flows annularly around the recuperator to the annulus between the hot duct and the connecting vessel. The helium exits the connecting vessel and flows around and down through the core barrel outer annulus to the lower plenum below the core.

The reactor vessel is also connected to two 100%-redundant DRACS systems (only one is shown in Fig. 3). Natural circulation flow paths are provided by vertical concentric pipes to helium-to-water heat exchangers. The maintenance circulators, which are normally valved off, are used for low-pressure maintenance conditions. The PCS includes a helium purification system (HPS) and inventory control system. The HPS also operates in conjunction with the fission product collection system (FPCS) to minimize the radioactivity in the primary system.

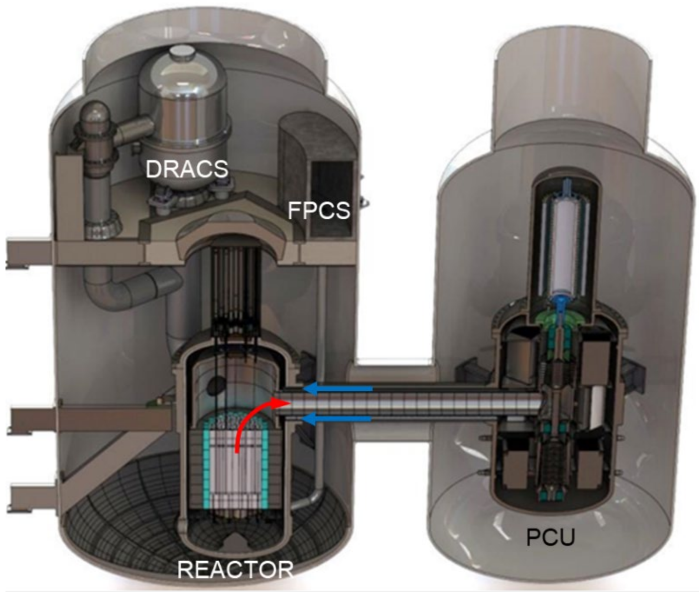

Figure 3 EM² primary heat transport system enclosed in two-chamber sealed containment

The EM² power conversion uses a combined cycle with a direct Brayton cycle and an organic Rankine cycle (ORC) using waste heat from the precooler in a bottoming cycle to achieve high net plant efficiency. The helium Brayton cycle is located in the PCU vessel shown in Figure 4. The ORC is located outside the reactor building near the cooling towers (see Figure 2). The turbo-compressor (T/C) and generator are mounted on an in-line vertical shaft suspended by active magnetic bearings. The T/C is mounted on a stiff cartridge frame that enables it to be removed and reinstalled as needed. The cycle incorporates two heat exchangers: a recuperator and a precooler. The recuperator is helium-to-helium in a plate-fin configuration. The precooler is helium-to-water in a diffusion-bonded configuration.

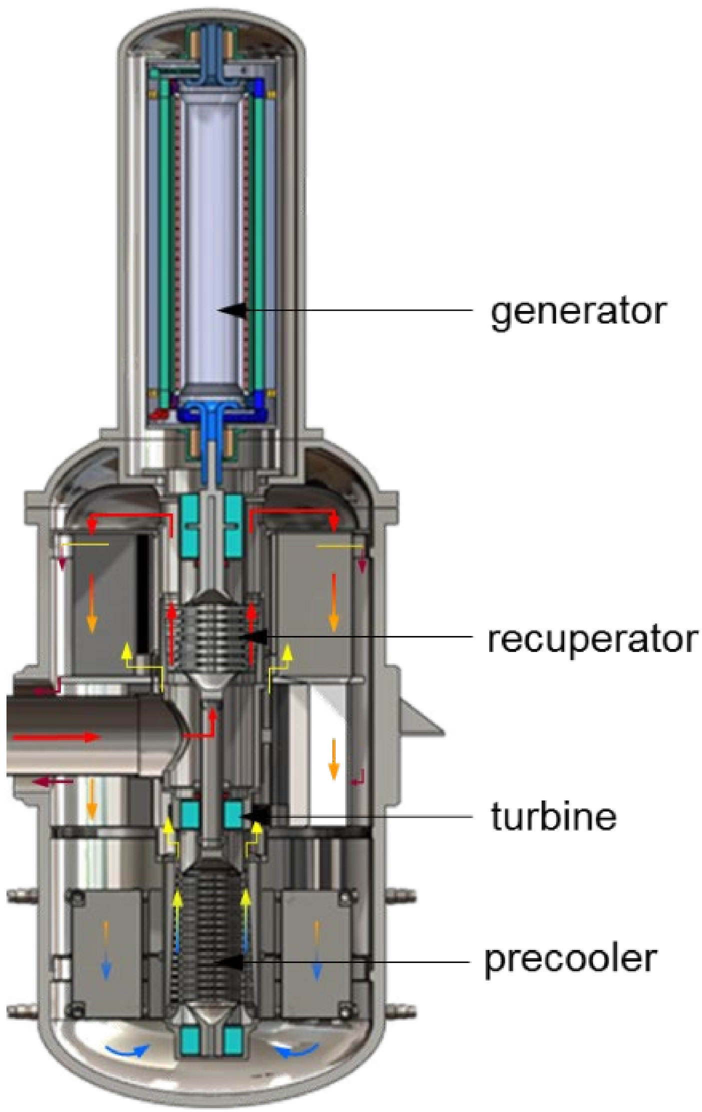

Figure 4 EM² PCU components and Brayton cycle helium flow

3.2 EM² Fuel System

The reactor core consists of 85 hexagonal fuel assemblies: 55 standard assemblies, 18 control assemblies, and 12 shutdown assemblies as shown in Figure 5. The standard fuel assembly has 91 fuel rods made of UC fuel pellets with a SiGA (SiC composite) cladding. The control and shutdown assemblies have 84 fuel rods. In order to achieve high fuel utilization, the EM² core utilizes the convert-and-burn concept in which the core is divided into three sections: fissile, fertile, and reflector. The fissile section contains low-enriched uranium (LEU) at an average ^{235}U enrichment of 14.5 wt% to sustain the chain reaction and provide excess neutrons to convert depleted uranium (DU) from fertile to fissile material. The average enrichment of the total active core (fissile and fertile sections) is 7.7 wt%. The reflector consists of an inner section of Zr_3Si_2 blocks and an outer section of graphite blocks. Table 4 summarizes the design parameters the EM² core.

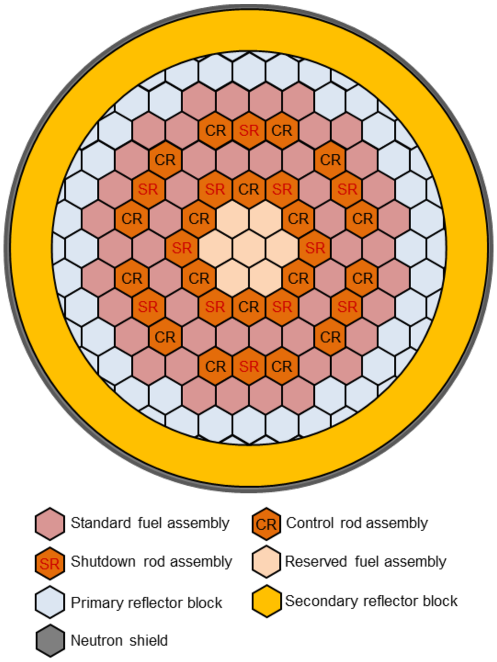

Figure 5 Configuration of EM² reactor core

Table 4 EM² core characteristics

Reactor power	500 MWth
Fuel material	Uranium carbide
Cladding/structural material	SiC composite
Coolant	Helium
Cycle length	32 years
Fuel loading	
Fissile fuel	21.3 tonnes
Fissile enrichment	14.5 wt%
(average)	19.8 tonnes
Fertile fuel	0.35 wt%
Fertile enrichment	7.7 wt%
Core average enrichment	
Fuel Conditions	300 GWD/t
Burnup, maximum	350 dpa
Cladding damage	9.5×10^{23} n/cm²
Neutron fluence, > 0.1	
MeV	13.3 MPa
Primary System	320 kg/s
Coolant pressure	550°C
Core flow rate	850°C
Core inlet temperature	
Core outlet temperature	

The basic building block of the EM² fuel system is the hexagonal fuel assembly. Three assemblies are joined into a tri-bundle as shown in Figure 6 for handling. The tri-bundle is located between separate upper and lower reflector blocks. It has a bottom alignment grid, an upper manifold assembly, and one intermediate spacer grid. The fuel is contained in cylindrical cladding tubes arranged in a triangular pitch. The specifications for the EM² fuel rod are presented in Table 5. Due to the high operating temperatures and long fuel cycle, all tri-bundle structural components and cladding are made of SiC composite. The fuel rod is 21 mm in diameter.

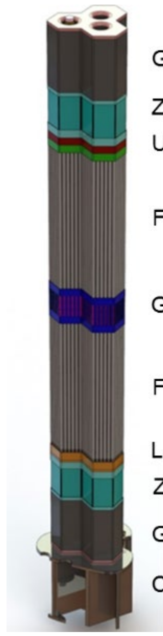

Figure 6 EM^2 tri-bundle fuel assembly

Table 5 Summary of EM^2 fuel specifications

Parameter	Value
Pellet material	UC_{1+x}
Pellet outer diameter	1.9 cm
Pellet inner diameter	0.5 cm
Pellet porosity (smeared)	25.3%
Element outer diameter	2.11 cm
Clad thickness	0.95 mm
where x is a small fraction much less than 1	

The fuel is in the form of UC annular pellets. The UC fuel meets the high uranium loading requirement, has a very high thermal conductivity, and is compatible with the SiC composite cladding. The UC is fabricated through a sol-gel process that produces uranyl nitrate spherical kernels containing carbon. After drying and calcining, the kernels are then heated and sintered to convert them to UC at ~200 mu diameter. The kernels are packed and sintered into annular pellets with a specified interstitial and internal porosity. The interstitial porosity allows for faster transport of volatile fission products, which reduces fuel swelling. Figure 7 shows UC kernels and pellets fabricated at GA. Fuel fabrication has successfully produced fuel pellets with grain size less than 10 m and 25% porosity.

The fabrication process of SiC composite starts with the braiding of SiC fiber into a woven cylindrical tube with a fiber volume fraction between 30% and 40%. A pyrolytic carbon interface layer around the fiber is formed by the decomposition of methane diluted in argon, while the SiC matrix is deposited from methyltrichorosilane. Deposition is carried out under vacuum and at temperatures greater than 900°C. A GA-proprietary □-SiC hermetic joining method is also used for end-plug sealing. These fabrication techniques are being extended to construction of large and complex SiC structures within the core.

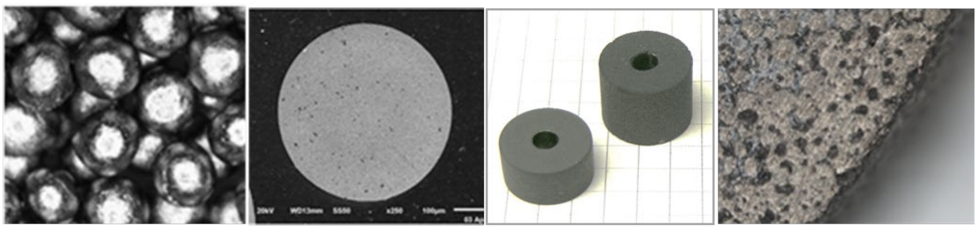

UC kernel via sol-gel | 200 μm diameter high density kernel | Annular pellet via hot pressing | Porous UC pellet

Figure 7 GA-fabricated bulk kernels and pellets with magnified cross-sections

3.3 EM² Safety Features

The selection of core materials is crucial in achieving a long-burn core with inherent and passive safety features. The carbide fuel is used to increase fuel loading to increase core lifetime and thermal inertia. A large core thermal inertia is provided by the ~41 tonne heavy metal loading. For a sodium fast reactor with similar power rating, the heavy metal loading is approximately 3 tonnes. The SiC composite cladding and core structures are used to survive high-temperature operation and high neutron damage. Due to high thermal conductivity of UC (~20 W/m-C), the peak fuel temperature during normal operation is kept below 1500ºC (See Sec. 6.2). The cladding temperature during normal operation is also in the range that keeps radiation-induced swelling of the cladding very low. Additional ceramic materials are used in the control and shutdown rods, reflector, upper plenum thermal barrier, internal vessel insulation cover plates and hot duct assembly to withstand high temperature operation.

The FPCS removes fission gases from the fuel and is located in the reactor containment. The FPCS maintains the pressure in the fuel rods slightly lower than the primary system pressure. The collection manifolds are routed from the fuel assemblies through the reactor vessel within a doubly contained pipe to the high-temperature absorber (HTA) of fission gases above the reactor as shown in Figure 8.

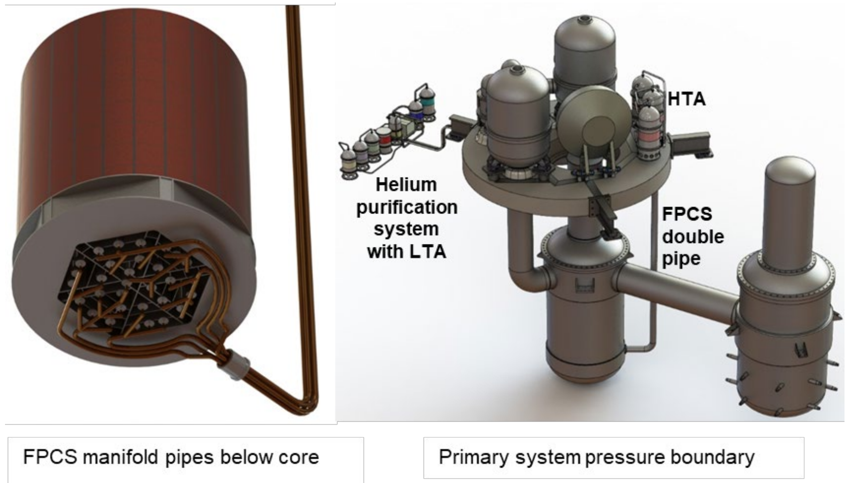

Figure 8 Routing of FPCS collection lines to HTA

The HPS maintains the coolant at low oxidant levels, i.e. < 0.35 parts per million by volume (ppmv). The SiC composite cladding is relatively inert to oxidation. In the event of a small cladding breach, the fuel would slowly oxidize. Therefore, oxidant levels in the primary coolant are kept low. This low oxidant level assures that even if the breach lasts the life of the core, the oxidation would not cause further cladding damage.

EM^2 has three systems for core afterheat removal to protect the fuel system – two are active and one is passive. (1) The normal method of shutdown core cooling is the PCU, which remains operational following reactor trip. Core afterheat is sufficient to drive the turbo-compressor for about 20 minutes after shutdown at which time the generator is converted to the motor mode to maintain primary system flow. Heat is rejected through the precooler to the cooling tower. (2) If the PCU is not available but either offsite on onsite electrical power is available, either one or both of the DRACS systems and be operated in the active mode supplying forced convection cooling. (3) If the DRACS circulators fail to operate, core flow continues without interruption by reverting to natural circulation of primary coolant helium to the DRACS. When forced helium flow from the PCU is terminated, the by-pass prevention valve (BPV) is passively opened in the DRACS loop allowing natural circulation heat exchange in the loop. The DRACS layout in Figure 9 shows how heat is transferred from the circulating helium to a closed intermediate water loop and to the cooling tower for heat rejection. The passive capability of DRACS for heat removal during all accident conditions assures EM^2 passive safety.

Heat rejection through the redundant water and air loops of DRACS is completely passive. It requires no active actuation, electric power or operator action to fulfill its passive safety function. The intermediate loop water flow from the DRACS helium-to-water heat exchanger is driven by natural circulation and heat is rejected at the elevated water-to-air heat exchanger (WTA-HX). The air flow is driven by the differential head provided by the cooling tower. A small amount of leakage through the BPV occurs during normal operation so that the water cooling loops and air cooling loops are always in a flowing condition so that core heat removal is not interrupted. The

DRACS water loop also provides heat rejection for the containment passive cooling system to mitigate direct containment heating. The freestanding steel containment has water-cooling channels on the outside to maintain the wall temperature at an acceptable level if the normal containment heat removal system is not operational. The containment and spent fuel storage facility are below-grade and the integrated aircraft crash protection structure that forms the maintenance hall roof provides additional protection to the containment and fuel storage. The primary coolant system, containment and reactor auxiliary building are seismically isolated to reduce fragility and cost of SSCs within those buildings.

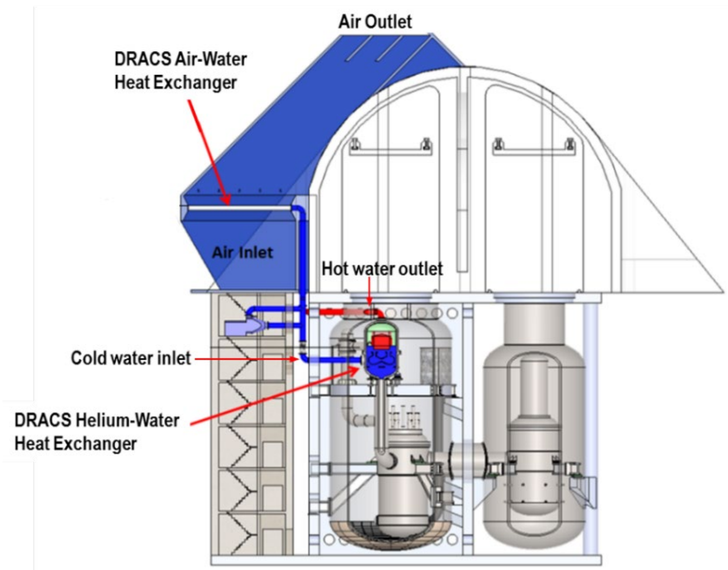

Figure 9 Passive DRACS heat exchangers and water loops

4 FUEL DESIGN BASES AND CRITERIA

Fuel element should maintain its structural integrity during the normal operation and anticipated over-power transients. Therefore, the fuel element is designed to comply with the nuclear, thermal, mechanical, and chemical requirements of the reactor system without fuel failure. This section describes design bases and criteria of the EM² fuel.

4.1 Thermal Design Bases and Criteria

4.1.1 Fuel Temperature

The peak fuel temperature shall be kept below the melting point during the steady-state operation and AOOs. The melting temperature of un-irradiated UC fuel is 2530°C and decreases by ~6°C per 10 MWd/kgU. The burnup-dependence of melting temperature was obtained from the melting temperature of mixed carbide fuel [1-7], shown in Figure 10, and plutonium buildup from uranium transmutation. It is a traditional practice to assume that fuel failure will occur if fuel centerline melting takes place [8]. Therefore, the design analysis is performed for the maximum power density anywhere in the core, including all hot spots and hot channel factors, and should account for the effect of burnup and composition on the melting point.

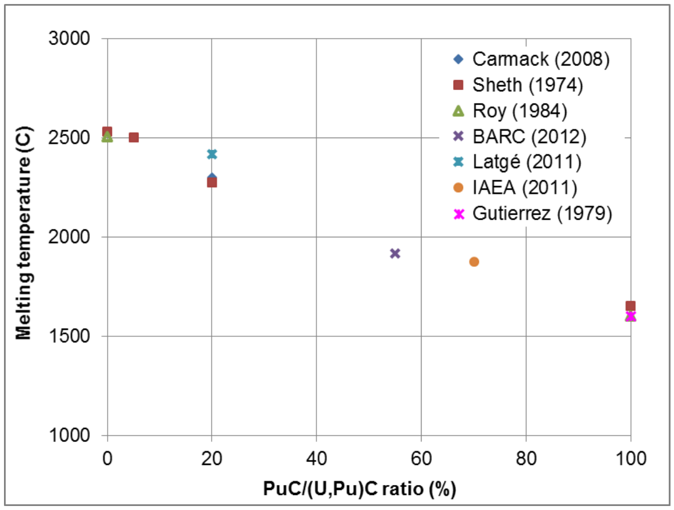

Figure 10 Melting temperature of carbide fuel as a function of plutonium content [1-7]

4.1.2 Cladding Temperature

The SiC composite cladding will be bombarded by high-energy neutrons (1 – 2 MeV) and damaged through displacement of atoms and helium/hydrogen formation. The cladding temperature shall be kept between 800 K and 1400 K to promote annealing of neutron irradiation-induced damage and achieve a long-life of cladding material. In the temperature range for point defect swelling (696–1546 K) where vacancies of both Si and C have no or very limited mobility, the matrix defects build up until pseudo-equilibrium is reached [9]. Above the critical amorphization temperature, the swelling decreases with increasing irradiation temperature and reaches a minimum at ~1300 K as shown in Figure 11. This reduced swelling is primarily attributed to the enhanced recombination of cascade-produced Frenkel defects at higher temperatures, which is commonly referred to as in-situ annealing. For temperatures exceeding ~1300 K, the presence of both Frank loops and tiny voids are observed, indicating limited mobility of vacancies [10]. The neutron damage of the cladding is dominated by displacement of atoms from the lattice rather than helium/hydrogen formation.

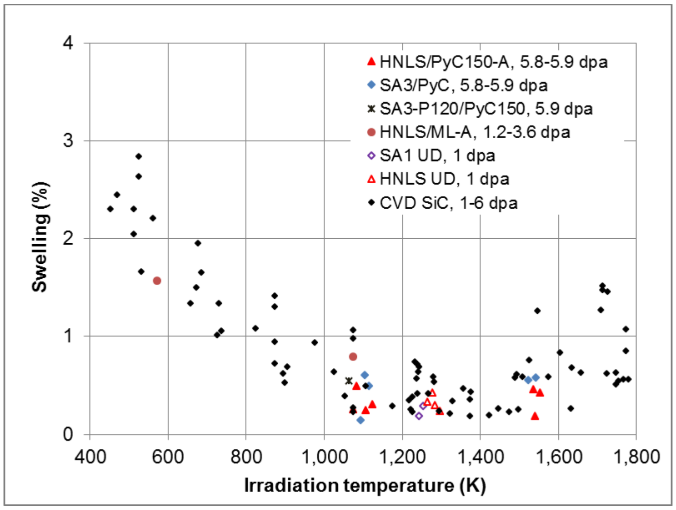

Figure 11 Radiation induced swelling in bulk SiC as a function of irradiation temperature [9].

SiC retains full strength at long-term duration at 1473 K (1200°C) and 75% of its strength at 1723 K (1450°C). SiC does not go through a melt phase, and instead decomposes at 2818 K. For β-SiC decomposition appears to be a function of temperature and rate of decomposition (k_d) in static argon has been reported as follows [11]

$$k_d\left(\frac{\mu g}{m^2 s}\right) = 2.95 \times 10^{13}\, exp\left(-\frac{56{,}252}{T}\right) \quad (4\text{-}1)$$

where T is in Kelvin.

4.2 Mechanical Design Bases and Criteria

4.2.1 Cladding Stress Limit

The general guidelines for stress categories and strength limits are defined in American Society of Mechanical Engineers (ASME) Code Section III [12]. Under normal and abnormal operating conditions (Condition I and II), the maximum primary tensile stress in the cladding shall not exceed one-third of the specified minimum tensile strength or two-thirds of the minimum un-irradiated yield strength of the cladding material at the applicable temperature. The corresponding limit under emergency conditions (Condition III and IV) is the material yield strength. The use of the un-irradiated material yield strength as the basis for allowable stress is conservative because the tensile strength of SiC composite increases with irradiation as shown in Figure 12 for SiC fiber (Hi-Nicalon Type-S) [13]. It should be noted, however, that the use of safety factors such as one-third and two-thirds would require further review by the NRC when applied to ceramic cladding materials.

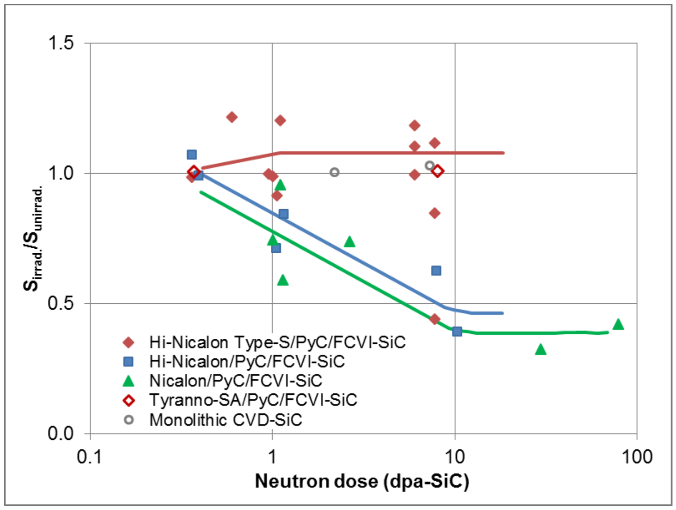

Figure 12 Irradiation stability (irradiated-to-non-irradiated ultimate strength ratio) of different SiC_f/SiC composite types [13].

4.2.2 Cladding Strain Limit

During normal operation or following any single upset or emergency event, the net unrecoverable parallel strain of Zircaloy cladding is typically limited to 1% during the fuel lifetime considering cladding creep and fuel-cladding interaction effects. This strain limit needs to be determined based on maximum strain of the material at its point of plastic instability. An analytical failure curve may be used during the early design stage and should incorporate anisotropy, stress states and strain rates. Then the design limit is determined conservatively by selecting adverse initial conditions, material behavior, and operating history. Instability strain is a property of metals that occurs due to necking at large deformation. This strain is used to trigger the ballooning, which is not observed to occur with SiC composite cladding.

For multi-layer SiC composite cladding, impermeability is provided by a monolithic SiC (mSiC) layer, while the structural integrity is maintained by the composite layer. If the composite layer exceeds its ultimate tensile stress (UTS), it is considered failed even if the mSiC is below its fracture stress. The measured helium leak rate of fully sealed SiC composite rodlets is 3.0×10^{-8} atm·mL/s by Deck et al. [14]. The SiC composite has inherent porosity and is considered to be permeable. As such, the SiC composite was engineered to allow the stresses in the composite layer to exceed the proportional limit stress (PLS), but remain below the UTS, and position mSiC layers to minimize their exposure to tensile stresses.

Stone et al. [15] constructed a stress-strain curve as shown in Figure 13 through a statistical approach using measured data from open literature [9] and measurements of tubular materials [16]. Because the mSiC layer is not structurally significant, the curve is primarily the characteristics of the composite layer. The best estimate of hoop strain limit was determined to be 0.62% based on the composite layer UTS, beyond which the impermeability of the SiC composite would be exacerbated. When the PLS is exceeded, the composite layer undergoes matrix cracking. However, as the internal pressure of the EM^2 fuel is kept lower than the system pressure, cladding failure and loss of hermeticity even at UTS does not have an immediate impact of safe operation of EM^2.

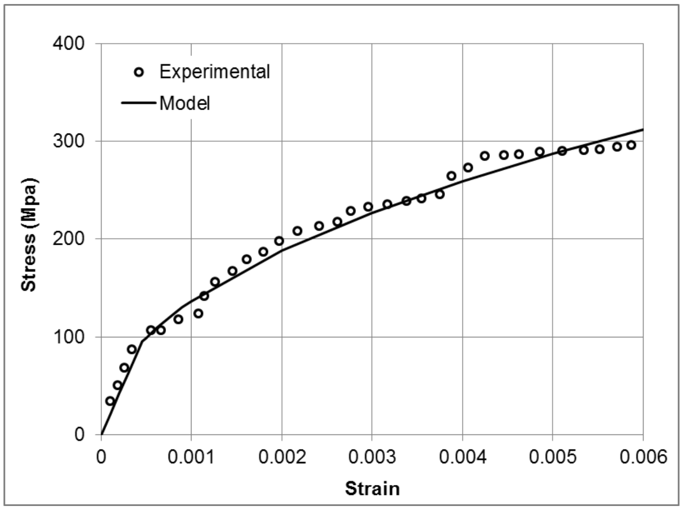

Figure 13 Components and distribution types for simplified stress-strain model of SiGA cladding using GA analysis and data [15].

4.2.3 Fuel Element Fatigue

The cladding creep and cumulative fatigue are considered together when determining end-of-life (EOL) cladding strain for metals. Cumulative cyclic strain ratio, defined as the number of cycles in a given effective strain range over the permitted number at that range, is limited to 0.8 for Zircaloy cladding, as an example. No detailed fatigue studies have been performed on SiC composite in tubular geometry. In general, specimens subject to cyclic stresses up to 80% of their UTS for 10^7 cycles at room temperature have the same UTS as the original specimens. At a higher temperature above 1273 K, however, effects from oxidation, fiber creep, and changes in the fiber/interphase sliding resistance begin to play a role. At these temperatures, fatigue-related decrease in UTS was observed after 10^4 cycles by Zhu et al. [17], which is tentatively used as the permitted number of cycles. Over a 30 year fuel lifetime, the tentative 10^4 cycle limit is equivalent to just over 1 cycle per day.

4.2.4 Element Internal Pressure

Fuel element internal pressure increases as fission gases are released from the fuel. The EM^2 fuel element is designed to collect fission gases through a continuous flow path to the FPCS and the internal pressure is maintained lower than the system pressure. The maximum fuel element internal pressure shall satisfy the following criteria:

- The primary stress of the cladding resulting from differential pressure will not exceed the PLS.
- The internal pressure will not cause the cladding to creep outward from the fuel pellet surface at the peak power density position during normal operation.

However, these criteria do not necessarily limit fuel element internal pressure less than the primary coolant pressure (13 MPa) and the occurrence of positive differential pressures would not adversely affect normal operation if appropriate criteria for the cladding stress, strain, and strain rate are satisfied.

4.3 Chemical Design Bases and Criteria

Chemical reaction between fission products and SiC composite cladding should be prevented. Some fission products are prone to attack SiC, form a carbon compound and deteriorate cladding strength. The SiC layer thinning (μm) is approximately $0.18\sqrt{t}$, where t is in hours, for UC_2 fuel heated at 1784 K as an example [18], which is ~17 μm loss after one year. Maximum EM^2 cladding temperature is less than 1400 K as presented in Section 6.2 in addition to having a cladding thickness of 0.95 mm. The EM^2 fuel was designed as hyper-stoichiometric UC_{1+x} to minimize the SiC loss due to fission products, where x is a small fraction much less than 1.

4.4 Summary of Design Bases and Criteria

The design features of the EM^2 core include high temperature operation and long-burn fuel cycle. Therefore, it is a prerequisite to choose materials that are inherently resistant to temperature and neutron irradiation with high core thermal inertia. UC has been selected for its high thermal conductivity, high melting point, high density, and high uranium content. SiC has exceptionally strong radiation resistance as well as high melting point. The operating temperature range of the cladding is also favorable to keep the swelling rate low owing to in-situ annealing effect.

The current thermal-mechanical design of the cladding tentatively follows ASME Code Section III (rules for construction of nuclear facility components) stress limits with the same safety factors. The strain limit has been estimated based on the composite UTS to maintain hermeticity of the cladding. It should be noted that the internal pressure of the fuel rod is kept lower than the system pressure by design. Micro-cracking of the cladding could be allowable from the viewpoint of cladding hermeticity because the cladding internal pressure is kept below the primary system pressure.

The EM^2 core does not require refueling until the end of fuel life by design. Therefore, cyclic stresses are expected to be minimal due to operation scheme. The oxidation of the SiC composite cladding are significantly lower when compared with the conventional zircaloy cladding with water coolant. Nonetheless, quantitative analyses are recommended for the cumulative fatigue and chemical reactions.

5 ANALYSIS METHODS AND MATERIAL PROPERTIES

Thermal-mechanical design and analysis of the fuel element involves thermal analysis of individual rods followed by calculation of the stress and strain that result from the differential thermal expansion between the cladding and the fuel pellet. Stress is caused by the non-linear temperature distribution within the fuel pellet. The local power distribution, helium flow and material properties determine the axial and radial temperature distributions. The fuel element is treated as a linear elastic solid at the operating temperature. Typically, these thermal and mechanical behaviors are analyzed by a finite element method (FEM).

5.1 Thermal-Mechanical Analysis Methods

In this study, the FEM codes, i.e. FRAPCON-4.0 [1] and FRAPTRAN-2.0 [2], are used to numerically discretize the fuel rod geometry using constituent material properties models and to solve the stiffness equation. The FRAPCON-4.0 and FRAPTRAN-2.0 codes were modified for UC fuel and SiGA cladding properties and models (See Sec. 5.2), i.e. FRAPCON-4.0GA and FRAPTRAN-2.0GA, respectively. As the physical parameters are inter-related, the solution is obtained by successively substituting physical parameters such as stress, strain, temperature, etc., i.e. the stiffness equation is iteratively solved. There are several simplifications or approximations applied to the model as follows:

- Heat conduction in the axial direction is negligible relative to radial heat conduction due to the large length-to-diameter ratio and is ignored, as is common in nuclear fuel thermal analysis.
- Heat conduction in the azimuthal direction is ignored, i.e. an axisymmetric model.
- Constant boundary conditions are maintained during each time step.
- Steady-state heat flow is assumed during each time step.
- The fuel rod is a right circular cylinder surrounded by coolant.
- Deformation is calculated as a linear sum of multiple strains, which is acceptable when the magnitude of strain is small.

The FRAPCON-4.0 code has been extensively validated against experimental data for LWR fuel, including 45 test rods for EOL power ramping and 92 steady-state cases of UO_2, mixed oxide, and urania-gadolinia fuels. Overall, the code gives reasonable predictions of fuel centerline temperature with standard error of less than 5%. The cladding hoop strain is slightly over-predicted by 0.1% up to 62 GWd/t [3]. However, there are several issues that should be considered when this code is used for non-conventional fuel and cladding materials as follows:

- The hard pellet model may not be valid when a hard cladding material like SiC composite is used. The thermal and mechanical strains of the pellet should be estimated in conjunction with the cladding deformation.
- For high temperature and high burnup carbide fuel, a restrained swelling model is required.

- The fuel pellet is either a solid or an annular cylinder. Particle fuel model is not available.
- A single material is used for the cladding. The SiC composite is a multi-layered design and a full model is under development, so at present the structure of the cladding is approximated by a single layer of composite.

5.2 Material Properties

The UC material properties have been collected from open literature and additional data will be collected. For consistency in data use, data from Preusser's publication [4] is preferentially used. Regarding SiGA cladding, most of material properties are architecture and manufacturer dependent. GA has published a material property manual for SiGA [5], including thermal conductivity, mechanical properties, corrosion rates, and others. Due to the manufacturer dependence, preference is given to measurements performed on GA's accident tolerant fuel (ATF) design using SiGA cladding. When GA properties are not available, the most relevant literature data is used.

5.2.1 Fuel Material Properties

Melting temperature - The melting point is 2803 K and 2780 K by Sheth and Leibowitz [6] and Roy and Ganguly [7] for UC. The burnup-dependence of the melting point was estimated based on uranium-plutonium ratio as follows [10-16]:

$$T_{melt}\ (K) = 2787.0 - 0.621\ B \tag{5-1}$$

where *B* is fuel burnup in GWd/t.

Specific heat - Preusser and De Coninck et al. [8] processed specific heat data from the early measurements. Preusser's equation is used as follows:

$$C_p\ (J/kg\text{-}K) = 217.8 + 0.03852\ T \tag{5-2}$$

where *T* is in Kelvin.

Thermal conductivity - The thermal conductivity is a critical property when calculating the peak fuel temperature, but includes multiple influencing factors such as temperature, porosity, alloy composition, burnup, fission gas content, etc. As such, many formulations have been recommended by Preusser, De Coninck et al., Bates [9], Wheeler [10], and Russell [11]. Preusser's formulation is used as follows:

$$\begin{aligned} \lambda\ (W/m\text{-}K) &= 20 \text{ for } T < 773.15\ K \\ &= 18.9949 + 0.0013\ T \text{ for } T \geq 773.15\ K \end{aligned} \tag{5-3}$$

The effect of porosity was considered by Steiner [12] as follows:

$$\lambda_p = \lambda \frac{1-P}{1+P} \quad (5\text{-}4)$$

where λ_p is the thermal conductivity with a porosity *P*.

The thermal conductivity of carbide fuel is affected by the combined effects of carbon concentration and volume concentration of second phase dicarbide and sesquicarbide, concentration of oxygen and nitrogen, porosity, and presence of sintering aid. Thermal conductivity decreases when the oxygen content increases due to a decrease in both the lattice and electronic components, with the larger decreases at lower temperatures due primarily to changes in lattice conduction. The effect of oxygen can be approximated by Bates' calculation results [13] of uranium oxycarbide thermal conductivities. The effect of sesquicarbide can be considered by interpolating the thermal conductivities of UC and U_2C_3 provided by Lewis and Kerrisk [14].

Emissivity - The emissivity was measured by De Coninck et al. and Corradetti et al. [15]. For stoichiometric or slightly hyper-stoichiometric UC, De Coninck et al. provided the mean value of the spectral emissivity between 1375 K and 2273 K as follows:

$$\epsilon = 0.57 - 8.5 \times 10^{-5}\, T \quad (5\text{-}5)$$

where *T* is in Kelvin.

Coefficient of thermal expansion - The coefficient of thermal expansion is influenced by temperature, alloy composition, stoichiometry, manufacturing process (structure, impurities), etc. Typically, the thermal expansion of stoichiometric carbide increases with temperature as formulated by Preusser, Stahl et al. [16], Nickerson and Kastenberg [17] and Matzke [18]. Preusser's equation is used as follows:

$$\alpha\ (1/K) = 9.7504\times10^{-6} + 1.17\times10^{-9}\, T \quad (5\text{-}6)$$

where *T* is in Kelvin.

Density - The fuel density of UC is 13.63 g/cm^3, of which the fraction of uranium is 12.97 g/cm3 and the carbon fraction is 4.8%. Assuming that the number of atoms is same for mono-UC and metal-poor UC_{1+x}, the estimated UC_{1+x} density is 13.04 g/cm3. The temperature dependency of UC density is provided in International Atomic Energy Agency (IAEA) publication [19] as follows:

$$\rho\ (g/cm^3) = 13.63\,(1 - 3.117\times10^{-5}\, T - 3.51\times10^{-9}\, T^2) \quad (5\text{-}7)$$

where *T* is in Kelvin. This correlation has been derived based on the measurement of linear expansion coefficient in the temperature range from 273 K to 3073 K.

Elastic modulus - The elastic modulus is influenced by temperature, porosity, stoichiometry, grain size, and alloy composition. Preusser, Nickerson and Kastenberg and Singh [20] formulated the UC elastic modulus as a function of temperature and porosity. Preusser's equation is as follows:

$$E\ (MPa) = 2.15{\times}10^{5}\ (1 - 2.3\ P) - [1 - 9.2{\times}10^{-5}\ (T - 298.15)] \tag{5-8}$$

where T is in Kelvin and P is porosity. The equation was experimentally established up to 1523 K and $P \leq 0.3$.

Poisson's ratio - The Poisson's ratio is directly related to the elastic modulus and the bulk modulus, and is dependent on the temperature and the structure of the working material. Padel and De Novion [21] formulated a porosity-dependent Poisson's ratio, which was measured in the same test as the elastic modulus, and is valid in the range from 5 to 27% porosity. Preusser used Padel and De Novion's formulation without temperature-dependency as follows:

$$\nu = 0.288 - 0.286\ P \tag{5-9}$$

where P is porosity.

Yield stress - The yield stress specifies the tension over which permanent inelastic deformation takes place. Preusser developed a formulation of UC yield stress for the URANUS code [22], considering experimental results quoted by Matthews [23], as follows:

$$\sigma_y\ (MPa) = 135.57 - 0.02943\ T \tag{5-10}$$

where T is in Kelvin.

Fracture stress - The fracture behavior of carbides is dependent on temperature. At low temperatures, it has a brittle behavior. At high temperatures, the breaking strength remains constant or decreases slightly with increasing temperature. The plastic deformation occurs before fracture, giving a higher breaking elongation, ductile behavior. The fracture stress is reported between 35 and 210 MPa for temperature range of 298 K and 1473 K, depending on manufacturing process and stoichiometry [23].

Swelling - The swelling is affected by temperature, burnup, stoichiometry, alloy composition, porosity, grain size, and neutron flux. It was measured by many authors [17, 24-30], but the individual measurements are not comparable as the sample fuels have different characteristics as well as the irradiation conditions and cladding material. The total swelling rate typically lies between 1.6 and 3.0% volume per percent of burnup. Free swelling rate is much higher up to 10.1% volume per percent burnup [27]. Preusser reported a total swelling rate, including the hot pressing effect for hard contact, as follows:

$$\Delta V/V = 0.4667 + 1.711\ f(P,pc)\ \text{for}\ T < 973.15\ K \tag{5-11}$$

$= 0.4667 + 1.711\, f(P,pc) + [(12.954 - 0.0281\, T + 1.52{\times}10^{-5}\, T^2)\, f(BU)\, f(P,pc)]$

for $T \geq 973.15$ *K*

The upper limit of $\Delta V/V$ was set 4.558%. The correction terms are as follows:

$$f(BU) = \left(\frac{BU}{BU_0} - a\right), f(BU) \geq 0 \tag{5-12}$$

$$f(P,pc) = \exp[-(P-0.04)]\, exp\left[-\left(\frac{pc}{pc_0}\cdot b\right)\right], (P-0.04) \geq 0 \tag{5-13}$$

where $\Delta V/V$ is in volume % per 10 MWd/kg, T is in Kelvin, BU is burnup in MWd/kg, P is porosity, pc is contact pressure in MPa, BU_0 is 10 MWd/kg and pc_0 is 1 MPa. The recommended values for constant a and b are 0 to 5 and 0 to 1, respectively.

Fission gas release - Fission gas release (FGR) is a complicated process affected by various parameters such as temperature, burnup, porosity and grain size. It is also known that the manufacturing parameters such as density, stoichiometry, impurity and pore size distribution influence the gas release process. Historically, measurements have been made to investigate radial fission gas distribution in bubbles, pores and matrix. Analytic models have also been developed that decompose the fission gas release into multiple processes from the gas production to the release [31-34]. At the moment, both the experimental and analytic models are applied to UC fuel because the experimental data is sparse and analytic models based on microscopic data are not available. As such, the fission gas release from UC fuel is tentatively calculated using the fission gas release model of UO_2 fuel, i.e. FRAPFGR, but with a UC diffusion constant.

The values reported for the out-of-pile diffusion of ^{133}Xe in irradiated UC vary by more than 3 orders of magnitude [33]. For example, the result of an earlier experiment by Rough and Chubb [35] is very high (2.9×10^{-13} cm²/s at 1273 K), while an experiment by Shaked et al. [36] showed much lower (4.4×10^{-16} cm²/s at 1273 K) values possibly due to a large grain size (700 to 1000 μm). The choice of diffusion coefficient will depend on how it is used in the formulation of the fuel performance code. For the diffusion in the solid, the Shaked et al.'s model is used, as the effect of grain size is explicitly considered in the fuel performance code:

$$D\left(\frac{cm^2}{s}\right) = 1.7\times10^{-6}\, exp\left(-\frac{54{,}900}{RT}\right) \tag{5-14}$$

where T is in Kelvin and R is universal gas constant (1.987 cal/mol·K).

Relocation - The pellet fragments which result from cracking at the start-up stage expand thermally and do not fully retract relative to the adjoining pellet fragments at shutdown.

Consequently, the gap is narrowed as the fragment is ratcheted outward. This phenomenon is called relocation. There is no known relocation data for UC fuel, particularly for the EM² porous pellet design. Therefore, the UO_2 relocation model of FRAPCON code is tentatively used, which is a function of linear heat generation rate, burnup and shutdown cycles. The fuel-cladding gap size of the thermal and internal pressure calculations includes the fuel relocation, while the fuel-cladding gap size of the mechanical calculations allows for 50% of the relocation to be recovered.

Densification - For a porous sintered fuel, the pores are transported up the temperature gradient to the fuel center, resulting in irradiation-induced densification. Dienst [31] reported that carbide fuel of high porosity will increase in density as an exponential function of burnup with a maximum volume change of 3.4%. However, previous simulations of carbide fuels irradiated in JRR-2 and JMTR test reactors have shown that this value could be too high when the fuel density is in an intermediate range of 83% to 90% and therefore it was adjusted to 1.5% [37]. The maximum volume change of 1.5% is used.

5.2.2 Cladding Material Properties

Melting temperature - SiC does not go through a melt phase, and instead decomposes at 2818 K. For β-SiC decomposition appears to be a function of temperature and rate of decomposition in static argon has been reported as follows [38]:

$$k_d\left(\frac{\mu g}{m^2 s}\right) = 2.95 \times 10^{13}\, exp\left(-\frac{56{,}252}{T}\right) \tag{5-15}$$

where T is in Kelvin.

Specific heat - Specific heat is a function of temperature and relies on bulk material properties. The SiC composite specific heat capacity is similar to that of monolithic SiC measured by Katoh et al. [39]. As density is minimally affected by irradiation, changes in the specific heat of the SiC composite as a function of irradiation are considered negligible. GA has measured the heat capacity of its prototype cladding and obtained results similar to those in the literature for chemical vapor deposition (CVD) SiC. For modeling purposes, the equation can be mechanically represented as follows [38]:

$$C_p\left(\frac{J}{kgK}\right) = 925.65 + 0.3772\, T - 7.9259 \times 10^{-5}\, T^2 - 3.1946 \times 10^7 \left(\frac{1}{T^2}\right) \tag{5-16}$$

where T is in Kelvin.

Thermal conductivity - The thermal conductivity drops significantly after irradiation. Due to the magnitude of this drop it is important to appropriately understand this phenomenon based on unirradiated data. A correlation between irradiated and unirradiated data has been developed based on thermal resistivity, i.e. the inverse of thermal conductivity. The thermal resistivity of the irradiated specimen is sum of the unirradiated resistivity and the radiation defect resistivity [40]. The radiated defect resistivity is largely proportional to material swelling. Literature values for the proportional constants for SiC composite is 15.1 m·K/W and for monolithic SiC is 6.1 m·K/W [39, 41]. The thermal conductivities of un-irradiated and irradiated SiC composite are as follows [42]:

$$k_{un-irr}\left(\frac{W}{m \cdot K}\right) = 7.97 + 0.061\,T - 1.10 \times 10^{-4}T^2 + 7.35 \times 10^{-8}T^3 - 1.71 \times 10^{-11}T^4$$

$$\frac{1}{k_{irr}} = \frac{1}{k_{un-irr}} + R_{rd} \qquad (5\text{-}17)$$

$$R_{rd} = c \times S$$

where T is in Kelvin, R_{rd} is a defect thermal resistivity in m·K/W and S is irradiation-induced swelling in percent. The proportional constant c is as follow:

$c = 1.47872 \times exp(-0.002507\ T)$, for SiC composite, (5-18)
$c = 0.5103526 \times exp(-0.0025277\ T)$, for monolithic SiC.

Emissivity - Emissivity is a surface phenomenon and small changes in surface roughness and microstructure can alter measured emissivity greatly. Based on literature data an emissivity of 0.8 or 0.9 is recommended [43], depending upon whether a high emissivity or a low emissivity yields a conservative value for the analysis.

Coefficient of thermal expansion - Thermal expansion is temperature-dependent and starts out at about 3 part per million (ppm)/K at room temperature. Coefficient of thermal expansion (CTE) as a function of temperature for planar material is assumed to behave similar to tubes [39, 40]. The data also shows CTE does not appear to be affected by irradiation, up to the irradiation temperature. At temperatures above the irradiation temperature CTE drops due to recovery of swelling by defect recovery. The CTE equation is given as follows [42]:

$$\alpha\left(\frac{1}{K}\right) = 3.5347 \times 10^{-15}T^3 - 1.2370 \times 10^{-11}T^2 + 1.5339 \times 10^{-8}T - 0.7362 \times 10^{-6} \qquad (5\text{-}19)$$

where T is in Kelvin.

Density - While fully dense β-SiC has a theoretical density of 3.2 g/cm^3 [38, 40], in practice due to the inherent porosity of the chemical vapor infiltration (CVI) process, a SiC composite based material will never reach this density. Instead densities of 2.6 - 2.8 g/cm^3 are common from the CVI process. While irradiation does have a small effect on density due to irradiation induced dimensional swelling, this swelling is typically under 2% and from a density standpoint has a minimal effect. Density of cladding is 2.8 g/cm^3 as measured using X-ray Computed Tomography (XCT) and confirmed with Archimedes method [42].

Elastic modulus - Typical values for the axial direction have been measured in the 200 - 250 GPa range and for the hoop direction 160 - 250 GPa. These properties are dependent on fiber architecture and manufacturer. For SiGA cladding, an axial modulus of 171 GPa and a hoop modulus of 207 GPa have been measured [42]. Elastic modulus can be assumed to stay at its room temperature value up to 2073 K. Due to the relatively small change, as a simplifying assumption it is recommended that no change in elastic modulus occurs as function of irradiation. A general formulation can be written as follow:

$$E\ (GPa) = 207\ (1 - 10 \times S/3) \tag{5-20}$$

where S is volume swelling fraction. A constant value of 207 GPa is used.

Poisson's ratio - The Poisson's ratio is 0.13 and 0.12 for the axial and the hoop direction, respectively [42].

Yield stress - Once the stress reaches the matrix cracking stress, stress-strain curve starts to deviate from the linear relationship; this threshold stress level is typically called Proportional Limit Stress (PLS). Typical values for the PLS in the axial direction have been measured in 80 - 100 MPa and for the hoop direction 100 - 160 MPa. These properties are dependent on fiber architecture and manufacturer. For SiGA cladding, an axial PLS of 98 MPa has been measured with corresponding strain of 0.000586 [42]. Hoop PLS of 153 MPa has been measured with corresponding strain of 0.000593 [42]. PLS strength is unaffected by irradiation and room temperature properties are maintained up to 2073 K.

Fracture stress - In the inelastic region crack propagation in both the matrix and fiber takes place, although the interphase plays an important role in crack deflection. Eventually enough localized damage occurs that the material fractures on the macro scale and the ultimate tensile strength (UTS) is reached. The UTS for composite material varies greatly with architecture/manufacturer and is anisotropic. Typical values range from 230 - 270 MPa for axial UTS and 200 - 340 MPa for hoop UTS. Strains at failure tend to range from 0.6 - 0.85%. Weibull moduli of 7 - 12 are typically observed. For SiGA cladding, an axial UTS of 224 MPa has been measured with corresponding strain at failure of 0.005896 [42]. Hoop UTS of 346 MPa has been measured with corresponding strain at failure of 0.006183 [42]. A Weibull modulus in 12 - 14 range has been obtained. The strength is unaffected by irradiation and formulated from room temperature to 2073 K.

$$UTS\ (MPa) = 355.49 - 0.0423 \times T \tag{5-21}$$

where T in Kelvin.

Swelling - Irradiation swelling in SiC composite has been measured up to ~100 displacement per atom (dpa) at a variety of temperatures. Swelling increases with dose up to approximately 1 dpa, at which point swelling saturates and minimal further changes occur [39]. Almost identical swelling rates are observed for CVD SiC and SiC composite [40]. At lower temperatures greater irradiation induced swelling is observed. GA has confirmed similar swelling values for its SiC composite as observed in the literature for material irradiated at 1003 K and 4.5 dpa. Katoh et al.'s swelling rate is used as follows:

$$\dot{S}\left(\frac{1}{dpa}\right) = K_s(T)\gamma^{-1/3}\, exp\left(-\frac{\gamma}{\gamma_{sc}}\right) \tag{5-22}$$

$$K_s\ (T) = 0.10612 - 1.5904\times10^{-4}\ T + 6.0631\times10^{-8}\ T^2$$

$$\gamma_{sc}\ (dpa) = 0.51801 - 2.7651\times10^{-3}T + 9.4807\times10^{-6}\ T^2 - 1.3095\times10^{-8}\ T^3 + 6.7221\times10^{-12}\ T^4$$

for 473 K < T < 1073 K

where the swelling rate is in $\Delta V/V$ per dpa.

Creep - Creep coefficient for CVD SiC have been experimentally measured as a function of dose and temperature for a number of different manufacturers [39, 44-46]. The instantaneous creep coefficient appears to decrease rapidly with increasing fluence in the transient regime up to the saturation point of 1 dpa, at which point it stabilizes at 1×10^{-7} per dpa·MPa or becomes negligible. Thus creep coefficient can be defined as a combination of swelling coupling + secondary creep. In the transition regime, swelling coupling dominates and is a function of applied stress and swelling rate. Secondary creep has a constant creep coefficient of 1×10^{-7} (dpa·MPa)$^{-1}$. The instantaneous strain rates are shown in Figure 14 for neutron flux of 1.0×10^{14} n/cm^2-s at 1073 K and 100 MPa as an example using Koyanagi et al.'s plot [46]. For comparison, perturbed strain rates are also plotted for 5.0×10^{14} n/cm^2-s, 1800 K and 50 MPa. As Koyanagi et al. didn't provide the temperature dependence of the creep rate, the effect of temperature on the creep rate was approximated by using an exponential function of temperature.

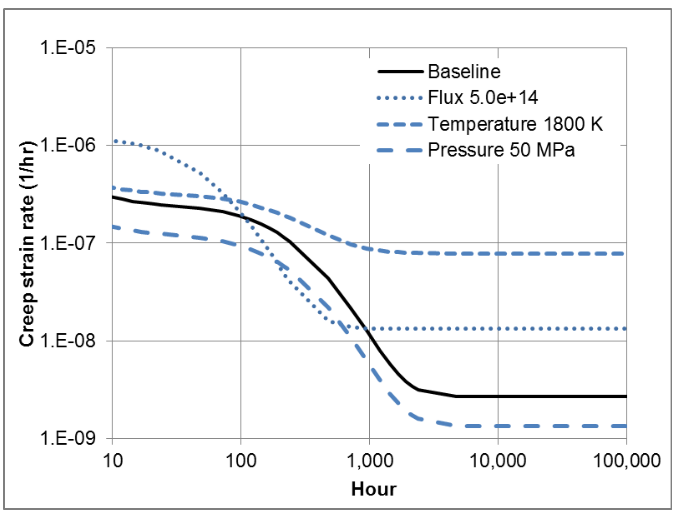

Figure 14 Tentative instantaneous creep rate model of SiGA under different operating conditions [46].

The total creep rate is determined by secondary creep once the irradiation creep drops. However, this secondary creep could seriously overestimate the total creep strain for the high burnup fuel like EM^2. For the Zircaloy-2 tubular cladding, as an example, Ibrahim [47] measured that the strait line model of log-strain vs. log-time reduced predicted strains after 30 year by a factor of ~3 when compared with the constant secondary creep rate model. So far, a long-term creep model of SiGA tube is not available. Therefore, a baseline creep model of SiGA was formulated based on general creep models of CVD SiC and SiC composite material summarized in Table 6. Snead et al. [38] model is for CVD SiC, but include the neutron irradiation effect. Zhu et al. [48] and Bhatt [49] models are for SiC composite but no irradiation effect is included. In general, the total creep rate is represented as a product of neutron flux, stress, and time with appropriate indices. The temperature effect is typically represented as an exponential function of activation energy, gas constant and temperature.

Table 6 Comparison of CVD SiC and SiC-SiC creep strain models

Snead et al. for CVD SiC	Zhu et al. for SiC-SiC	Bhatt for SiC-SiC
Primary creep $\varepsilon_c = A_p(\sigma / G)^n (t / \tau)^p$ n=1.63, p=0.2-0.4 Steady-state creep rate $\dot{\varepsilon} = A_s(\sigma / G)^n \exp(-Q/k_b T)$ n=2.3 Irradiation creep rate $\dot{\varepsilon} = \sigma (B\varphi + D\dot{S})$	Time-dependence $\dot{\varepsilon} = A\, t^{-0.75}$ Stress-dependence $\dot{\varepsilon} = B\, \sigma^{1.5}$ Temperature-dependence $\dot{\varepsilon} = C \exp(-Q/RT)$ General form $\dot{\varepsilon} = k\sigma^n t^{-q} \exp(-Q/RT)$	Thermal creep $\varepsilon_p = C\, \sigma_m [t \exp(-B/T)]^{1/3}$

In general, the total creep rate is represented as a product of neutron flux, stress, and time with appropriate indices. The temperature effect is typically represented as an exponential function of activation energy, gas constant, and temperature. The time indices of the above formulations are between -0.8 and -0.6. As such, the transient creep rate of SiGA was formulated as follows:

$$\dot{\varepsilon} = \mathrm{K}(\varphi + \varphi_0)\, (\sigma + \mathrm{b} \exp(\mathrm{c}\sigma)) \exp(-\mathrm{Q/RT})\, \mathrm{t}^{-0.6} \tag{5-23}$$

The baseline creep rate is compared with the constant secondary (steady-state) creep rate in Figure 15 in which two curves intersect at around 2000 – 3000 hours. This trend is the same for the perturbed cases of the neutron flux, stress and temperature. In summary, the baseline creep calculation uses Koyanagi et al.'s [46] primary creep model during early irradiation, followed by a reduced secondary creep model during long-term irradiation.

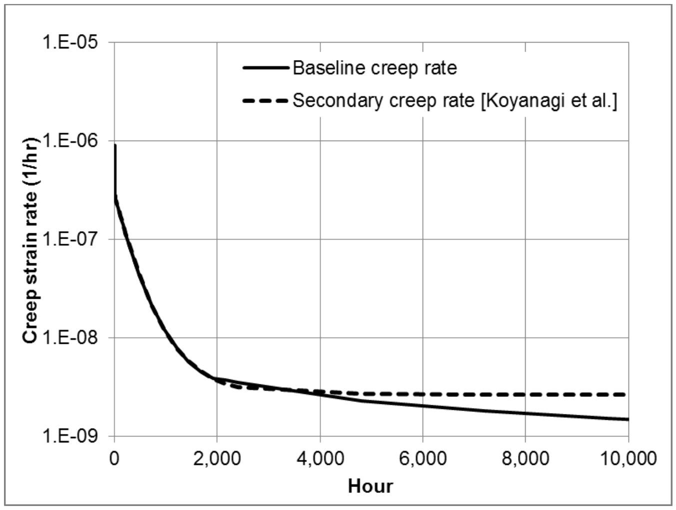

Figure 15 Tentative transient creep rate model of SiGA [46].

Stress-strain - The stress-strain formulation follows the general form such as

$$\sigma = k\varepsilon^{n}\left(\frac{\dot{\varepsilon}}{10^{-3}}\right)^{m} \quad (5\text{-}24)$$

where σ is the total stress, k is the strength coefficient, ε is the total strain, n is the strain hardening exponent, and m is the strain rate sensitivity constants. Values of k, n, and m were estimated based on homogenized values of equivalent stress and strain taken from an ANSYS model of internal pressurization of a SiC composite tube [41]. The stress-strain curve was initially constructed from average values throughout the cladding thickness, using equivalent stress and strain. However, as initial inclusion of the monolithic outer layer provides a nearly linear stress-strain curve, the stress-strain curve was conservatively reconstructed using only the composite layer and compared to the experimental data. While this model is not perfect, it provides a reasonable fit for the reactor operating condition. The fitting formulation was set such that k = 3.32 GPa, n = 0.462, and m = 0.001 (set to a small value as the strain rate sensitivity is unknown and not expected to be large). The temperature dependence of the stress-strain curve was derived from the UTS, which is shown in Figure 16.

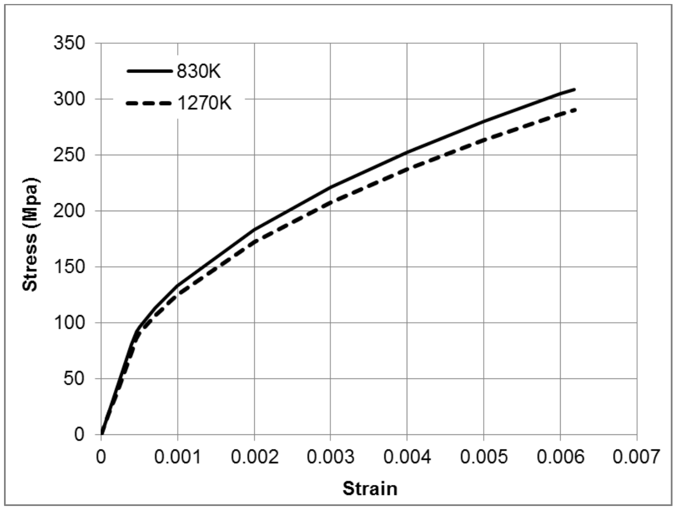

Figure 16 SiGA stress-strain model for selected temperatures of 1270K and 830K [41].

5.3 Uncertainties in Properties and Models

The fuel performance analysis includes uncertainties in simulation results due to imperfectness of material properties and models, geometry modeling, and solution methods. The accuracy of the design and analysis is required not only for the safety analysis but also for the licensing. This section summarizes issues of existing material properties and models of the UC and SiC composite.

5.3.1 Uranium Carbide Fuel

Uranium carbide fuel properties have been collected from legacy publications. These properties were formulated by many different authors, but details of measurements such as fabrication process, impurities, stoichiometry, etc. are not always well known. Nonetheless, thermal properties such as thermal conductivity and coefficient of thermal expansion are in general consistent from each other, while irradiated fuel properties such as swelling and diffusion coefficient show large discrepancies. The current status of UC fuel properties is as follows:

- *Melting temperature* is in the range of 2250 and 2530ºC. The property was formulated as a function of burnup based on plutonium/uranium ratio.
- *Specific heat* was measured from freezing to melting points as a function of temperature.
- *Thermal conductivity* is given as a function of temperature and adjusted by porosity. The legacy data show that measurements were conducted up to 2400ºC.
- *Emissivity* is formulated as a function of temperature from 1102 to 2000ºC.
- *Coefficient of thermal expansion* depends on temperature was measured between 400 and 1700°C, and formulated as a function of temperature.
- *Density* is given as a function of temperature with a full density of 13.63 g/cm^3 based on the measurement of linear expansion in the temperature range from 0 to 1800°C.
- *Elastic modulus* is formulated as a function of temperature and porosity up to 1250ºC with porosity less than 0.3.

- *Poisson's ratio* is given as a function of porosity in the range from 0.05 to 0.27.
- *Yield stress* is given as a function of temperature in the range from 25 to 1200°C without considering manufacturing process and stoichiometry.
- *Fracture stress* is reported between 35 and 210 MPa for temperature range from 25 to 1200ºC, depending on manufacturing process and stoichiometry.
- *Swelling* is formulated as a function of temperature, porosity, burnup and contact pressure. Apparently the formulation is applicable up to ~6% burnup and 2000ºC.

Fuel properties depend on various parameters including fabrication process and stoichiometry. For example, Carniglia quoted by Matthews [23] reported the fracture stress changing from 100 to 210 MPa at room temperature depending on fabrication process and stoichiometry. As the EM^2 fuel is slightly hyperstoichiometric and the pellet includes both closed and open pores, it is recommended to measure all the properties of the as-fabricated EM^2 fuel. There are specific issues of certain properties as described below. These could be the priority of measurements too.

- *Thermal conductivity* has non-negligible dependence on impurity, e.g. oxygen, and stoichiometry ty. However, manufacturing campaign at GA has shown that nearly pure UC kernels are fabricated. Therefore, the effects of these parameters could be excluded assuming that the fabrication process consistently produces qualified kernels. The effect of hyperstoichiometry on the thermal conductivity is unknown for EM^2 fuel and needs to be tested. As the EM^2 fuel is slightly hyperstoichiometric and the temperature is the most influencing parameter of all other properties, the thermal conductivity of as-fabricated EM^2 fuel should be measured as a first priority. As the fuel burns, fission gases are accumulated in the fuel kernel while the open pore could absorb the fuel swelling, resulting in solid fission products buildup in the kernel and complicated pore distribution in the pellet. The relationship between the thermal conductivity and fuel burnup needs to be formulated considering the effect of both the solid and gaseous fission products.
- *Swelling* formulation provided by Preusser is a restrained swelling model that includes two correction factors. These correction factors were supposedly determined based on measurements. Once the swelling rate reaches its limiting value, the total swelling becomes a linear function of burnup. This formulation needs to be properly revised based on EM^2 fuel measurements or a new swelling formulation is required to model swelling accommodation by the open pores.
- *Mechanical strength* needs to be properly formulated as a function of temperature, burnup, stoichiometry, and porosity based on measurements as the mechanical properties, e.g. yield stress and fracture stress, are to be used to determine the swelling accommodation by the open pores based on Dienst's observations, i.e. external pressure up to 30 MPa doesn't result in any noticeable change in the swelling rate up to 1300ºC and carbide fuel can be considered unable to bear any appreciable mechanical load resulting from the cladding restraint at high temperatures above ~1200°C.
- *Creep rate* of the fuel could be neglected when the fuel is considered to be hard compared with the metal cladding. Because the cladding is a hard material too, this assumption is no longer valid and appropriate creep models will be needed for the stress-strain analysis.
- *Diffusion coefficients* have a significant variation by more than 3 orders of magnitude, possibly due to different microstructure of the sample used in the legacy measurements. The diffusion coefficient of the as-fabricated EM^2 fuel will need to be measured as a

function of temperature.

- *Fission gas release* – A simplified fission gas release model was provided by Preusser above 1000ºC. Theoretical models are also available by Prajoto et al. and others. However, as was noted from UO_2 fuel case, both the experimental and theoretical models may have limitations in correctly predicting the fission gas release. It will be required to update the UC fission gas release model based on targeted measurements or theoretical models.
- *Densification* – There is no densification data specific to the UC pellet. Preusser reported that high density fuel (96 to 99% TD) undergoes no restructuring, including densification. However, Dienst reported that porous mixed carbide densifies to ~90% TD. Recent simulations of the legacy carbide fuel irradiation tests showed that the maximum densification needs to be formulated in terms of initial fuel density. There is no procedure to measure densification by resintering tests either. A new procedure is underway to measure the UC densification.
- *Relocation* – There is no relocation model specific to the UC pellet. This model affects the temperature and strain calculations until the fuel gap is closed. A theoretical model is recommended, but an experimental model can also be developed from targeted fuel rod irradiation tests.

5.3.2 Silicon Carbide Composite Cladding

SiGA cladding properties depend on fabrication architecture and manufacture. The properties were formulated based on measurements performed on GA-EMS's accident tolerant fuel (ATF) design and most relevant open literature. Currently the irradiation property is available only up to 75 dpa. It should be noted that the SiC composite properties are also available from non-nuclear community that measured thermal and mechanical properties for a wide range of temperature and time.

- *Specific heat* is formulated as a function of temperature. The irradiation effect is neglected as the density is not affected.
- *Thermal conductivity* is formulated as a function of temperature, irradiation, and composite structure. The irradiation effect is considered by incorporating irradiation-induced swelling.
- *Emissivity* is conservatively used between 0.8 or 0.9 as a constant value.
- *Coefficient of thermal expansion* is formulated as a function of temperature.
- *Elastic modulus* is assumed to be independent of temperature and irradiation. Directional moduli were measured for specific fiber architecture and manufacturing process.
- *Poisson's ratio* is assumed to be constant.
- *Yield stress* measured at room temperature is used up to 1800ºC and is assumed to be independent of irradiation.
- *Fracture stress* is unaffected by irradiation. A linear dependence on temperature is included.
- *Swelling* is formulated in the temperature range from 200 to 800ºC. It was measured up to 75 dpa at a variety of temperatures. Swelling was formulated such that it increases with dose up to ~1 dpa, at which point it saturates.

- *Creep coefficient* for CVD SiC was experimentally measured as a function of dose and temperature. The instantaneous creep coefficient decreases up to the saturation point of 1 dpa. Secondary creep has a constant creep coefficient. The effect of temperature was approximated by an exponential function of temperature. Out-of-pile tests SiC show that the creep rate slowly decreases as a function of time rather than being a constant value, which was also reported for the zircaloy tube. As such, the long-term creep rate was formulated as a function of time.
- *Stress-strain* formulation follows the general form such that the stress is a function of strain and strain rate. Values of strength coefficient, strain hardening, and strain rate sensitivity constants were estimated based on homogenized values of equivalent stress-strain taken from an ANSYS model of internal pressurization of a SiC composite tube. The temperature dependence of the stress-strain curve was added based on UTS. However, the effect of strain rate is neglected. The strain limit should consider hermeticity, mechanical integrity and fission gas release all together.

6 PERFORMANCE EVALUATION

The EM^2 fuel performance was evaluated by FRAPCON-4.0 and FRAPTRAN-2.0 code [1, 2] modified for UC fuel and SiGA cladding properties and models (See Sec. 5.2), i.e. FRAPCON-4.0GA and FRAPTRAN-2.0GA, respectively. The reference fuel element for the thermal-mechanical analysis is the hot rod with average linear power of 34 kW/m at the BOL and the inlet temperature of 823 K. The fuel element geometry and dimensions have been derived from preliminary analysis and passed down as fuel element specifications given in Table 2. The fuel element is a rod of 2.11 cm diameter. The fuel pellet has 0.5 cm inner and 1.9 cm outer diameter (sintered UC with smeared porosity of ~25%) and is enclosed in a 0.95 mm thick SiC composite ceramic cladding.

6.1 Approach to EM^2 Fuel Performance Evaluation

The baseline fuel element calculation uses the restrained swelling model for the annular pellet. The follow-on sensitivity calculations model the swelling accommodation by the open pore (or restructuring of fuel kernels) using both annular and solid pellet configuration as described below. In both cases, the amount of fuel is the same.

- *Restructured annular pellet* - The use of the restrained swelling model of the baseline case could be limited as the fuel and cladding materials and their operating conditions, used when developing the formulation, are not the same as those of the fuel and cladding analyzed here. As such, the free swelling formulation developed by Harrison [3] is used along with the assumption that the fuel swells into the open pores when the fuel and cladding are under a hard contact.
- *Restructured solid pellet* - The cladding strain can be relieved when the fuel swelling is absorbed by the open pores even though this assumption requires experimental verification in the near future. Under this assumption, it will be more effective to increase the open pore volume of the fuel rather than increasing the fuel gap. It is expected that the central hole of the annular pellet will be eventually filled by kernel swelling. If the central

hole is included in the open pore volume, the smeared density of the pellet is reduced to 69.53% from 74.7% of the annular pellet. In addition, if the kernel density of 95%TD is used, the solid fuel pellet will have the open pore volume fraction of 26.8% while it was 17% for the annular fuel pellet model. However, use of the solid fuel pellet model will increase the fuel centerline temperature when compared with the annular pellet model. It should be noted that the purpose of using the solid pellet model is to evaluate the effect of open pore to the cladding stress and strain not the fuel temperature.

6.2 Normal Operation

The long-term power histories of the fuel rods were calculated using MCNP6 [4] from the beginning-of-life (BOL) to the end-of-life (EOL) as shown in Figure 17 for the average and peak power rods. The axial power peaking is 2.02 at BOL and reduces to 1.42 at EOL, which is typical during normal long-term operation due to fissile burning, transmutation and xenon buildup. The linear power history and its axial distribution are used to calculate long-term phenomena such as burnup, fuel swelling, relocation, densification, and cladding deformation.

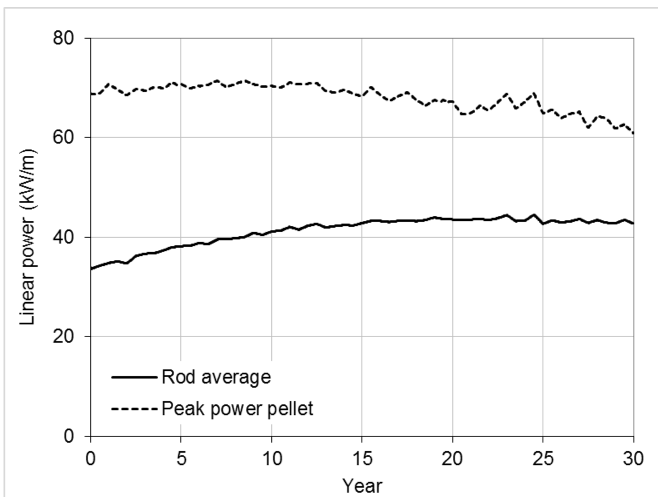

Figure 17 Power history of reference EM^2 fuel element

The fuel, cladding and channel outlet temperatures of the baseline case are shown in Figure 18 at the peak fuel temperature position. The peak fuel temperature is 1746 K after 33 days of irradiation, which is a 38% margin to the melting point. The corresponding cladding temperatures are 1398 and 1248 K on the inner and outer surface, respectively. During the cycle, the cladding temperature varies between 1248 K and 1398 K with an average value of 1326 K. Under these operating temperature conditions, it is expected that radiation-induced swelling of the cladding is expected to be minimal.

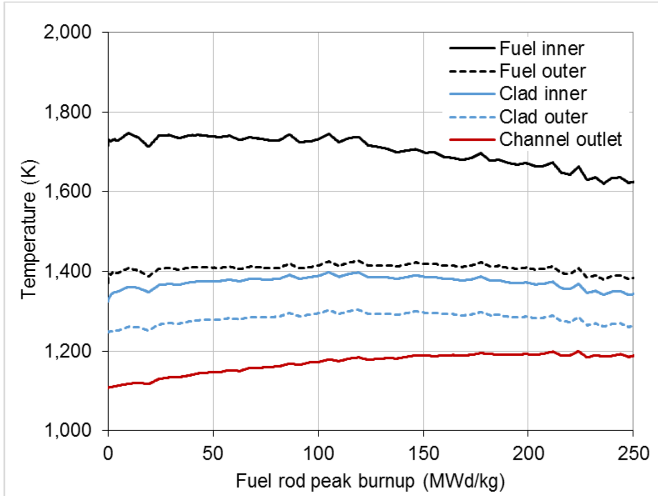

Figure 18 Reference EM² fuel element operating temperature profile

The operating temperature profile through the radius of the pellet is shown in Figure 19. The cladding temperature difference varies by 76 – 100 K linearly through the thickness of the SiC composite cladding. The parabolic temperature distribution in the fuel pellet increases by 232 – 345 K from the outer surface of the fuel to the inner surface. The temperature drop through the fuel-cladding gap is 26 – 61 K. Though the thermal conductivity of the cladding decreases with irradiation, the linear power at the peak temperature position also decreases.

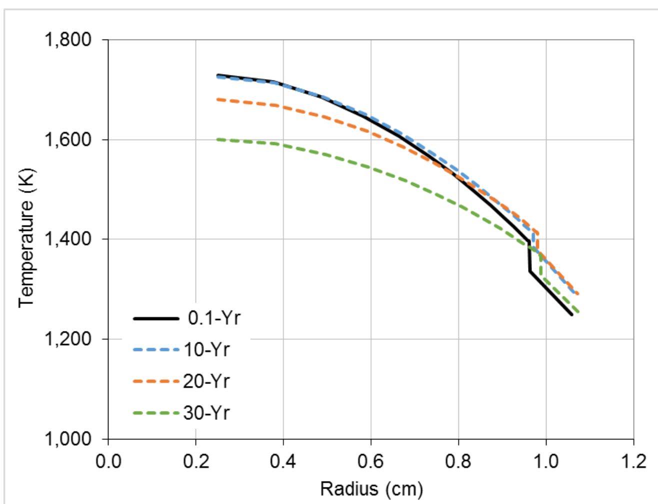

Figure 19 Reference EM² fuel pellet radial temperature distribution

The cladding hoop stress and strain states of the baseline case are shown in Figs. 20 and 21, respectively, along with the restructured pellet cases. The fuel gap is closed at 165-day and then the cladding is under tension. The peak hoop stress is ~32 MPa, which is far below the 1/3 of UTS (115 MPa). The cladding hoop strain increases up to 2.48% for the baseline case which is beyond the current design limit of 0.62%. However, if the fuel kernels are restructured, the time at the hoop strain limit is reached is 18.8 years (175 MWd/kg) and 22.5 years (208 MWd/kg) for the annular and solid pellet model, respectively. It is obvious that the strain will increase fast if the swelling is no longer accommodated by the open pore in the fuel. It is also true that the results include uncertainties as the restructured pellet model has not yet been experimentally verified for the specific design of EM² fuel. However, results of early studies support the design concept of the porous fuel to mitigate the swelling effect. For example, Chubb et al. patented a non-swelling uranium nitride fuel based on 20% to 30% interconnected porosity [5]. The sphere-pac nuclear fuel program confirmed the propagation of kernel restructuring inside the fuel rod through high temperature irradiation tests [6-8].

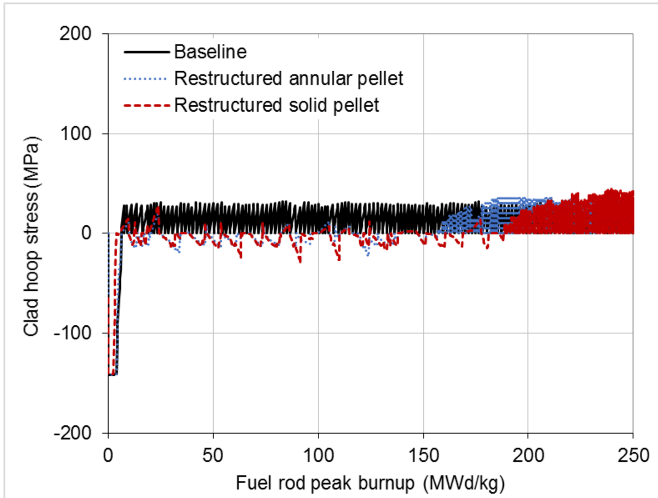

Figure 20 Comparison of EM² fuel element cladding hoop stresses.

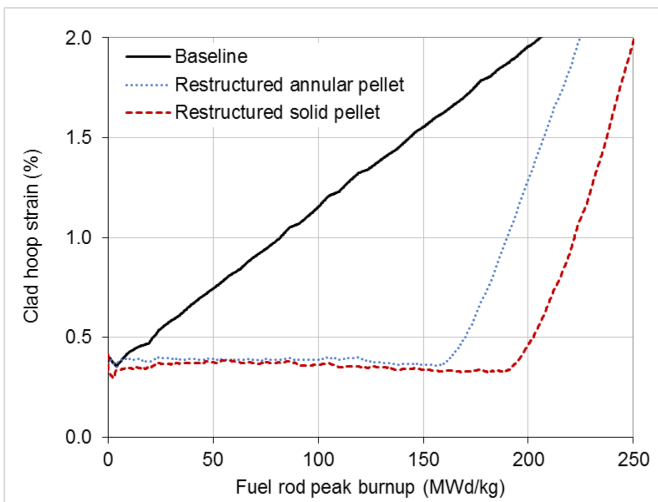

Figure 21 Comparison of EM² fuel element cladding hoop strains.

6.3 Accident Conditions

Representative accident scenarios have been selected for EM² such as uncontrolled control rod (CR) withdrawal, loss-of-flow accident (LOFA), and loss-of-coolant accident (LOCA). The uncontrolled CR withdrawal is a reactivity-initiated accident (RIA) resulting from malfunction of the reactor control system or failure in the CR system. A LOFA could occur due to loss of off-site power, compressor failure, or heat exchanger / pipe blockages. A LOCA causes rapid changes in pressure and flow within the primary cooling system due to breaks in the primary coolant pressure boundary.

6.3.1 Control Rod Withdrawal

The design requirements on the fuel system imposed by reactivity initiated accidents are represented by the uncontrolled CR withdrawal. The limiting CR withdrawal occurs during the middle-of-life (MOL) core conditions when CRs are the most inserted at ~70%. At BOL and EOL conditions the CRs are close to fully withdrawn. The operation time at MOL is 13.5 years. At this time in the fuel life, the peak local fuel burnup of the hot rod is 132 MWd/kgU. The average CR worth of 173 pcm at MOL is used for simulation. During the CR withdrawal, the PCU remains connected to the electrical grid. When the CR is withdrawn from fully inserted position, the core power reaches the maximum value of 109% at 31 sec and drops as shown in Figure 22.

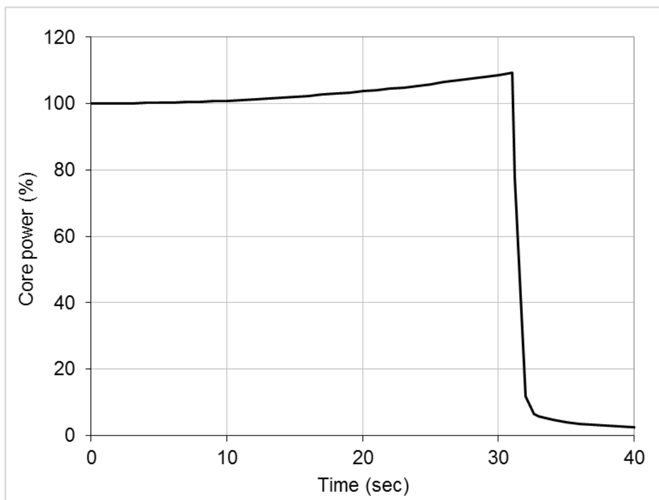

Figure 22 Transient EM² reactor core power during a single CR withdrawal

The reactor core is tripped at 31 sec into the transient and the shutdown rods drop after a 0.6 sec delay. The peak fuel and coolant outlet temperatures are 1789K (1516ºC) and 1215K (942ºC), respectively, for the hot rod as shown in Figure 23. The margin to fuel melting point (2705K) is 34%. As the fuel temperature increases during the transient, so does the cladding circumferential stress. At the peak fuel temperature point, the cladding circumferential stress jumps to 169 MPa and then drops, shown in Figure 24, which exceeds circumferential PLS of 153 MPa, but is below circumferential UTS of 346 MPa. The peak cladding circumferential strain is 0.59%, shown in Figure 25, which is below the strain limit of 0.62%. Though the fuel has a sufficient thermal margin to the melting, the mechanical deformation of the pellet imposes an excessive stress on the ceramic cladding even though the strain is below the limiting value. The results indicate that the design parameters of the fuel as well as the reactor trip system need to be adjusted. This does not exclude the effects of uncertainties associated with the property parameters and numerical scheme of the analysis tool.

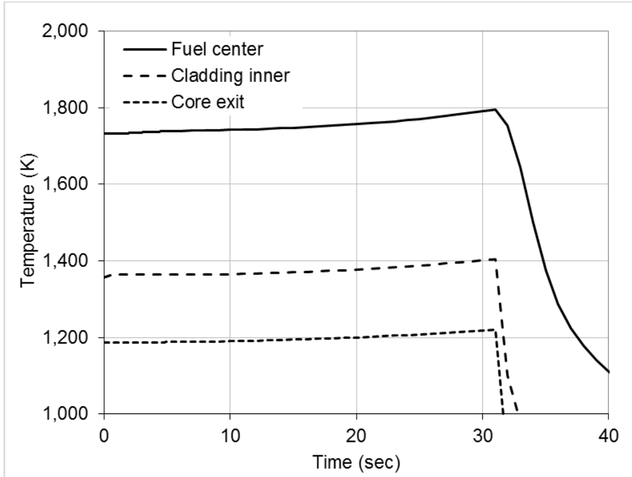

Figure 23 Transient EM² temperatures during a single CR withdrawal

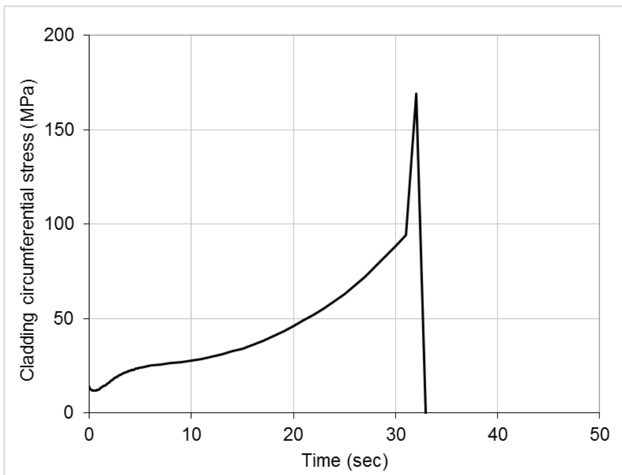

Figure 24 Transient EM² cladding circumferential stress during a single CR withdrawal

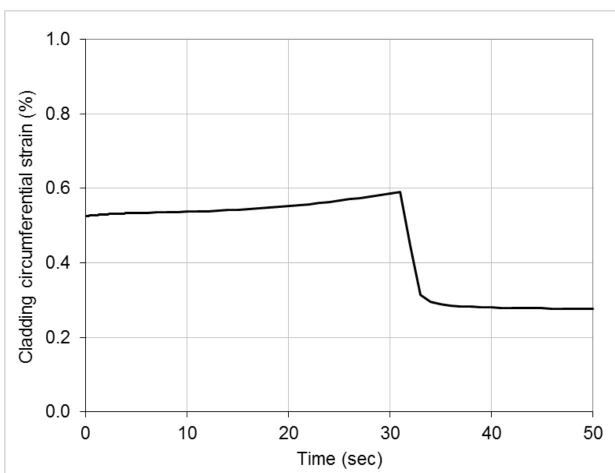

Figure 25 Transient EM² cladding circumferential strain during a single CR withdrawal

6.3.2 Loss of Primary Cooling Capability

The design requirements on the fuel system imposed by loss of primary cooling accidents are represented by two classes of accidents: LOFA and LOCA. The LOFA was initiated by tripping the PCU which then trips the reactor core. It was assumed that only one of two passive DRACS loops is operating. The LOCA analysis includes two different break sizes: small break (SB) resulting in a slow depressurization, and large break (LB) resulting in a rapid depressurization. The SBLOCA has a break size of 10 cm^2 equivalent to a 3.6 cm (1.5 inch) inner diameter (ID) pipe. The LBLOCA has a break size of 400 cm^2 equivalent to a rupture of a 23 cm (9 inch) ID pipe or the maximum crack and displacement of a cross-duct allowed by the concrete supports.

The reactor transient conditions were obtained by DRACSMAT [9] that simulates the shutdown cooling capability of the DRACS via natural circulation. It should be noted that *the reactor core is already shut down at time zero in DRACSMAT simulation models*. Due to unavailability of the transient conditions between the onset of accident and reactor shutdown, the fuel analyses based on DRACSMAT simulation results provide the fuel performance only for the after-shutdown transient. Figure 26 shows the primary system pressure transients. The SBLOCA primary pressure equilibrates with the containment in ~30 min. The LBLOCA equilibrates in less than one minute. In all cases, the cooldown assumes only one DRACS loop is operational. Mass flow and core cooling are directly related to the pressure and coolant density in the primary system. The slow depressurization of the SBLOCA results in a slow decline in core mass flow rate as shown in Figure 27.

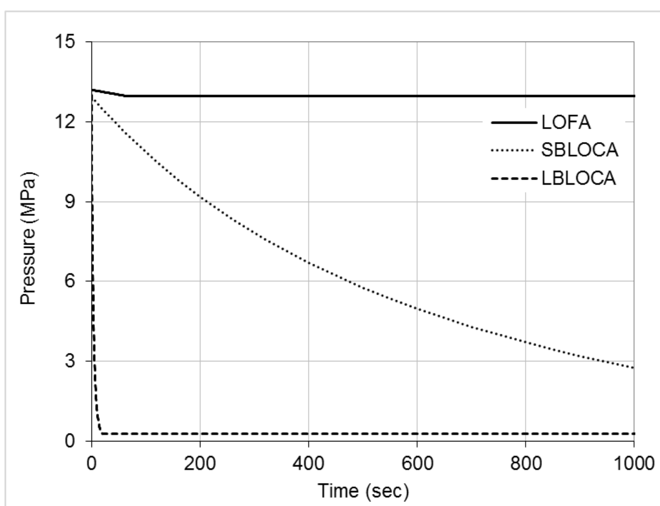

Figure 26 Comparison of EM^2 primary system pressure with cooldown on one DRACS loop

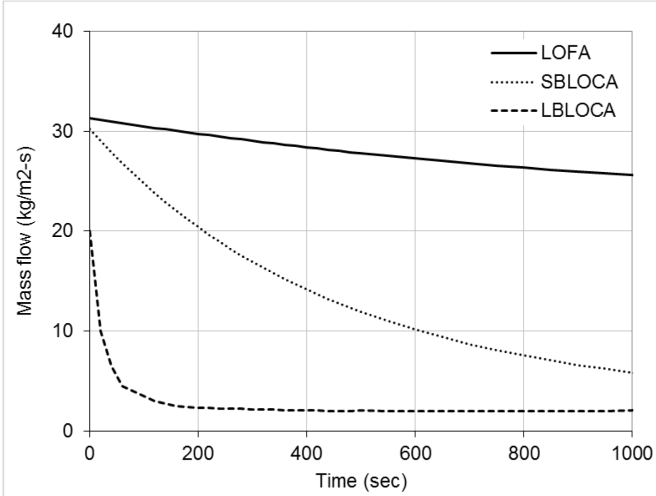

Figure 27 Comparison of EM² helium mass flow during LOFA and LOCA

It should be noted again that the simulations of the LOFA and LOCA in this study are limited to the evaluation of fuel performance after shutdown due to nature of the DRACSMAT that generates the fuel boundary conditions. The fuel temperature drops immediately as the reactor trips, shown in Figure 28. For the LBLOCA, however, the fuel temperature increases again up to 1384K because the cooling condition is seriously exacerbated due lower pressure when compared with the LOFA and SBLOCA. Both the circumferential stress and strain are below the limiting values during the shutdown as shown in Figs. 29 and 30, respectively.

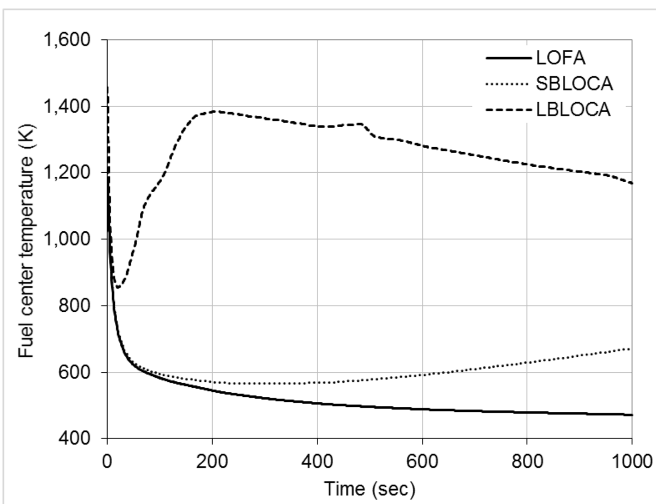

Figure 28 Comparison of EM² transient temperatures during LOFA and LOCA

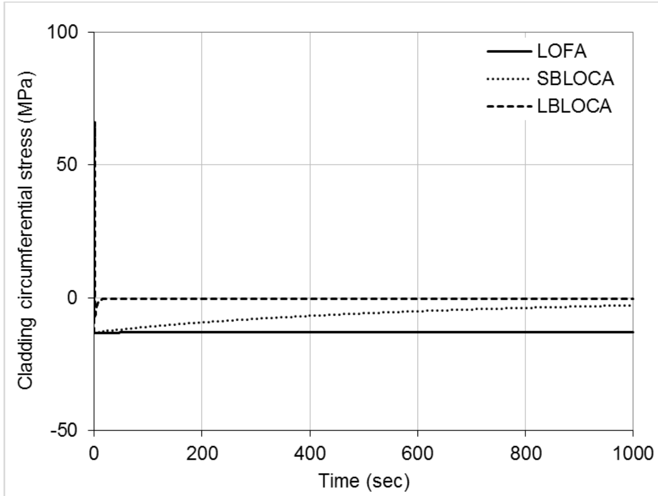

Figure 29 Comparison of EM² transient cladding circumferential stress during LOFA and LOCA

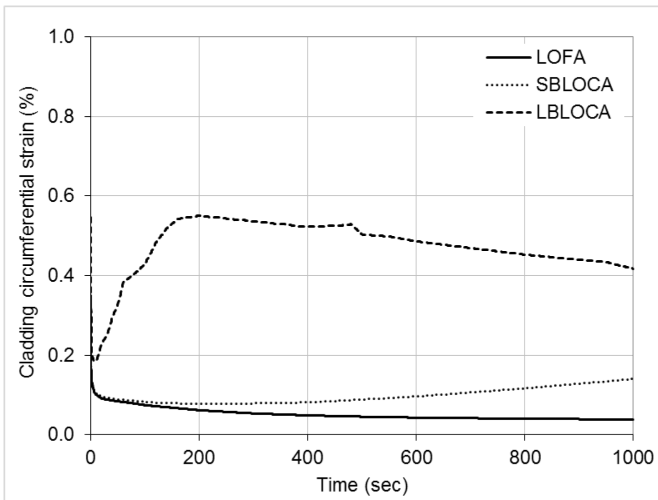

Figure 30 Comparison of EM² transient cladding circumferential strain during LOFA and LOCA

6.4 Remarks

The analyses have been conducted for the hot rod, including the evaluation of the restructured pellet models to accommodate excessive fuel swelling of the high burnup fuel. Findings from this preliminary evaluation are as follows:

- The fuel temperature is well below its melting point, which is attributable to the use of UC fuel and annular pellet geometry.
- The cladding hoop stress is well below 1/3 of UTS when the restrained swelling model is used.
- If the fuel kernels are restructured such that the swelling is fully accommodated by the open pore of the fuel pellet, the cladding hoop strains could be kept below the current design limit of 0.62% up to 22.5-year.

It should be, however, addressed that these results are based on several critical assumptions such as dense fuel kernels, solid and gaseous fission product accommodation, and fuel kernel restructuring during pellet-cladding hard contact, which requires experimental or theoretical verifications. Regarding the carbide fuel swelling, it is worth noting some of observations provided by Preusser and Dienst based on their early experimental results. These are very important in developing future experimental plans and understanding fuel behavior during high-burnup irradiation as summarized below:

- The middle and low density (77 to 90% TD) carbide fuels can swell into the pores.
- At high temperatures above about 1473 K, mixed carbide fuel can be considered unable to bear any appreciable mechanical load resulting from the cladding restraint in fuel pins. Therefore, the fuel swelling rates at lower temperatures are more important with regard to mechanical interaction between fuel and cladding.
- Fuel-cladding mechanical interaction during steady-state operation is mainly determined by the swelling rate of the outer fuel zone, which is at lower temperatures. Swelling of the hotter fuel inside can be absorbed in the available void space such as pores and cracks.

7 LEGACY APPROACH TO FUEL QUALIFICATION

The approach to fuel development and qualification is generally estimated to take as long as 20 years due to the long time durations associated with irradiation, post-irradiation examination (PIE), and safety testing. In 2007, Crawford, et al. [1] documented the approach and rationale, describing a program structure in four phases based on their observations and experience. While sound, the approach is very serial, and thus very time-consuming. Making use of today's multi-scale modeling and simulation tools and enhanced experimental capabilities, fuel qualification can be done more efficiently and still maintain the high safety standards. This section will describe the legacy approach for comparison with the emerging new Accelerated Fuel Qualification (AFQ).

Crawford, et al. [1] summarized the objectives of fuel development programs as follows:

1. Develop the fuel system design specifications
2. Produce databased of fuel properties and irradiation behavior

Their paper describes that the two objectives as linked because as the fuel specifications are finalized, they are used to produce the test specimens that create the database of fuel properties and irradiation behavior. The fuel fabricator must ensure that the fuel can be manufactured to meet specifications and achieve economic goals. The fuel properties and irradiation behavior database is used to calculate the fuel performance and associated uncertainties that are needed for the licensing safety analyses.

To classify maturity in the US Department of Energy Advanced Fuel Cycle Initiative (AFCI) program, they adopted a NASA-like Technology Readiness Level (TRL) scale for fuel development. As described in Table 7, they categorized fuel development in four phases: 1) fuel candidate selection, 2) concept definition and feasibility, 3) fuel design improvement and evaluation, and 4) fuel qualification and demonstration.

Phase 1 – fuel candidate selection can rely on past experience and data supplemented by limited laboratory testing when needed. Fortunately, the early history of nuclear power investigated a wide variety of fuel forms so that this phase of fuel development often involves literature searches and data retrieval.

Phase 2 – concept definition and feasibility are shown when initial radiation testing is performed on a small number of test samples. Irradiation testing and post-irradiation examination (PIE) are both costly and time-consuming. Typically, phase 2 could take 8 years to complete. Fortunately, phase 3 can begin before phase 2 is finished assuming positive results.

Phase 3 – design improvement and evaluation are concluded when irradiation testing and property measurement for model development result in a defendable safety case. This phase requires a significant amount of irradiation space in test facilities with prototypic environments followed by PIE in shielded hot cells. Irradiation tests must also assess fuel performance at operating limits of heat generation and coolant temperatures. Safety testing of the fuel under design-basis and beyond-design-basis accident conditions is also required to establish margin to fuel failure. The schedule for completing phase 3 is highly dependent on available irradiation space which is extremely limited in the US. Phase 3 could take 8 years to complete but can begin 3 to 5 years before the completion of phase 2 if programmatic risk is assessed to be acceptable. With limited irradiation space, the time to complete phase 3 can easily double.

Phase 4 – fuel qualification and demonstration are focused on fuel performance using fuel manufactured according to specification with a specified quality assurance (QA) and control program. Irradiation for fuel qualification can proceed along a few different paths. For LWRs, qualification can use existing reactors by adding lead test rods (LTRs) and/or lead test assemblies (LTAs) as part of a core reload. The reactor/fuel vendor may also use a special purpose-built test reactor or demonstration reactor to qualify the fuel. The demonstration reactor could be reduced-scale or a full-scale prototype reactor. The same test facilities used in phase 3 could also be used in phase 4. Phase 4 could take 8 years to complete but the start of phase 4 would be delayed if a test, demonstration or prototype reactor is built specifically to qualify the fuel.

For a long-life fuel form like EM^2, it is impractical to obtain end-of-life (EOL) data before qualifying fuel. Following the pathway above, a typical 20-year schedule could stretch out to 60 years. This necessitates a new methodology for accelerated fuel qualification (AFQ), as mentioned earlier, which is the subject of the next section.

Table 7 Application of TRLs to reactor fuel development and qualification [1]

TRL	TRL Function	Generic Definition	Fuel Development-Specific Definition	Fuel Dev. Phase
1	Technology Down-Selection	Basic principles observed and formulated	Technical review leading to identified technical options. Identification of criteria for candidate selection	1
2		Technology concepts and/or applications formulated	Fuel candidates selected from options, based on selection criteria	
3		Analytical and experimental demonstration of critical function and/or proof of concept	Calculational analysis and lab-scale experimentation and characterization addressing feasibility, including: fabrication process development, property measurement, and ex-pile tests	2
4	Final Process Selections and Integration	Component and/or bench-scale validation in a laboratory environment	Establish proof of concept. Fabrication of irradiation testing samples in accordance with QA requirements. Design parameters and features established. Performance phenomena identified with proof-of-concept irradiation testing.	
5		Component and/or breadboard validation in a relevant environment	Irradiation testing of prototypic rods/compacts under nominal representative conditions (e.g., fission densities, fuel and cladding temperatures, cladding damage rates) is performed and assessed.	3
6	Full-Scale Integrated Testing	System/subsystem model or prototype demonstration in relevant environment	Prototypic rod/compact and assembly/element irradiation in representative environment, under full range of relevant normal and off-normal conditions. Representative compositions. Design parameters investigated. Information is sufficient to support a Fuel Specification and a Fuel Safety Case (which, in turn, support larger System Demonstration to achieve TRL 7)	
7		System prototype demonstration in prototypic environment	Fabrication of reference fuel derived from production supply sources irradiated to design conditions and utilization. Irradiation in representative environment. Prototypic design. Prototypic fabrication processes. Representative compositions.	4
8	Full-Scale Demonstration	Actual system completed and qualified through test and demonstration		
9		Actual system proven through successful mission operations		

8 STRATEGY FOR ACCELERATED FUEL QUALIFICATION

New nuclear fuel systems such as EM^2 UC/SiC composite fuel are needed to improve the economic outlook of nuclear power. Innovative fuels that are capable of high-temperature operations at high burnup (and long core life) can increase reactor safety and offer sustainable solution to high-level waste disposal. However, as noted in Sec. 7, using the legacy approach for qualification of a new fuel would be a decades-long, data-intensive undertaking, and is prohibitive for the long-lived fuels in advanced reactor designs.

The AFQ methodology brings together a combination of physics-informed advanced nuclear fuel performance modeling and simulation (M&S) with targeted experiments in order to significantly reduce the cost and time for qualification of new fuels while still maintaining the highest levels of safety. It aims to consolidate and reduce the number of required integral irradiation tests by developing and using models that represent the underlying physics by making use of separate effects test to validate those models and simulations. These models and simulations can then be used to optimize fuel designs more efficiently before undertaking the complex integral irradiation experiments. This approach takes advantage of advances made in microstructurally-informed fuel performance M&S tools and new advanced irradiation capabilities.

The advances in capabilities enable the AFQ methodology to be employed today. Modeling and simulation have advanced orders of magnitude in computational speed and employ sophisticated algorithms. As a result, in some cases, like for UO_2, predictions of fuel behavior are effectively based on first principles calculations. In characterization and experimental test capabilities, new diagnostics make measurements at higher resolution than ever before, and new techniques enable precision in separate effects testing. These enable a better understanding of the underlying behavior of materials and structures so that performance of fuel forms does not have to be solely dependent on empirical data.

After initial formulation of the concept, this methodology as noted in section 1, reference 2, it is further described in a paper by Terrani, et al. [1] that further articulates a three-phase approach to fuel qualification. Savings in time and cost arise from early identification and focus on the key drivers of the safety case for efficient use of resources. In addition, modeling and simulation is performed in parallel with experiments, in an iterative fashion. Importantly, fuel performance codes can make use of empirical materials property data, as before, and also use "data" from validated models. It should not be overlooked that the development of codes and simulations require experiments to validate them. The end result is that use of targeted separate effects and accelerated experiments enables higher quality and fewer integral irradiation experiments to achieve data needed to support the safety case.

An example of how a reduced number of data points can accurately represent behavior (strain) as a function of an important parameter (time) when a good physics-based model exists can be seen in the paper by Wen et al. [2], which shows a mechanism-based model of the thermal and irradiation creep of HT-9 and experimental data. A rate-theory-based dislocation climb law was developed including the contribution of irradiation-induced point defects. The climb approach is coupled with a constitutive model describing the effects of solute strengthening and Coble creep mechanisms. The model was benchmarked using the experimental results of Toloczko et al. [3] for both thermal and irradiation creep tests in Figure 31. The comparison shows that the model can quantitatively assess the relative roles of the physical mechanisms. This also indicates that the model can be effectively used to predict the thermal and irradiation behaviors of the SiC composite being developed for the application to the high temperature and high-dpa applications.

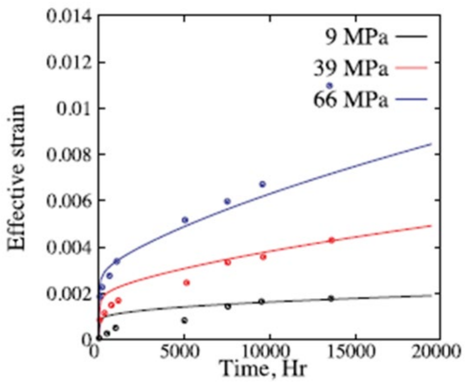

The circles are the experimental measurements

Figure 31 Predicted thermal creep behavior of HT9 steel as a function of von-Mises stresses at 600ºC

In comparison to the approach outlined in the Crawford paper, the AFQ methodology essentially consolidates Phases 2 and 3 into a single phase. The initial Phase 1, selection of a fuel form and matrix, is still the starting point for both approaches as shown in Table 8. However, many irradiation experiments have now produced useful materials property data which can already be used to refine the initial selection, potentially obviating some of the Crawford Phase 2 activities. Such is the case for the use of SiC, which relies on over 20 years of irradiation data showing temperature and dpa dependence of the thermophysical properties. Depending on extant data and models, the Crawford Phases 2 and 3 essentially overlap and become a single phase as described in the Terrani paper. Furthermore, modeling and simulation can be pursed in parallel with separate effects measurements of material properties and component level tests. Both of these enable a time-savings.

Table 8 AFQ Phases

PHASE	FUEL SYSTEM COMPONENT	AFQ ACTIVITY
Phase 1	Fuel-cladding/matrix selection	Choice of fuel system components for the expected operating environment based on irradiation, thermochemical, and thermodynamic behavior from literature searches, separate effects data, etc.
Phase 2	Fuel	Fissile material properties and component level performance testing and M&S
	Material encapsulating the fuel (tube, plate or matrix)	Non-fissile material properties and component level performance testing and M&S
	Prototypic combinations of Fuel and encapsulating material	Thermochemical and thermomechanical prototypic interaction testing and M&S
	Analysis by modeling and simulation and testing, where possible	Determination of uncertainties and safety margins in transients, DBA
Phase 3	Integral fuel+cladding/matrix	Fuel system performance in prototypic conditions - fuel burnup
	Integral fuel+cladding/matrix	Fuel system performance in prototypic conditions - cladding/matrix corrosion, heat transfer
	Integral fuel+cladding/matrix	Transient testing
	Integral fuel+cladding/matrix	AOO, DBA

The AFQ methodology will now be discussed more specifically for the EM^2 fuel system. The first phase has already been articulated in the description of the EM^2 reactor in the previous sections of this document and will not be repeated here since the fuel system has already been identified. The active efforts and most crucial activities for pre-licensing are in Phase 2 in the modeling and simulation as well as the separate effects experiments in progress now. However to set the context, a brief discussion of the gaps in the fuel system components is presented in Tables 9 and 10. Phase II will address filling the gaps through low-scale modeling for material properties, and engineering-scale modeling for the UC pellet and SiC composite cladding behavior separately. Phase III of modeling and testing addresses integral effects in combining the UC pellets and SiC composite cladding that collectively confirms the performance of the as-fabricated fuel. Although each phase builds upon the models and data from the previous phase, they can overlap in time rather than be performed sequentially.

The following steps will be covered below:

Phase 1:

1. Compile and evaluate existing data exists - sections 5.3
2. Identify gaps in data - see tables 5 and 6 below
3. Develop physics-based models that describe that phenomena - for UC leverage existing work on UO_2 and adapt it to UC; for SiC models have been developed on independently-funded R&D and are being implemented in BISON
4. Identify the driving physics phenomena and experimental observables that are important to the safety case

Phase 2:

1. Use the physics-based models that describe the phenomena of interest, do not just rely on empirical models
2. Validate the model(s) with targeted experiments (separate effects testing) - i.e. measure key experimental observables and results compare to simulations
3. Use the models to perform more simulations in order to optimize and help define the bounding variables (pressure, temperature) and determine/define an operating envelope of parameters in which the simulations are validated.
4. Use modeling and simulation to determine sensitivities and uncertainties with more fidelity than can be obtained with empirical models. Continue doing separate effects testing and integral testing as necessary

Phase 3:

1. Carry out essential integral tests which are expected to be limited in number given information already obtained in Phases 2 and 3.
2. Produce a final fuel qualification topical report for licensing purposes.

8.1 AFQ Phase 1 for EM^2 Fuel

Tables 9 and 10 summarizes the gaps in properties for the EM^2 fuel and cladding, respectively. The bases for the table ratings are described in Sec. 5.3. The “uncertainty ratings” are based on the quality and consistency of existing data due to availability of measurements and their variations. The “importance ratings” are based on the impact of the property/model on fuel damage, fuel failure, and coolability. The “priority ratings” reflect the combined impacts of uncertainty and importance so that they indicate the relative need and urgency to collect new data and improve modeling to reduce uncertainties in the fuel safety analysis. The objective of modeling and measurement data gathering is to reduce the uncertainties in the safety decision-making such that reasonable and acceptable design margins exist to preclude fuel damage, fuel failure and loss of coolability.

Table 9 Gap assessment in uranium carbide fuel properties and models

Property/Model	Uncertainty	Importance	Priority
Melting temperature	Low	High	Moderate
Specific heat	Low	High	Moderate
Thermal conductivity	Low	High	High
Emissivity	Low	Moderate	Low
Density	Low	Moderate	Low
Elastic modulus	Moderate	Moderate	Moderate
Poisson's ratio	Moderate	Moderate	Moderate
Yield stress	High	High	High
Fracture stress	High	High	High
Thermal Expansion	Low	High	Moderate
Swelling	High	High	High
Creep	High	High	High
Diffusion coefficients	High	High	High
Fission gas release	High	High	High
Densification	High	High	High
Relocation	High	High	High

Table 10 Gap assessment in silicon carbide composite cladding properties and models

Property/Model	Uncertainty	Importance	Priority
Specific heat	Low	Low	Low
Thermal conductivity	Low	High	High
Emissivity	Low	Moderate	Moderate
Thermal expansion	Low	Moderate	Moderate
Elastic modulus	Low	Moderate	Moderate
Poisson's ratio	Low	Moderate	Moderate
Yield stress	Low	High	High

Property/Model	Uncertainty	Importance	Priority
Fracture stress	Low	High	High
Swelling	Moderate	High	High
Creep	High	High	High
Stress-strain	Moderate	High	High

8.2 AFQ Phase 2 for EM² Fuel

In this phase, the modeling and simulation will be discussed in detail for the low-length scale modeling. Also, the first separate effects test on UC kernels has been started under a separately funded DOE cooperative agreement DE-NE0008819 named “Combining Multi-scale Modeling with Microcapsule Irradiation to Expedite Advanced Fuels Deployment” and will be described in detail. It is a separate eff tests to measure fission gas release and fuel kernel swelling. Future modeling and simulation will examine the sensitivity and uncertainty of the model and relevant simulations. The experimental conditions are chose to measure the performance of the UC material under the operating conditions of the EM², and determine bounding ranges of validity that can inform the operational envelop of the fuel.

Figure 32 below portrays as flow chart in detail of Phase 2. It is consistent with that found in the Terrani paper [1], but is more explicit in showing the fabrication/characterization steps, and the contribution of the low-length and engineering scale modeling as they contribute to the “evaluated material properties” and the “predictive model of integral fuel performance”.

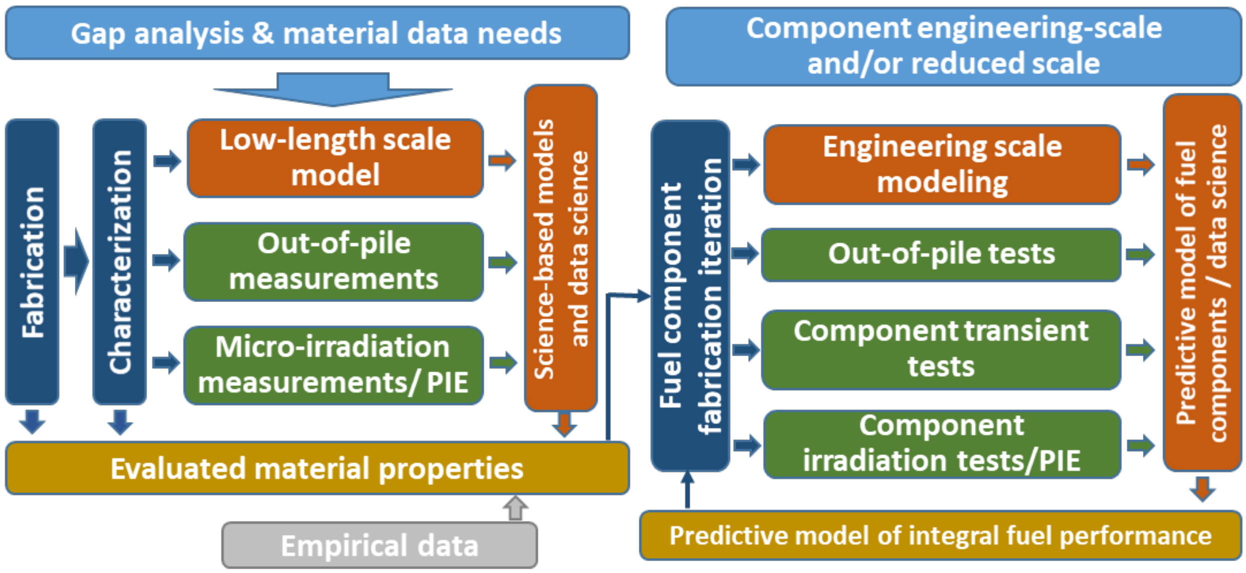

Figure 32 Detail of Phase 2 of the Accelerated Fuel Qualification Methodology

8.2.1 Fundamental material properties and characterization of UC

Modeling and testing initially focus on the UC kernel properties and fabrication. GA has developed UC fuel fabrication process, conducted kernel and pellet fabrication campaign, and characterized them. Under the GA-EMS DOE-funded program, Prof. B. Wirth at the University of Tennessee at Knoxville is developing a theoretical model of the fission gas release and swelling of the UC kernel in parallel with kernel irradiation in HFIR at ORNL. The outcome of this R&D is the physics-based models of the fission gas release and swelling, verified by targeted irradiation tests of limited number of samples..

As such, the physics-based model would:

- Reduce the amount of empirical data required to develop models and to verify the performance
- Incorporate underlying physics of the material behavior to enable prediction of material response to operating conditions and fabrication parameters.
- Enable the developed models to be applicable to a wide range of operating conditions while the data-based model is limited by its measurement range
- Utilize the relevant legacy measurements to verify the models and to identify the missing physics.

An example of the atomic scale model of ^{133}Xe diffusion coefficient is shown in Figure 33 along with measurement data. The solid circles represent specimens of grain size as large as 700 to 1000 μm. The open circles represent specimens with grain size from 20 to 150 μm [4]. The small grain specimens deviate substantially from the high temperature trend. Such behavior strongly suggests that grain-boundary diffusion can be important at temperatures below 1400 to 1500°C, whereas lattice diffusion is the predominant release mechanism at higher temperatures. Bévillon et al. [5] estimated the diffusion coefficient of ^{133}Xe using the migration energy calculated by atomistic model. This model best fits to Lindner and Matzke's measurements [6], when compared with Auskern and Osawa [7] and Ritzman et al. [8]. Bévillon et al. assumed that the entire sample behaved as a single crystal as far as the diffusion process was concerned. The shaded area in Figure 33 covers the GA-EMS data range from post-irradiation heat tests of UC kernels planned after the MiniFuel Irradiation Tests presented in Section 8.2.3.

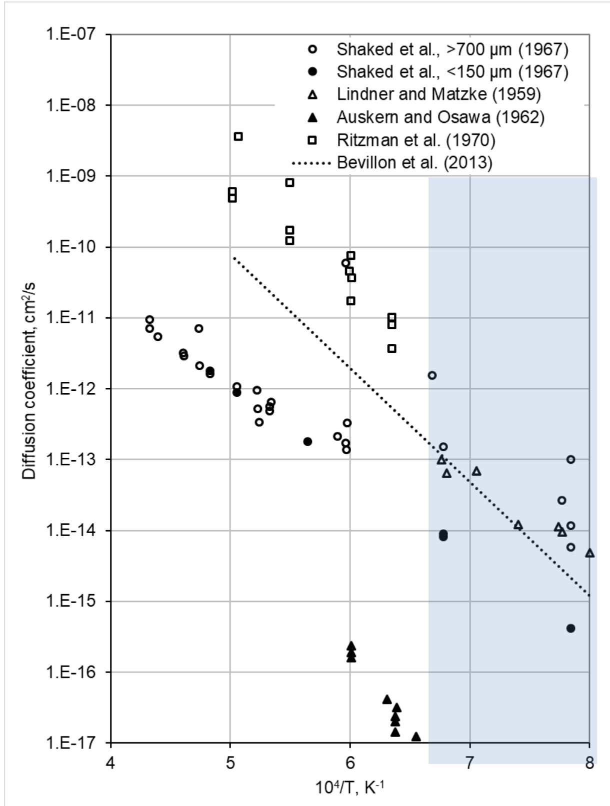

Figure 33 Comparison of diffusion coefficient of ^{133}Xe in UC

8.2.2 Atomistic to Mesoscale Modeling and Simulation - Low Length-Scale Models

Given the tremendous progress made in the development of atomistic and mesoscale computational tools in recent years, it is now possible to derive material properties using lower length scale models, which can provide consistent material property correlations. In addition, simulations can provide insight into the temperature and irradiation behavior of materials, providing data that is otherwise difficult to measure, either due to harsh environments (e.g. in-pile measurements), or expansive time scales of multiple decades. The advantage of the low-length scale modeling is that it can generate the data in a consistent way, extend the application range purely based on physics, and can be validated by the existing data, thus reducing the number of required experimental measurements.

The DOE NEAMS program has established a framework for multi-scale simulation of fuel properties and demonstrated application of reduced order models for fission gas release and thermal conductivity [9]. In addition, the combination of the phase field and cluster dynamics techniques is being developed in a NE-SciDAC project [10]. A number of atomistic to mesoscale computational tools are used in those programs: Vienna ab initio simulation package (VASP) [11] is frequently-used density functional theory (DFT) code; XOLOTL [12] is a cluster dynamics code which can provide predictions of fission gas behavior using fission gas diffusivity and point defect behavior; MARMOT [13] is a phase field code under MOOSE framework [14]; and LAMMPS [15] is a molecular dynamics (MD) code being used for mechanical property evaluation and chemical reaction modeling.

The DFT method has been successfully applied in several studies to investigate thermo-physical properties of UC, such as lattice constants [16], elastic constants [17], enthalpy and heat capacity [18], and dynamic fracture [19], as well as some thermodynamic and kinetic properties of point defects and fission products [21, 5]. In particular, it was determined that the thermal conductivity of UC is of electronic origin rather than phonon dominated transport as in UO_2, which implies that electronic structure methods must be used, following those already applied to other nuclear fuels [21]. It is of great importance to understand the degradation of thermal conductivity due to chemical changes (impurities, non-stoichiometry) and irradiation damage. These relative changes will be the focus of the atomistic to mesoscale simulation that provides physics interpretation of the relationship between the material property and physical parameters and enables formulating property models calibrated by a finite number of measurements.

Xenon diffusion from UC - The behavior of point defects and fission gas atoms in UC can directly feed into the engineering scale fission gas release and swelling model similar to those derived by Prajoto et al. [22]. This has been conceptually and quantitatively demonstrated for UO_2 [23, 24] and uranium silicide [25]. Under subcontract to GA through DOE funding, University of Tennessee – Knoxville has performed VASP calculations of a 3x3x3 supercell, shown in Figure 34, to quantify electronic potentials of vacancies and interstitials. The lowest energy configuration is a xenon atom on a uranium lattice site with a neighboring carbon vacancy. Activation energies for xenon diffusion for vacancy-mediated and interstitial-assisted mechanisms have been calculated and compared with experimental values as was discussed in Section 8.2.1. Assessment of radiation-enhanced diffusion is in progress. Results from these DFT calculations provide input to parameterization of XOLOTL calculations of bubble populations.

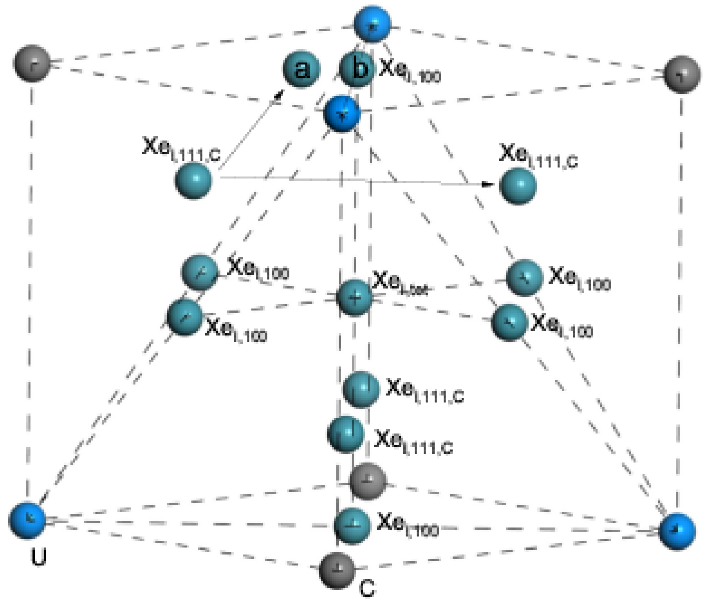

Figure 34 Possible sites for Xe within the UC lattice (courtesy UT-Knoxville)

UC thermal conductivity - One of the high priority data and modeling needs is UC thermal conductivity, especially at high burnup which is problematic data to acquire with the long-life fuel cycle proposed for EM². Recent success in microstructural modeling of mixed oxide high burnup fuel suggests that approach can be applied to UC thermal conductivity [26]. Highly-irradiated mixed oxide fuel is radially inhomogeneous in both composition and microstructure. The high burnup structure (HBS) forming at the rim region in uranium oxide fuel pellets has counterintuitive physical properties such as improved thermal conductivity even though it contains a high density of grain boundaries and micro-size gas bubbles. Before the HBS forms, the fuel grain size is about 10 microns with some pores resulting from the fuel fabrication process. After the HBS forms, the grain size decreases to about 0.1-0.3 microns. At the same time, many micro size pores or bubbles are formed. HBS starts to form at a local burnup of about 50 GWd/tHM and is fully developed at about 75 GWd/tHM. Similar surface structures have been found in samples of advanced fast reactor fuel $(U_{0.8}Pu_{0.2})C$ irradiated in the Dounreay Fast Reactor [27]. Microstructural modeling of UC is likely to undergo a similar process and will need to be confirmed by targeted experiments.

For a deeper understanding, mesoscale heat conduction simulations with inputs from atomistic simulations and experiments were recently conducted to study these phenomena [28]. The study examined the phonon scattering effects caused by small point defects such as dispersed Xe atoms in the grain structure. The high-density grain boundaries in the HBS act as defect sinks and can reduce the concentration of point defects in its grain interior and improve its thermal conductivity compared to typical large grain structures. Such microstructural and multiscale modeling improves fundamental understanding which can be applied to uranium carbide thermal conductivity modeling. Effects of accelerated testing can be compensated in the modeling to reduce uncertainties associated with extrapolating test results to nominal irradiation condition and to allow the extension of the model to higher burnups than practical testing can afford.

Mechanistic modeling of thermal conductivity includes contributions from lattice vibration or phonon transport and electron-hole pair effects. Thermal conductivity is primarily dependent on temperature with phonon transport dominant below 1500 K and electronic contributions dominant above 2000 K. Porosity and burnup, which increases porosity, are known to degrade thermal conductivity. The Lucuta model for UO_2 thermal conductivity accounts for degradation of thermal conductivity due to burnup, porosity, fission products and radiation [29]. This model was further modified by Nuclear Fuels Industries (NFI) and later modified by including the Duriez stoichiometry-dependent correlation [30]. Similar modeling can be applied to UC fuel accounting for intergranular and intragranular bubbles. The model would likely be a function of temperature, local temperature gradient, and burnup in terms of fission density.

Fission gas release from UC - FGR mechanisms in UC are similar to those in UO_2 due to their crystalline grain structure. FGR occurs through three stages: fission gas generation and transport within the grain; grain face bubble nucleation, growth and interconnection with grain edge bubbles; and fission gas transport through interconnected grain edge tunnels to free surfaces for release [31]. The diffusion of fission gas within the grain is effected by the fuel microstructure, the capture of gas atoms by intragranular bubbles, and resolution of gas atoms from these bubbles due to the impact of highly energetic fission fragments. An empirical diffusion model for UO_2 contains three contributions: intrinsic diffusion, irradiation enhanced diffusion, and athermal diffusion. The first two contributors can be obtained from a reaction-diffusion model of defect evolution parameterized by DFT and empirical potential calculations. The third contributor is obtained from direct molecular dynamics cascade and thermal spike simulations. Recent analysis of athermal diffusion for U_3Si_2 is predicted to be two orders of magnitude slower than UO_2 primarily due to its high thermal conductivity which transfers the heat in the thermal spike from the fission fragment so quickly that no displacement occurs [32, 33]. Preliminary calculations for UC, which also has a high thermal conductivity, suggest a similar conclusion.

UC creep - Creep modeling of UC can follow the same first principles approach applied to uranium silicide. The model developed by Metzger accounts for irradiation-induced creep below a homologous temperature through a Nabarro-Herring mechanism [34]. Above the homologous temperature, creep can be driven by either a Coble grain boundary creep mechanism or a dislocation creep mechanism depending on the stress state derived from a generalized Ashby diagram. The transition from irradiation-induced creep to thermal creep for UC is a factor of 0.45 times the melting temperature which Metzger also applied to uranium silicide. The grain size dependent creep model uses pre-sintering particle size data in conjunction with post-sintering grain size data to estimate grain boundary activation energies and diffusion coefficients.

Physical and mechanical properties - Mechanical testing can also be applied to investigate material properties and microstructure relationships. Microindentation techniques can be used to assess hardness, fracture toughness and related properties [35]. Results show a softening of the fuel as a result of porosity increase in the HBS. Microacoustic techniques can also be used to determine local elastic properties [36]. Young's modulus results show a decrease in UO_2 at burnup up to 100 GWd/tHM. These techniques have been applied to high burnup UO_2 to study the effects of HBS [37]. Hardness versus porosity dependence has been analyzed on the basis of the minimum solid area (MSA) model [38] which allows predictions and correlations to other properties such as thermal conductivity and Young's modulus.

SiC irradiation effect - SiC data is also available in the open literature. The effect of radiation damage has been measured up to ~100 displacement per atom (dpa) [39]. Although less than the anticipated maximum of ~350 dpa predicted for EM^2, the phenomena causing change in the material properties saturate. Thus degradation of SiC thermal conductivity and mechanical strength at such large doses are observed to plateau after ~ 2 dpa. The MD simulations have been widely used for SiC to investigate the mechanisms of deformation in the presence of a crack [40]; swelling due to intrinsic point defects and strain reduction during annealing [41]; transition from pure elastic to elastic-plastic deformation [42]; and directional amorphization due to shear-driven defects [43]. These preceding works will be translated to SiC composite to predict thermal and mechanical properties. This involves dislocation dynamics (DD) simulations, visco-plastic self-consistent models of heterogeneous microstructures, and finally development of a reduced order models using data science approach [44]. The data science approach characterizes the complex microstructures and its salient features at a higher scale that can be used to predict the effective thermal and mechanical properties of the material using a low-cost computational model. The atomistic to mesoscale modeling will supplement the existing data gap for dependency of the SiC composite properties on physical parameters.

8.2.3 Phase 2 Targeted Experiments: MiniFuel Irradiation Tests

ORNL has developed an experimental capability to perform separate effects irradiation testing of miniature fuel specimens in the High Flux Isotope Reactor (HFIR) [45]. These "MiniFuel" irradiation vehicles have a small sample size (<4 mm^3) which simplifies the design, analysis, and PIE. By reducing the fuel mass, the total heat generated inside the test capsule can be dominated by gamma heating in the structural materials instead of fission heating in the fuel.

Initial tests using the MiniFuel capsules were performed using uranium nitride (UN) kernels and UN TRISO particles [45]. Under a US DOE award to GA, ORNL and UTK, UC and UO_2 kernels will be irradiated in 2020 and 2021 in HFIR. The objective of the irradiation is to measure fission gas release and fuel swelling. The microspheres are placed in small hemispherical holes in molybdenum (Mo) cups. The capsules are seal-welded with internal helium. Figure 35 shows the parts of the MiniFuel capsule with a 6-mm inner diameter. Two target rods will each contain 6 capsules that are loaded into one of the inner small vertical experimental facility (VXF) locations in the reflector of HFIR. Two of the six capsules will contain UO_2 kernels and the other 4 capsules will contain UC kernels.

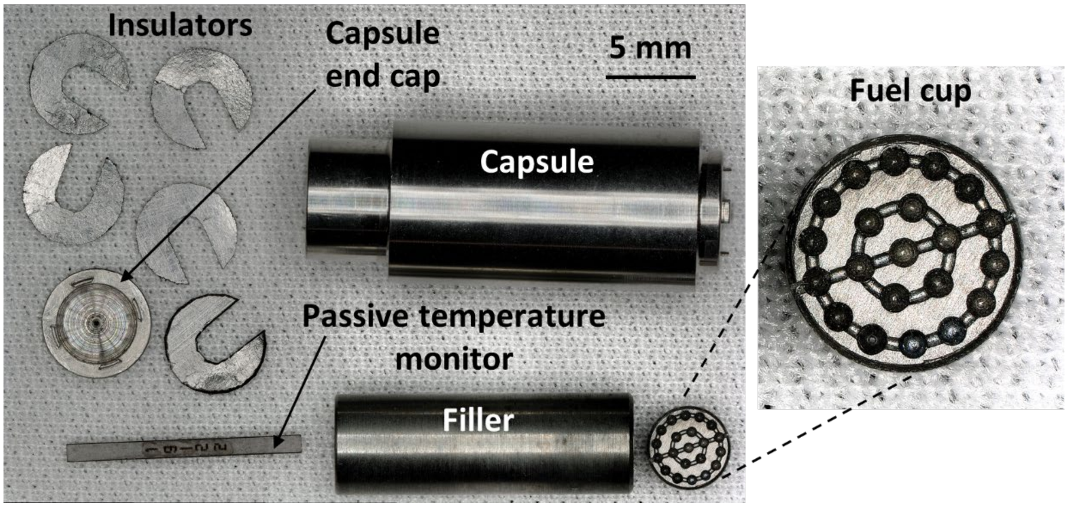

Figure 35 MiniFuel capsule for irradiation of UC kernels in HFIR (courtesy ORNL)

For the proposed irradiations, the important parameters to be controlled are burnup and temperature. One of the target rods will be irradiated for 3 cycles (1-2 at.%) and the other will be irradiated for 6 cycles (2-4 at.%). The kernels will be irradiated at two different temperatures: 850±50°C and 700±50°C. The total irradiation period is expected to be approximately one year. The ability to irradiate numerous fuel samples at the same time and to isolate the effect of variables such as burnup, temperature, and temperature gradients during irradiation testing within a reasonable time and cost is highly beneficial to accelerate the fuel qualification process.

At the end of irradiation, the target rods will be relocated to a hot-cell facility where they will be cut open to extract the capsules to measure the fission gas release and swelling. The resolution of the gas-collection system is on the order of a fraction of one μCi of Kr-85 activity. Gamma spectra from the traps will be measured to determine the xenon (Xe) and krypton (Kr) isotope content for comparison with predicted amounts from fission and fission product decay from neutronics calculations. This will give a release-to-birth ratio (R/B) for comparison with multi-scale modeling and simulation predictions.

The volumetric swelling of the UC kernels will be determined by x-ray computed tomography (XCT) of individual kernels. A 2-D image and 3-D projection of one of the UC kernels are shown in Figure 36. Volume measurements are highly repeatable indicating that the swelling measurements will have an uncertainty of ~0.5%. Depending on time and budget, microstructural examination will be performed, including energy-dispersive X-ray spectroscopy to determine distribution of solid and gaseous fission product in the irradiated samples, and electron microscopy to determine grain size, pore size, and pore distribution.

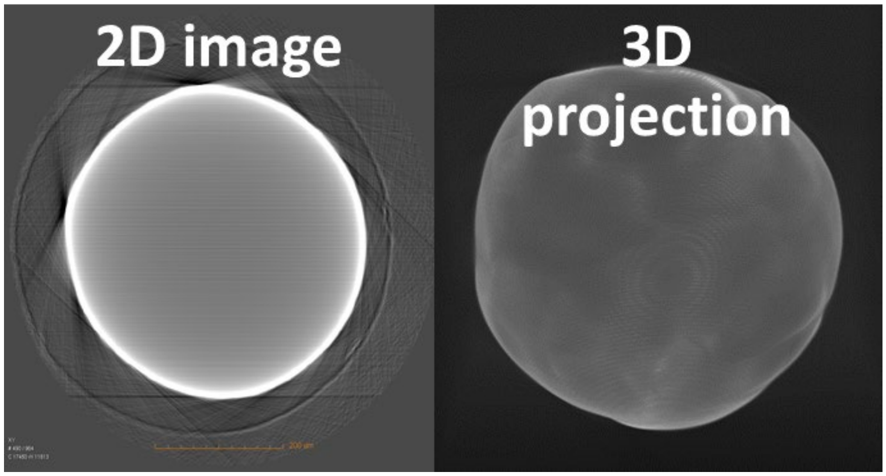

Figure 36 X-ray computed tomography images of UC kernel (courtesty ORNL)

Preliminary fuel performance analysis has been completed using BISON and post-irradiation heating tests are proposed to measure FGR at elevated temperatures. Figure 37 shows the proposed temperature profiles for UC kernels irradiated for 3- and 6-cycles and the corresponding FGR. Additional UC kernel and mini-pellet discs will be proposed to obtain irradiation data at higher temperatures, longer exposure and higher burnup.

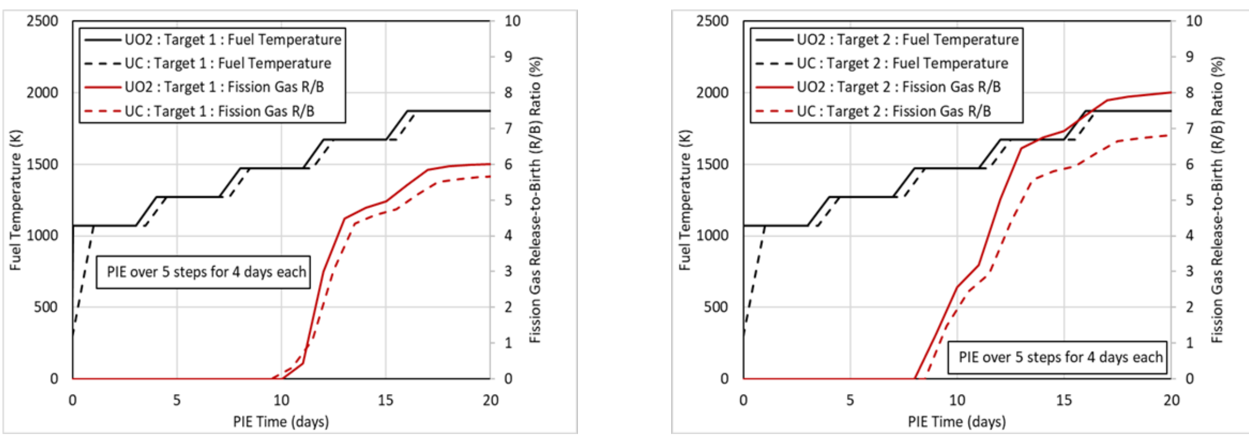

Figure 37 GA Simulation of Post-Irradiation Heating of 3- and 6-Cycle HFIR Irradiated UC Kernels

8.2.4 Phase 2 **Models and Tests for Fuel Form (Pellet) Design and Analysis: Fission Accelerated Steady-state Testing (FAST)**

For testing the fuel form, the UC pellet, INL has developed a revised capsule design for the accelerated testing of advanced reactor fuels which exploits the use of smaller diameter rodlets to increase power densities and correspondingly reduce the irradiation time required to reach high burnup [46]. An irradiation that would take 12 years to complete could be reduced to approximately 2-3 years if the fuel diameter is reduced by one-half and to around 1-2 years if the diameter is reduced by one-third. In addition, reducing fuel diameter improves radial power distribution in the fuel without the use of cadmium shrouding. This observation opens up the possibility of testing advanced reactor fuels in small irradiation locations in the ATR at INL.

The revised capsule design and approach is referred to as Fission Accelerated Steady-state Testing or FAST. With a reduction of fuel diameter and an increase in enrichment, power density is increased which produces the accelerated burnup. The capsule design can be tailored to either maintain similar cladding temperatures or similar peak fuel temperatures as compared to the reference fuel design.

Based on this revised capsule design, INL has funded a three-year laboratory-directed research and development (LDRD) project to achieve accelerated burnup of GA-fabricated UC fuel pellet [47]. The approach is prototypic in some respects since peak temperature is maintained but non-prototypic in others since temperature gradient is steeper. The first two years of the LDRD focus on fabrication and modeling of UC pins with GA as a contracted supplier of UC pellets and consultant to ensure the experiments meet GA needs. Over 24 reduced size UC pellets would be fabricated by GA during Fiscal Year 2021 (FY21) and assembled into three target rods for ATR insertion in January 2022. Two target rods would be irradiated at the same time with staggered removal so that the irradiation covers 1-, 2-, and 3-cycles of 60-day ATR exposure. Subsequent PIE work would answer critical issues of fission gas release and fuel swelling from UC pellets. Successful demonstration of this approach will lead to additional FAST irradiation of UC pellets in ATR and future fast reactor test facilities such as the VTR planned for construction at INL.

The purpose of accelerated fuel irradiation test is obtain data on the irradiated fuel form, an annular pellet, for a variety of operation conditions and design variables. The intent is to conduct all the experiments typically required for the licensing, e.g. steady-state, transient and design basis accident cases, including out-of-pile tests but with a reduced fuel size which is amenable to accelerate the fuel irradiation. However, due to the space constraints of the irradiation capsule, the physical size of the pellet will be small than the designed fuel size for EM^2. The smaller size also presents a benefit because the fuel irradiation time is reduced by a factor of ~10 when reducing the physical size of the planned test article, multiple irradiation tests can be launched simultaneously under different operating condition and with different fabrication parameters.

As the size of the fuel pellet is reduced to accelerate the irradiation when compared with the as-fabricated fuel, the models developed from the accelerated irradiation tests need to be scaled up to be applicable to the as-fabricated fuel. For the purpose of scaling up, the irradiation data should be generated with different fuel sizes. The analysis will adopt machine learning algorithm to develop the scaling model. This algorithm uses computational methods to “learn” information directly from data without assuming a predetermined equation as a model and adaptively improves its performance as the number of samples available for learning increases. Therefore, it finds natural patterns in data that generate insight and helps make better decisions and predictions by discovering the underlying correlations behind the data and the fundamental phenomena.

8.2.5 Phase 3: Integral Fuel Testing

As discussed in the previous sections, in the AFQ Phases 1 and 2, the modeling of the UC kernel uses atomistic and meso-scale approaches to derive key model parameters and to inform irradiation testing. These material properties and models of UC kernels are used to build continuum-scale models of the UC pellets. The SiC composite cladding also uses continuum-scale modeling and test data due to its engineered composite structure. With science-based models, integral irradiation tests can be more focused on validating parameters and confirming expected trends and inflection points in the models. Science-based models may also allow greater flexibility in interpolation and extrapolation beyond the irradiation database.

Phase 3 will be informed by Phase 2 for integral testing. Integral fuel testing may initially be performed using reduced size rodlets of UC pellets within SiGA cladding. These rodlets could be irradiated in Advanced Test Reactor (ATR) in a test capsule adopted from the Advanced Gas Reactor (AGR) fuel program. When the Versatile Test Reactor (VTR) has been built and finished commissioning tests, the gas-cooled cartridge test loop being designed by GA-EMS will be used to irradiate EM^2 rodlets under more prototypical conditions of temperature and fast neutron flux. Both the ATR and VTR tests can be accelerated using higher than normal fission density. The enrichment in ^{235}U may have to be greater than 20 weight % in order to accelerate the burnup. The data from these integral fuel tests will be used to establish the safety case for the fuel sufficient for use in a reduced-scale demonstration reactor with prototypic conditions.

Engineering-scale modeling and simulation tools along with early irradiation testing provides feedback to the materials data and design parameters to refine subsequent integral fuel testing. Targeted separate-effects testing can further refine the safety case and minimize efforts on parameters with little or no effect on fuel performance. Integral tests under prototypical conditions to full burnup will ultimately be required to fully qualify the fuel system for its entire life cycle. For a long-life fuel, this testing to acquire qualification data may be obtained in a bootstrapping way with a demonstration reactor.

8.3 Overall EM^2 Qualification Plan

For the safety analysis and licensing of the fuel, computer simulations are required to predict the fuel behavior during normal and abnormal operations by simultaneously treating all aspects of fuel performance in a self-consistent way. The need for best estimate simulations of the fuel necessitates the validation of the computer code against good quality data produced from experiments under relevant as-fabricated fuel operating conditions. Initial testing in HFIR and ATR using thermal spectrum neutron exposure will produce the data to enable identification and planning for future targeted experiments to provide fast spectrum data needed for licensing. The experiments could be conducted in a designated test loop of a test reactor like VTR [48, 49] or other fast reactors with appropriate experimental loops. The validation tests will be conducted for the as-fabricated fuel rodlet and the results will be used for benchmarking computer codes. These activities will raise the TRL up to 6, which is required to license the fuel for a demonstration reactor.

The validation tests would focus on fuel behavior such as radial flux depression, fuel creep, fuel densification, fuel swelling and cladding creep down, which are essential when evaluating the material properties and models being used in the code. On the other hand, for the licensing purpose, the code should provide reliable calculation results of fuel temperatures, stored heat, fission product release, rod internal pressure, and corrosion effect. Therefore, these data are also of particular interest of the code validation. For example, assessment of a licensing code FRAPCON-4.0 included validation against experimental data such as fuel center temperature vs. burnup, steady-state and power-ramped FGR, internal rod void volume, cladding corrosion, and cladding hoop strain during power ramp [50]. For the transient code FRAPTRAN-2.0, the experimental data of cladding hoop strain, cladding failure, and FGR are used for RIA, while those of cladding ballooning, failure, and pressure; residual hoop strain; and high-temperature oxidation were used for LOCA [51].

GA expects that it is impractical for the irradiation test for validation to continue to the end of life of the EM^2 fuel prior to licensing a full-scale EM^2 power plant. However, it should be noted that the primary objective of the AFQ is to reduce the number of measurements by adopting mechanistic property models in the code and to evaluate those models through the accelerated irradiation tests, which could be either prototypic or non-prototypic. The non-prototypic fuel irradiation conditions by the nature of the accelerated irradiation tests will actually enable the property models to be evaluated for a wide range of application. As such, the validation tests will be conducted to confirm the functionality of integrated property models for the as-fabricated EM^2 fuel. The measurements shall focus on the fuel rod deformation and other key performance parameters. It is expected that the appropriate burnup range would be 35 to 50 GWd/t, where the fuel is already densified, the cladding swelling is in an asymptotic range, significant amount of fission gases are released, fuel and cladding creeps are developed, and the fuel swelling is accommodated by the open pore to a certain extent. The recommended validation plan is as follows:

- Perform appropriate phenomena identification and ranking tables (PIRTs) for key safety phenomena.
- Define evaluation models and perform assessment matrix table (AMT) to determine how well phenomena are modeled and identify data and modeling gaps
- Steady-state irradiation of the as-fabricated fuel rod up to 35-50 GWd/t, followed by measurements of the fuel rod deformation, fission gas release, pellet deformation, porosity, microstructure, etc.
- Transient tests of irradiated fuel for RIA and LOCA conditions and measurements of the fuel rod deformation, fission gas release, and fuel failure.

- Steady-state irradiation of the as-fabricated fuel rod up to 100 GWd/t, followed by measurements of the fuel rod deformation, fission gas release, pellet deformation, porosity, microstructure, etc.

Accelerated fuel irradiation using the FAST approach can reach EOL burnup but is not prototypic due to the high fission density. Due to the long-life of the EM^2 fuel, prototypic irradiation to EOL burnup is not practical. Advanced M&S tools can greatly reduce the uncertainties in the safety case to qualify EM^2 fuel for long irradiation exposure. The licensing path for the first demonstration reactor, chosen in consultation with the NRC, will be either as a 10 CFR 50 commercial application under Sec. 103, or as a test reactor under Sec. 104c. In either licensing path, a phased prototype testing approach, such as described in the Massachusetts Institute of Technology (MIT) report [52], may also be appropriate. The licensing, design, and construction data from the demonstration reactor will become the foundation of design certification of commercial units. Since fuel performance in a fast neutron flux is the most critical data to obtain, designation as a test reactor may be a more expeditious option that would still allow for up to 50% cost recovery from electricity revenue. Fast spectrum fuel irradiation is a prerequisite for post-irradiation testing of representative fuel samples. Testing activities will include:

- Integral testing of fuel, along with appropriate modeling and simulation working hand-in-hand to achieve accelerated fuel qualification.
- Accelerated testing, PIE, and post-irradiation heating tests of fuel irradiated in the gas cartridge loop of the VTR. Unlike the ATR testing, these tests will be more representative of EM2 fast spectrum conditions.
- Verification of demonstration reactor and fuel performance during low power testing during a slow power ascension testing phase with data gathering hold points.
- Fuel surveillance, inspection, and removal for testing in a hot cell during prototype testing phase of demonstration reactor. Fuel assemblies would be removed periodically during the first several years of prototype testing.

Commercial licensing will follow when enough data from the demonstration has been acquired for licensing. If burnup data for the full duration of the fuel element is unavailable at the time of design certification, as is likely, then conditional licensing will be pursued to operate the commercial plant, until full burnup data is available from the demonstration unit, or VTR testing.

The goal of the above testing plan is to refine and validate the fuel and cladding performance models to provide confidence in the safety performance sufficient for qualification in the design certification for commercial units either under 10 CFR 52 or 10 CFR 53, as appropriate. Advanced reactor licensing under the new licensing framework (10 CFR 53) is expected to be consistent with 10 CFR 50 and 52 but without the prescriptive requirements associated with the existing LWR licensing framework. When 10 CFR 53 is available, it would be the preferred licensing path.

8.4 Summary of Key Elements in Accelerated Fuel Qualification

Atomistic and mesoscale modeling will lead to development of mechanistic models that can be validated by experimental data to add confidence and reduce uncertainty particularly when extrapolating to higher burnup and when compensating for effects of accelerated irradiation at much higher than normal fission density. The mechanistic models will reduce the dependence on models derived from purely empirical data because the functional relationships of key dependent variables are science-based.

Pre-irradiation characterization and PIE require much more extensive microstructural measurements to support the advanced M&S tools. The result of using advanced M&S is a set of science-based models that can predict long-term irradiation behavior of the EM^2 fuel system to prevent fuel damage and failure, thus ensuring fuel coolability during severe accidents. Empirical models are inherently limited to the database used to create them. Science-based models use better mathematical descriptions of the physics and mechanisms of the underlying material properties to enable them to have better fidelity than the limitations purely empirical database. Variations and uncertainties in specifications can be accommodated in science-based models to reduce excess margin normally applied to empirical models.

Advanced M&S, FAST fuel irradiation, and MiniFuel capsule irradiation are all expected to reduce the number and cost of fuel irradiations. The number of irradiations is greatly reduced because the models are science based rather than empirically based. Empirically-based models require a much larger database to establish the foundation of the empirical model. Both the FAST and MiniFuel irradiations are accelerated which reduce both the cost and schedule as compared with prototypic irradiation. Fuel qualification will ultimately rely on integral fuel data from a reduced-scale prototype or demonstration reactor as described in Section 8.3.

9 REFERENCES

Section 1

[1] “Technical Program Plan for INL Advanced Reactor Technologies Technology Development Office / Advanced Gas Reactor Fuel Development and Qualification Program,” Idaho National Laboratory, PLN-3636 Rev. 6, June 2017.

[2] J. Opperman, “Original Proposal for DOE Award No: ARD-18-15066 – Combining Multi-Scale Modeling with Microcapsule Irradiation to Expedite Advanced Fuels Deployment,” General Atomics document GA-A29413, October 2020.

[3] S. Kwon, “Demonstrate Viability of Accelerated Fuel Qualification Approaches,” FY20 LDRD Proposal, Idaho National Laboratory, 2019.

[3] R. Faibish, “Accelerated Fuel Qualification (AFQ) Workshop I Summary Report,” General Atomics document GA-A29407, November 2020.

[4] R. Faibish, “Accelerated Fuel Qualification (AFQ) Workshop II Summary Report,” General Atomics document GA-A29408, November 2020.

Section 4

[1] A. Sheth, L. Leibowitz, "Equation-of-state for Advanced Fuels," ANL-AFP-2, Argonne National Laboratory, 1974.

[2] J. Carmack, K. O. Pasamehmetoglu, "Review of Transmutation Fuel Studies," INL/EXT-08-13779, Idaho National Laboratory, 2008.

[3] P. R. Roy, C. Ganguly, "Plutonium Metallurgy in India," *Bull. Mater. Sci.*, Vol. 6, No. 5, pp. 923-958, 1984.

[4] BARC, "Fuel Property Evaluation," Bhabha Atomic Research Centre; barc.ernet.in/publications/eb/ golden/nfc/toc/Chapter%203/3.pdf, 2012.

[5] C. Latgé, "Synergy between LFR & SFR," Helimnet Meeting, Bologna, Italy, Jan. 19, 2011.

[6] IAEA, "Status and Trends of Nuclear Fuels Technology for Sodium Cooled Fast Reactors," IAEA Nuclear Energy Series No. NF-T-4.1, International Atomic Energy Agency, 2011.

[7] R. L. Gutierrez, R. J. Herbst, K. W. R. Johnson, "Preliminary Fabrication Studies of Alternative LMFBR Carbide Fuels," LA-7901-MS, Los Alamos National Laboratory, 1979.

[8] NRC, "Standard Review Plan for the Review of Safety Analysis Reports for Nuclear Power Plants: LWR Edition - Reactor (NUREG-0800, Chapter 4)," NUREG-0800, U.S. Nuclear Regulatory Commission, 2007.

[9] Y. Katoh, K. Ozawa, C. Shih, T. Nozawa, R. J. Shinavski, A. Hasegawa, L. L. Snead, "Continuous SiC fiber, CVI SiC matrix composites for nuclear applications: Properties and irradiation effects," *J. Nuclear Materials* 448, pp. 448–476, 2014.

[10] L. L. Snead, Y. Katoh, T. Nozawa, Comprehensive Nuclear Materials, p.215, R. J. M. Konings, Ed., Elsevier, New York, 2012.

[11] L. L. Snead, T. Nozawa, Y. Katoh, T. Byun, S. Kondo, D. A. Petti, "Handbook of SiC properties for fuel performance modeling," *J. Nuclear Materials* 371, pp. 329-377, 2007.

[12] ASME, "2015 ASME Boiler and Pressure Vessel Code," ASME BPVC.III.1.NB-2015, The American Society of Mechanical Engineers, 2015.

[13] W. E. Windes, P. A. Lessing, Y. Katoh, L. L. Snead, E. Lara-Curzio, J. Klett, C. Henager, Jr., R. J. Shinavski, "Structural Ceramic Composites for Nuclear Applications," INL/EXT-05-00652, Idaho National Laboratory, 2005.

[14] C. P. Deck et al., "Demonstration of Engineered Multi-layered SiC-SiC Cladding with Enhanced Accident Tolerance," Reactor Fuel Performance 2018, Prague, Czech Republic, Sept. 3 – Oct. 4 (2018).

[15] J. G. Stone, R. Schleicher, C. P. Deck, G. M. Jacobsen, H. E. Khalifa, C. A. Back, "Stress analysis and probabilistic assessment of multi-layer SiC-based accident tolerant nuclear fuel cladding," *J. Nuclear Materials* 466, pp. 682-697, 2015.

[16] G. M. Jacobsen, J. G. Stone, H. E. Khalifa, C. P. Deck, C. A. Back, "Investigation of the C-ring test for measuring hoop tensile strength of nuclear grade ceramic composites," *J. Nuclear Materials* 452, pp. 125-132, 2014.

[17] S. Zhu, M. Mizuno, Y. Kagawa, Y. Mutoh, “Monotonic tension, fatigue and creep behavior of SiC-fiber-reinforced SiC-matrix composites: a review,” *Composites Science and Technology* 59, pp. 833-851, 1999.
[18] F. Montgomety, “Fission-product SiC reaction in HTGR fuel,” 905837, General Atomics, 1981.

Section 5

[1] K. J. Geelhood, W. G. Luscher, P. A. Raynaud, I. E. Porter, “FRAPCON-4.0: A Computer Code for the Calculation of Steady-State, Thermal-Mechanical Behavior of Oxide Fuel Rods for High Burnup,” PNNL-19418, Vol.1 Rev.2, Pacific Northwest National Laboratory, 2015.
[2] K. J. Geelhood, W. G. Luscher, J. M. Cuta, I. E. Porter, “FRAPTRAN-2.0: A Computer Code for the Transient Analysis of Oxide Fuel Rods PNNL-19400, Vol.1 Rev.2, Pacific Northwest National Laboratory, 2016.
[3] K. J. Geelhood and W. G. Luscher, “FRAPCON-4.0: Integral Assessment,” PNNL-19418, Vol. 2, Rev. 2, Pacific Northwest National Laboratory, 2015.
[4] T. Preusser, "Modeling of Carbide Fuel Rods," *Nuclear Technology* 57, pp. 343-371, 1982.
[5] G. Jacobsen, H. Chiger, “General Atomics Silicon Carbide Cladding,” GA-A28712, General Atomics, 2017.
[6] A. Sheth, L. Leibowitz, "Equation-of-state for Advanced Fuels," ANL-AFP-2, Argonne National Laboratory, 1974.
[7] P. R. Roy, C. Ganguly, "Plutonium Metallurgy in India," *Bull. Mater. Sci.*, Vol. 6, No. 5, pp. 923-958, 1984.
[8] R. De Coninck, W. Van Lierde, A. Gijs, "Uranium Carbide: Thermal Diffusivity, Thermal Conductivity and Spectral Emissivity at High Temperatures," *J. Nuclear Materials* 57, pp. 69-76, 1975.
[9] J. L. Bates, “Thermal Conductivity and Electrical Resistivity of Uranium Oxycarbide,” Battelle Memorial Institute report BNWL-989, 1969.
[10] M. J. Wheeler, “Thermal Conductivity of Uranium Monocarbide,” in *Carbides in Nuclear Energy*, Vol. 1, L. R. Russell et al., Eds. (Macmillan, London, 1964), pp. 358-364.
[11] L. E. Russell, “The Structure and Properties of UC and (U,PU)C Alloys,” Proc. Conf. on New Nuclear Materials Technology Including Non-Metallic Fuel Elements, pp. 409-423, Prague, Czech, July 1-5, 1963.
[12] H. Steiner, “Das Materialverhalten Der Karbidischen Brennstoff,” IMF-Bericht 229, PBSBericht 440 (1b), Kernforschungszentrum Karlsruhe (1975) (in German).
[13] J. L. Bates, “Thermal Conductivity of Uranium Oxycarbide,” Thermal Conductivity: Proc. 7th Conf.,
Gaithersburg, Maryland, Nov. 13–16, 1967.
[14] H. D. Lewis, J. F. Kerrisk, “Electric and Thermal Transport Properties of Uranium and Plutonium Carbide,” LA-6096, Los Alamos National Laboratory, 1976.

[15] S. Corradetti, M. Manzolaro, A. Andrighetto, P. Zanonato, S. Tusseau-Nenez, “Thermal conductivity and emissivity measurements of uranium carbides,” *Nuclear Instruments and Methods in Physics Research Section B: Beam Interactions with Materials and Atoms* 360, pp. 46-53, 2015.

[16] D. Stahl, A. Strasser, K. Taylor, J. Anderson, "Out-of-pile Properties of Mixed Uranium-Plutonium Carbides," UNC-5074, United Nuclear Corporation, 1963.

[17] G. M. Nickerson, W. E. Kastenberg, "Preliminary Assessments of Carbide Fuel Pins during Mild Overpower Transients in LMFBRs," *Nuclear Engineering and Design* 36, pp. 209-233, 1976.

[18] Hj. Matzke, *Science of advanced LMFBR fuels*, Chapter 4, North-Holland, p. 176, 1986.

[19] IAEA, "Status and Trends of Nuclear Fuels Technology for Sodium Cooled Fast Reactors," IAEA Nuclear Energy Series No. NF-T-4.1, International Atomic Energy Agency, p. 72, 2011.

[20] R. N. Singh, "Mechanical Property and Diffusion Data for Advanced Carbide and Nitride Fuels," ANL-AFP-15, Argonne National Laboratory, 1976.

[21] A. Padel, Ch. De Novion, "Constantes elastiques des carbures, nitrures et oxydes d'uranium et de plutonium," *J. Nuclear Materials* 33, pp. 40-51, 1969.

[22] K. Lassmann, "URANUS-A Computer Programme for the Thermal and Mechanical Analysis of the Fuel Rods in a Nuclear Reactor," *Nuclear Engineering and Design* 45, p. 325, 1978.

[23] J. R. Matthews, "Mechanical Properties and Diffusion Data for Carbide and Oxide Fuels," AERE-M 2643, U.K. Atomic Energy Authority, 1974.

[24] W. Dienst, “Swelling, densification and creep of (U,Pu)C fuel under irradiation,” *J. Nuclear Materials* 124, pp. 153-158, 1984.

[25] J. E. Frank, "Irradiation Behavior of Unalloyed Uranium Carbide," AI-CE-MEMO-9, Atomics International-Combustion Engineering, 1966.

[26] J. W. Harrison, “The Irradiation-Induced Swelling of Uranium Carbide,” *J. Nuclear Materials* 30, pp. 319-323, 1969.

[27] C. Grando, M. Montgomery, A. Strasser, "Unrestrained Swelling and Fission-Gas-Release Experiments of Fast Reactor Fuels," *Trans. Am. Nucl. Soc.* 14, Suppl. 1, p. 36, 1971.

[28] W. Chubb, R. F. Hilbert, V. W. Storhok, D. L. Keller, "Fission Gas Swelling of Refractory Nuclear Fuels," *Materials Science and Engineering* 9, pp. 293-300, 1972.

[29] H. Michailoff, "Fundamental Results on Irradiated Carbides: Fission Product Release, Fuel Swelling and Evolution of Composition," *Trans. Am. Nucl. Soc*. 19, p. 89, 1974.

[30] R. Lallement, H. Michailoff, J. Ravier, "Carbide Fuel Elements for Fast Reactors-Research and

Development Program," *Trans. Am. Nucl. Soc*. 20, p. 296, 1975.

[31] F. Caligara, "TPROF-A: A Computer Code for Analysing the Behaviour of the Advanced Fuels," European Institute for Transuranium Elements, Karlsruhe, 1978.

[32] H. G. Bogensberger, C. Ronchi, "Effects due to fission gas during unprotected overpower transients in a liquid metal fast breeder reactor," *Nuclear Technology* 29, p. 73, 1976.

[33] P. Prajoto, A. R. Wazzan, D. Okrent, "Computer Modelling of Steady State Fission Gas Behaviour in
Carbide Fuels," *Nuclear Engineering and Design* 48, p. 461, 1978.
[34] J. R. Matthews, M. H. Wood, "Modelling the Transient Behaviour of Fission Gas," *J. Nuclear Materials* 84, p. 125, 1979.
[35] F. A. Rough and W. Chubb, Eds., "Progress on the Development of Uranium Carbide-Type Fuels," BMI-1370, Battelle Memorial Institute, 1959.
[36] H. Shaked, D. R. Olander, T. H. Pigford, "Diffusion of Xenon in Uranium Monocarbide," *Nucl. Sci.*
Eng. 29, p. 122, 1967.
[37] H. Choi, "Evaluation of Carbide Fuel Property and Model Using Measurement Data from Early Experiments," *Nuclear Technology* 204, pp. 283-298 (2018).
[38] L. L. Snead, T. Nozawa, Y. Katoh, T. Byun, S. Kondo, D. A. Petti, "Handbook of SiC properties for fuel performance modeling," *J. Nuclear Materials* 371, pp. 329-377, 2007.
[39] Y. Katoh, K. Ozawa, C. Shih, T. Nozawa, R. J. Shinavski, A. Hasegawa, L. L. Snead, "Continuous SiC fiber, CVI SiC matrix composites for nuclear applications: Properties and irradiation effects," *J. Nuclear Materials* 448, pp. 448–476, 2014.
[40] T. Koyanagi, Y. Katoh, G. Singh, M. Snead, "SiC/SiC Cladding Materials Properties Handbook," ORNL/TM-2017/385, Oakridge National Laboratory, 2017.
[41] J. G. Stone, R. Schleicher, C. P. Deck, G. M. Jacobsen, H. E. Khalifa, C. A. Back, "Stress analysis and probabilistic assessment of multi-layer SiC-based accident tolerant nuclear fuel cladding," *J. Nuclear Materials* 466, pp. 682-697, 2015.
[42] G. Jacobsen and H. Chiger, "Materials Property Manual: General Atomics Silicon Carbide Cladding," General Atomics document GA-A28712, November 2017.
[43] R. Brandt, M. Friess, G. Neuer, "Thermal Conductivity, Specific Heat Capacity, and Emissivity of Ceramic Matrix Composites at High Temperatures," *High Temperatures-High Pressures* 35/36, p. 169-177, 2003.
[44] S. Zhu, "Monotonic tension, fatigue and creep behavior of SiC-fiber-reinforced SiC-matrix composites: a review," *Composites Science and Technology* 59, pp. 833-851, 1999.
[45] Y. Katoh, N. Hashimoto, S. Kondo, L. L. Snead, A. Kohyama, "Microstructural development in cubic silicon carbide during irradiation at elevated temperatures," *J. Nuclear Materials* 351, p. 228-240, 2006.
[46] T. Koyanagi, Y. Katoh, K. Ozawa, K. Shimoda, T. Hinoki, L. L. Snead, "Neutron-irradiation creep of silicon carbide materials beyond the initial transient," *J. Nuclear Materials* 478, pp. 97-111, 2016.
[47] E. F. Ibrahim, "In Reactor Tubular Creep of Zircaloy-2 at 260 to 300 C," *J. Nuclear Materials* 46, pp. 169-182, 1973.

[48] S. Zhu, J. Cao, M. Mizuno, Y. Kagawa, "Time-Dependent Deformation in an Enhanced SiC/SiC Composite," *Metallurgical and Materials Transactions A*, Vol. 35, Issue 9, pp. 2853–2859, 2004.

[49] R.T. Bhatt, "Creep/Stress Rupture Behavior of 3D Woven SiC/SiC Composites with Sylramic-iBN, Super Sylramic-iBN and Hi-Nicalon-S Fibers at 2700F in Air," 41th Annual Conference on Composites, Materials, and Structures, Cocoa Beach/Cape Canaveral, January 2017.

Section 6

[1] K. J. Geelhood, W. G. Luscher, P. A. Raynaud, I. E. Porter, "FRAPCON-4.0: A Computer Code for the Calculation of Steady-State, Thermal-Mechanical Behavior of Oxide Fuel Rods for High Burnup," PNNL-19418, Vol.1 Rev.2, Pacific Northwest National Laboratory, 2015.

[2] K. J. Geelhood, W. G. Luscher, J. M. Cuta, I. E. Porter, "FRAPTRAN-2.0: A Computer Code for the Transient Analysis of Oxide Fuel Rods PNNL-19400, Vol.1 Rev.2, Pacific Northwest National Laboratory, 2016.

[3] J. W. Harrison, "The Irradiation-Induced Swelling of Uranium Carbide," *J. Nuclear Materials* 30, pp. 319-323, 1969.

[4] J. T. Goorley et al., "MCNP6 User's Manual Version 1.0," LA-CP-13-00634, Los Alamos National Laboratory (2013).

[5] W. Chubb et al., "Nonswelling Uranium Nitride Fuel," U.S. Patent 3,661,709 (1972).

[6] R. W. Stratton and L. Smith, "The Irradiation Behavior of Sphere-pac Carbide Fuel," *Proc. Int. Meeting Advanced LMFBR Fuels*, pp. 348-360, Tucson, Arizona, Oct. 10-13 (1977).

[7] A. van der Linde, H. J. B. Luijckx, and J. H. N. Verheugen, "Fabrication, Irradiation and Post-irradiation Examinations of MO_2 and UO_2 Sphere-pac and UO_2 Pellet Fuel Pins Irradiated in a PWR Loop," EUR 7599 EN, Netherlands Energy Research Foundation (1982).

[8] K. L. Peddicord, R. W. Stratton, and J. K. Thomas, "Analytical and Experimental Performance of Sphere-pac Nuclear Fuels," *Progress in Nuclear Energy* 18, pp. 265-299 (1986).

[9] R. W. Schleicher, "Energy Multiplier Module Conceptual Technical Description: Volume VIII – Shutdown Heat Removal Systems," General Atomics, 2012.

Section 7

[1] D. Crawford et al., "An approach to fuel development and qualification," *J. of Nuclear Materials* 371, 232-242, 2007.

Section 8

[1] K. A. Terrani, et al., "Accelerating nuclear fuel development and qualification: Modeling and simulation integrated with separate-effects testing," J. of Nuclear Materials 539, 152267, 2020.

[2] W. Wen et al., “Mechanism-based modeling of thermal and irradiation creep behavior: An application to ferritic/martensitic HT9 steel,” LA-UR-19-28064, Los Alamos National Laboratory, 2019.
[3] M. Toloczko et al., “Comparison of thermal creep and irradiation creep of HT9 pressurized tubes at test temperatures from ~490ºC to 605ºC,” S. T. Rosinski, Ed., *Effects of Radiation on Materials: 20th International Symposium*, ASTM International, 2001.
[4] H. Shaked, et al., “Diffusion of xenon in uranium monocarbide,” *Nuclear Science and Engineering* 29, 122-130, 1967.
[5] Bévillon, et al., “Investigation of the diffusion of atomic fission products in UC by density functional calculations,” *J. of Nuclear Materials* 434, 240-247, 2013.
[6] R. Lindner and Hj. Matzke, “Diffusion radioaktiver Edelgase in Uranoxyden und Uranmonokarbid,” *Zeitschrift für Naturforschung* 14a, 1074-1077, 1959.
[7] A. Auskern and Y. Osawa, “Xenon Diffusion in Uranium Carbide Powder,” *J. of Nuclear Materials* 6, 334-335, 1962.
[8] R. L. Ritzman et al., “Interpretation of Fission Gas Behavior in Refractory Fuels,” *Nuclear Applications and Technology* 9, 167, 1970.
[9] M. R. Tonks et al., “Mechanistic materials modeling for nuclear fuel performance,” *Annals of Nuclear Energy* 105, 11–24, 2017.
[10] A. D. Andersson, “Simulation of Fission Gas in Uranium Oxide Nuclear Fuel,” NE SciDAC annual report, 2018.
[11] G. Kresse, M. Marsman, J. Furthmüller, “The VASP Manual,” Universität Wien, Austria, 2018.
[12] S. Blondel et al., “Xolotl: a cluster dynamics code to predict gas bubble evolution in solids,” 2018 Scientific Discovery through Advanced Computing (SciDAC-4) Principal Investigator Meeting, Washington DC, July 23 - 24, 2018.
[13] M. R. Tonks et al., “Assessment of MARMOT: A Mesoscale Fuel Performance Code,” INL/EXT-15-35108, Idaho National Laboratory, 2015.
[14] D. Gaston, G. Hansen, C. Newman, “MOOSE: A Parallel Computational Framework for Coupled Systems of Nonlinear Equations,” INL/CON-08-15008, Idaho National Laboratory, 2009.
[15] SNL, “LAMMPS Molecular Dynamics Simulator,” https://lammps.sandia.gov/index.html, 2019.
[16] M. Freyss, “First-principles study of uranium carbide: Accommodation of point defects and of helium, xenon, and oxygen impurities,” *Physical Review B* 81, 014101, 2010.
[17] B. D. Sahoo et al., “Ab initio study on structural stability of uranium carbide,” *J. of Nuclear Materials* 437, 81–86, 2013.
[18] S. Starikov, M. Korneva, “Description of phase transitions through accumulation of point defects: UN, UO2 and UC,” *J. of Nuclear Materials* 510, 373-381, 2018.
[19] S. Maiti, P. H. Geubelle, “Mesoscale Modeling of Dynamic Fracture of Ceramic Materials,” *Computer Modeling in Engineering and Sciences* 5, 91-101, 2004.
[20] É. Bévillon et al., “First-principles study of the stability of fission products in uranium monocarbide,” *J. of Nuclear Materials* 426, 189–197, 2012.

[21] Q. Yin et al., “Electronic correlation and transport properties of nuclear fuel materials”, *Physical Review B* 84, 195111, 2011.

[22] P. Prajoto, A. R. Wazzan, D. Okrent, “Computer modeling of steady state fission gas behavior in carbide fuels,” *Nuclear Engineering and Design* 48, 461-495, 1978.

[23] D. A. Andersson et al., “Atomistic modeling of intrinsic and radiation-enhanced fission gas (Xe) diffusion in UO2±x: Implications for nuclear fuel performance modeling,” *J. of Nuclear Materials* 451, 225–242, 2014.

[24] D. A. Andersson et al., “Multiscale simulation of xenon diffusion and grain boundary segregation in UO2,” *J. of Nuclear Materials* 462, 15–25, 2015.

[25] D. A. Andersson et al., “Density functional theory calculations of self- and Xe diffusion in U_3Si_2,” J. of Nuclear Materials 515, 312-325, 2019.

[26] M. Teague, M. Tonks, S. Novascone, S. Hayes, “Microstructural modeling of thermal conductivity of high burnup oxide fuel,” *J. of Nuclear Materials* 444, 161-169, 2014.

[27] I. L. F. Ray, Hj. Matzke, “Observation of a high burnup rim-type structure in advanced plutonium-uranium carbide fuel,” *J. of Nuclear Materials* 250, 242-243, 1997.

[28] X. Bai, M. Tonks, Y. Zhang, J. Hales, “Multiscale modeling of thermal conductivity of high burnup structures in UO_2 fuels,” *J. of Nuclear Materials* 470, 208-215, 2016.

[29] P. G. Lucuta, H. S. Matzke, and I. J. Hastings, “A pragmatic approach to modeling thermal conductivity of irradiated UO_2 fuel: review and recommendations,” *J. of Nuclear Materials* 232, 166-180, 1996.

[30] C. Duriez, J.-P. Allesandri, T. Gervais, and Y. Philipponnea, “Thermal conductivity of hypo-stoichiometric low Pu content $(U,Pu)O_{2-x}$ mixed oxide,” *J. of Nuclear Materials* 277, 143-158, 2000.

[31] M. Tonks et al., “Unit mechanisms of fission gas release: current understanding and future needs,” *J. of Nuclear Materials* 504, 300-317, 2018.

[32] T. Barani et al., “Multiscale modeling of fission gas behavior in U_3Si_2 under LWR conditions,” *J. of Nuclear Materials* 522, 97-110, 2019.

[33] B. Beeler et al., “Molecular dynamics investigation of grain boundaries and surfaces in U_3Si_2,” *J. of Nuclear Materials* 514, 290-298, 2019.

[34] K. E. Metzger, “Analysis of pellet cladding interaction and creep of U_3Si_2 fuel for use in light water reactors,” PhD thesis, University of South Carolina, 2016.

[35] J. Spino, J. Cobos-Sabate, F. Rousseau, “Room-temperature microindentation behavior of LWR-fuels, part 1: fuel microhardness,” *J. of Nuclear Materials* 322, 204-216, 2003.

[36] D. Laux et al., “Determination of high burn-up nuclear fuel elastic properties with acoustic microscopy,” J. of Nuclear Materials 420, 94-100, 2012.

[37] F. Cappia et al., “Microhardness and Young’s modulus of high burn-up UO_2 fuel,” *J. of Nuclear Materials* 479, 447-454, 2016.

[38] R. W. Rice, Porosity of Ceramics, Marcel Dekker, New York, 1998.

[39] T. Koyanagi et al., “In-pile tensile creep of chemical vapor deposited silicon carbide at 300ºC,” *J. of Nuclear Materials* 521, 63-70, 2019.

[40] A. Romano, J. Li, S. Yip, “Atomistic simulation of rapid compression of fractured silicon carbide,” *J. of Nuclear Materials* 352, 22–28, 2006.

[41] L. Pizzagalli, “Atomistic modeling of point defect contributions to swelling in Xe-implanted silicon carbide,” *J. of Nuclear Materials* 512, 349-356, 2018.

[42] K. Nishimura, K. Miyake, K. Saitoh, “Molecular dynamics study on defect formation in SiC film,” LAMMPS Workshop and Symposium, Albuquerque, Aug. 13-15, 2019.

[43] R. M. Flanagan et al., “Non-equilibrium simulations of shock-induced horizontal defects and amorphization in 4H silicon carbide,” LAMMPS Workshop and Symposium, Albuquerque, Aug. 1-3, 2017.

[44] P. Altschuh et al., “Data Science Approaches for Microstructure Quantification and Feature Identification in Porous Membranes,” J. of Membrane Science 540, 88–97, 2017.

[45] C. Petrie et al., “Separate effects irradiation testing of miniature fuel specimens,” J. of Nuclear Materials 526, 1-14, 2019.

[46] G. L. Beausoleil, B. J. Curnutt, and G. L. Povirk, “A Revised Capsule Design for the Accelerated Testing of Advanced Reactor Fuels,” Idaho National Laboratory, INL/EXT-18-45933, July 2018.

[47] S. Kwon, “Demonstrate Viability of Accelerated Fuel Qualification Approaches,” FY20 LDRD Proposal, Idaho National Laboratory, 2019.

[48] S. A. Balderrama et al., “Versatile Test Reactor: Irradiation Testing Vehicles for Fast Reactors and Proposed Experimental Loadings,” INL/EXT-18-15762, Idaho National Laboratory, 2018.

[49] S. Balderrama, P. Sabharwall, D. Wachs, “Versatile Test Reactor for Advanced Reactor Testing,” *Transactions of the American Nuclear Society*, Vol. 119, Orlando, Nov. 11–15, 2018.

[50] K. J. Geelhood, W. G. Luscher, “FRAPCON-4.0: Integral Assessment,” PNNL-19418, Vol. 2 Rev. 2, Pacific Northwest National Laboratory, 2015.

[51] K. J. Geelhood, W. G. Luscher, “FRAPTRAN-2.0: Integral Assessment,” PNNL-19400, Vol. 2 Rev. 2, Pacific Northwest National Laboratory, 2016.

[52] MIT Energy Initiative Study, “The Future of Nuclear Energy in a Carbon-Constrained World,” Sept. 2018.

GENERAL ATOMICS
P.O. BOX 85608 SAN DIEGO, CA 92186-5608 (858) 455-3000